AD-A066 794 BOEING VERTOL CO PHILADELPHIA PA F/G 1/3
HELICOPTER TRANSMISSION VIBRATION AND NOISE REDUCTION PROGRAM. --ETC(U)
JAN 79 J W LENSKI DAAJ02-74-C-0040
UNCLASSIFIED D210-11442-1 USARTL-TR-78-2C NL

1 OF 2
AD A066794

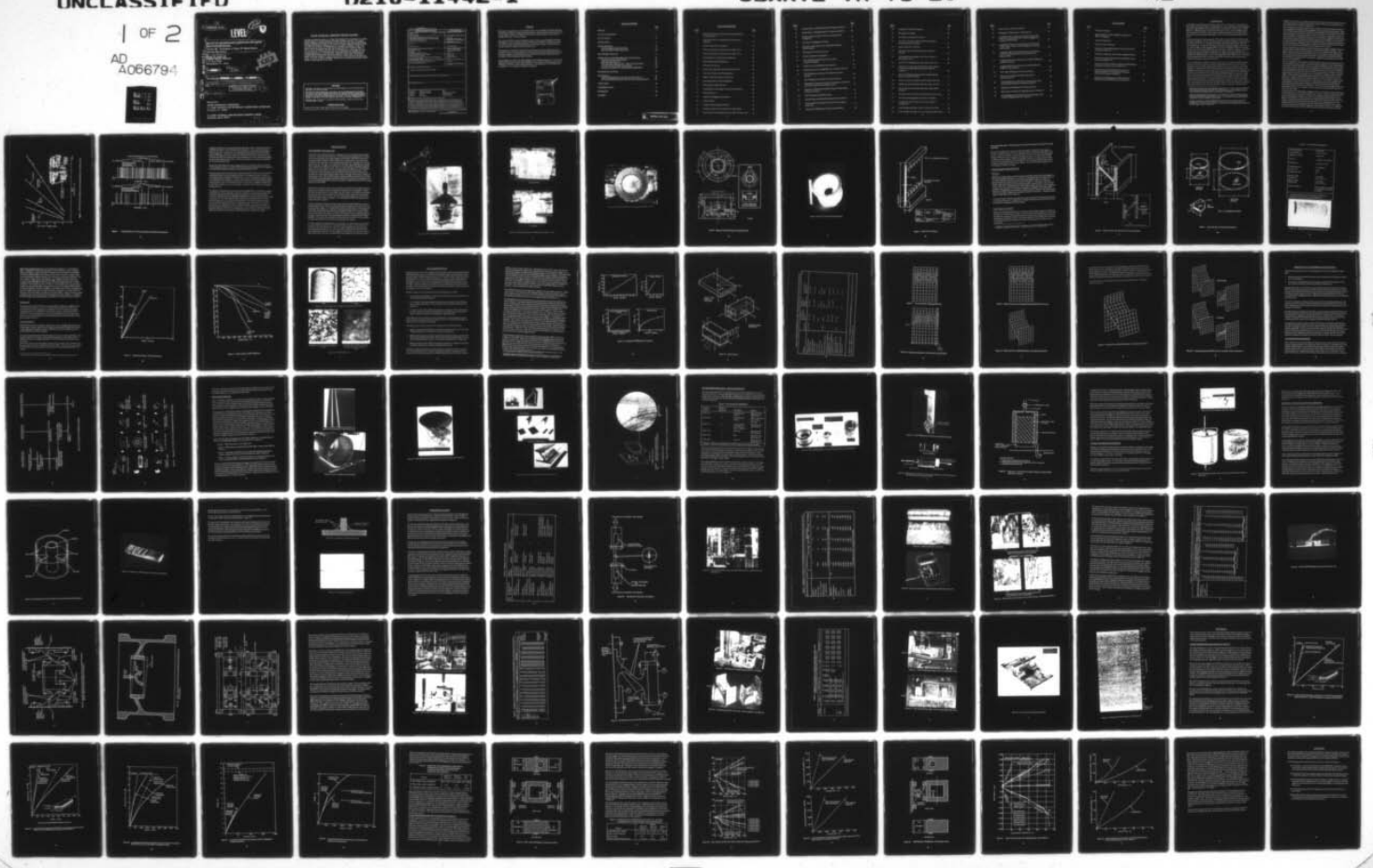

(18) USARTL (19) TR-78-2C

(12)

LEVEL II

AD A054827

(6) HELICOPTER TRANSMISSION VIBRATION AND NOISE REDUCTION PROGRAM.
Volume III, Evaluation of Fiber FP Metal-Matrix Housing Specimens.

(10) Joseph W. Lenski, Jr.
BOEING VERTOL COMPANY
P. O. Box 16858
Philadelphia, Pa. 19142

(11) Jan [redacted] 79

(12) 99 p.

1A AD55104
2B A051827

(9) Final Report, [redacted] Mar [redacted] — Oct [redacted] 78,

(15) DAAJ02-74-C-0040 (16) 1G262207AH89

Approved for public release; distribution unlimited.

(17) 02

(14) D210-11442-1

Prepared for

APPLIED TECHNOLOGY LABORATORY
U. S. ARMY RESEARCH AND TECHNOLOGY LABORATORIES (AVRADCOM)
Fort Eustis, Va. 23604

U.S. ARMY MATERIALS AND MECHANICS RESEARCH CENTER
Watertown, Mass. 02172

403 682

APPLIED TECHNOLOGY LABORATORY POSITION STATEMENT

This report provides the details of an effort that represents the continuation of an overall program designed to reduce helicopter transmission vibration and noise. The original program developed an analytical technique to determine the areas of high strain density, and hence, high acoustical energy, on the surface of a gearbox (USARTL-TR-78-2A & 2B). This effort has resulted in the development of a technique to selectively stiffen these areas of high strain density using high modulus aluminum oxide continuous fibers. A CH-47C forward transmission has been cast in three sections; i.e., outer ring, web and inner ring, and two "Z" sections have been cast to demonstrate the capability of incorporating these fibers into a complex shape. Subsequent testing has demonstrated the increased stiffness characteristics under both shear and moment loads. The ultimate benefit will be the reduction in internal noise levels in current and future US Army helicopters. Mr. Allen C. Royal, Propulsion Technical Area, Aeronautical Technology Division, served as project engineer for this effort.

UNCLASSIFIED
SECURITY CLASSIFICATION OF THIS PAGE (When Data Entered)

REPORT DOCUMENTATION PAGE

READ INSTRUCTIONS BEFORE COMPLETING FORM

1. REPORT NUMBER: USARTL-TR-78-2C	2. GOVT ACCESSION NO.
3. RECIPIENT'S CATALOG NUMBER	
4. TITLE (and Subtitle): HELICOPTER TRANSMISSION VIBRATION AND NOISE REDUCTION PROGRAM, Volume III – Evaluation of Fiber FP Metal-Matrix Housing Specimens	5. TYPE OF REPORT & PERIOD COVERED: Final Report, March 1978 – October 1978
	6. PERFORMING ORG. REPORT NUMBER: D210-11442-1
7. AUTHOR(s): Joseph W. Lenski, Jr.	8. CONTRACT OR GRANT NUMBER(s): DAAJ02-74-C-0040
9. PERFORMING ORGANIZATION NAME AND ADDRESS: Boeing Vertol Company, Box 16858, Philadelphia, Pennsylvania 19142	10. PROGRAM ELEMENT, PROJECT, TASK AREA & WORK UNIT NUMBERS: 62207A 1G262207AH89 02 004 EK
11. CONTROLLING OFFICE NAME AND ADDRESS: Applied Technology Laboratory, U.S. Army Research and Technology Laboratories (AVRADCOM), Fort Eustis, Virginia 23604	12. REPORT DATE: January 1979
	13. NUMBER OF PAGES: 99
14. MONITORING AGENCY NAME & ADDRESS (if different from Controlling Office): U.S. Army Materials and Mechanics Research Center, Watertown, Massachusetts 02172	15. SECURITY CLASS. (of this report): Unclassified
	15a. DECLASSIFICATION/DOWNGRADING SCHEDULE

16. DISTRIBUTION STATEMENT (of this Report)

Approved for public release; distribution unlimited.

17. DISTRIBUTION STATEMENT (of the abstract entered in Block 20, if different from Report)

18. SUPPLEMENTARY NOTES

19. KEY WORDS (Continue on reverse side if necessary and identify by block number)

Helicopters	Aluminum oxide fibers	Fibers
Transmissions	Metal matrix composites	Fiber-reinforced composites
Housings	Fiber FP	Magnesium matrix
Vibration	Noise reduction	Stress-strain relations

20. ABSTRACT (Continue on reverse side if necessary and identify by block number)

The objective of the work performed under this contract was to demonstrate selective reinforcement of a cast magnesium housing by the use of high-modulus FP fibers via casting technology. A series of housing element specimens were designed, fabricated, and tested to evaluate the application of state-of-the-art technology to the fabrication of a full-scale, fiber-reinforced metallic transmission housing. Several typical housing section specimens were fabricated and tested to determine material properties. These properties were compared with predicted values to develop the technology and analytical capability for the application of selective reinforcement of a full-scale helicopter transmission housing, with the final objective of reducing system deflections, noise, and vibration.

DD FORM 1 JAN 73 1473 EDITION OF 1 NOV 65 IS OBSOLETE

UNCLASSIFIED
SECURITY CLASSIFICATION OF THIS PAGE (When Data Entered)

PREFACE

This report is an appendix to work conducted under contract DAAJ02-74-C-0040, Helicopter Transmission Vibration and Noise Reduction Program. This initial work has been documented in two volumes. Volume I, USARTL-TR-78-2A, is the Technical Report, and Volume II, USARTL-TR-78-2B, is the User's Manual.

The work outlined herein has been performed under U.S. Army contract DAAJ02-74-C-0040, Mod. P00011, under the technical cognizance of Allen Royal, Applied Technology Laboratory, U.S. Army Research and Technology Laboratories, Fort Eustis, Virginia. The period of performance was from 13 March 1978 to 30 October 1978.

This program was conducted at the Boeing Vertol Company under the technical direction of Joseph W. Lenski, Jr. (Program Manager), of the Advanced Power Train Technology Department. Principal investigators for this program were Fred W. Brown (Analytical), Dale Austin (Test), and Robert Pinckney (Manufacturing Technology).

Acknowledgment is made to Dr. Ashok Dhingra and Dr. William Krueger of E. I. Du Pont de Nemours and Company, Textile Fibers Department, Pioneering and Textile Research Division, Wilmington, Delaware, for their technical assistance in the fabrication of the FP fibers and test specimens and consultation during the test program.

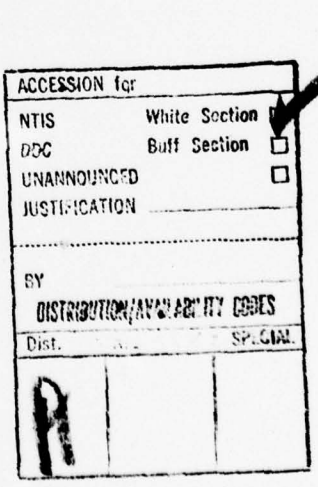

TABLE OF CONTENTS

LIST OF ILLUSTRATIONS

LIST OF TABLES

INTRODUCTION

Considerable attention has been focused in recent years on the reduction of noise levels for both military and civil helicopters, as evidenced by the noise requirements outlined in Military Specification MIL-A-8806, the Occupational Safety and Health Act (OSHA), and the Walsh-Healy Act. Helicopter noise emanates from three major sources: the rotor blades, engines, and transmissions. The effort of this contract and the Advanced Power Train Technology group has been directed toward reducing the noise level of the helicopter transmission at its source.

Boeing Vertol has been investigating since 1974, under contract DAAJ02-74-C-0040 entitled Helicopter Transmission Vibration and Noise Reduction Program, methods of reducing acoustical energy at the source by controlling the dynamic response through stiffness, mass, and inertia distribution. To provide a helicopter transmission housing meeting the criteria of low cost and low weight, as well as being capable of selective stiffening for efficiently reducing vibration and noise levels and deflections, it was necessary to assess the utility of new material concepts such as cast metal-matrix composites. The effect of selective stiffening can be evaluated by analytical techniques developed under Applied Technology Laboratory contracts DAAJ02-74-C-0040 (References 1 and 2) and DAAJ02-75-C-0053 (Reference 3). The results of these programs show that the techniques developed for predicting noise generated by a helicopter transmission correlate with test data.

Current cast-light-alloy transmission housing technology does not provide an optimum support structure for power train dynamic components under operational loads. These structures, limited by current materials and processing techniques that do not permit structural design optimization, exhibit excessive deflections and displacements under load which result in gear misalignment and vibration and noise generation. Increases in helicopter size, performance, and payload have intensified the need for high-strength, lightweight materials. The metal industry has been endeavoring to develop alloys with higher strength-to-weight and modulus-to-weight values. New alloys and new methods of working and heat-treating have brought about small improvements, but the gains are no longer proportional to the effort that must be expended. Since all of the widely used structural metals reach limits of specific strength at about 1 million inches and of specific modulus at about 100 million inches, a search was initiated for some way to get around these barriers. Several metal-matrix candidate systems have exhibited specific

---

1. Sciarra, John J., Howells, Robert W., Lenski, Joseph W., Jr., Drago, Raymond J., and Schaeffer, Edward G., HELICOPTER TRANSMISSION VIBRATION AND NOISE REDUCTION PROGRAM, Volume I – Technical Report, Boeing Vertol Company, Philadelphia, Pennsylvania; USARTL-TR-78-2A, Applied Technology Laboratory, U.S. Army Research and Technology Laboratories (AVRADCOM), Fort Eustis, Virginia, March 1978, AD A055104.

2. Sciarra, John J., Howells, Robert W., Lenski, Joseph W., Jr., and Drago, Raymond J., HELICOPTER TRANSMISSION VIBRATION AND NOISE REDUCTION PROGRAM, Volume II – User's Manual, Boeing Vertol Company, Philadelphia, Pennsylvania; USARTL-TR-78-2B, Applied Technology Laboratory, U.S. Army Research and Technology Laboratories (AVRADCOM), Fort Eustis, Virginia, March 1978, AD A054827.

3. Howells, R. W., and Sciarra, J. J., FINITE ELEMENT ANALYSIS FOR COMPLEX STRUCTURES (HELICOPTER TRANSMISSION HOUSING STRUCTURAL MODELING), Boeing Vertol Company, Philadelphia, Pennsylvania; USAAMRDL-TR-77-32, Applied Technology Laboratory, U.S. Army Research and Technology Laboratories (AVRADCOM), Fort Eustis, Virginia, January 1978, AD AD52749.

strength in the range of 2 to 3 million inches and specific modulus of 400 to 500 million inches. Thus, there are many areas where metal-matrix composites offer unique combinations of improved performance for helicopter applications.

The development of composite materials and the refinement of manufacturing technology for these materials have provided extended capabilities for the reinforcement of structures. Application of finite-element analyses to transmission housing design has permitted the use of optimization methods such as strain-energy analysis. Previous optimization work, although quite extensive, had been limited to varying the wall thickness of a conventional cast magnesium housing. The analytical techniques have indicated the potential for more efficient application of the optimization methods by taking advantage of the improved properties and capability for selective reinforcement offered by composite materials. The ability to build up composite material elements with specified property orientations allows selective reinforcement of predetermined housing regions and provides improved flexibility for optimization of the structure.

The use of metal-matrix composite materials for helicopter transmission housings has many potential benefits, including reduced vibration and noise levels and improved stiffness. These improved vibration and noise characteristics are due to the increased overall stiffness and the ability to further selectively stiffen identified areas. By increasing the housing wall stiffness, the resulting static and dynamic displacements will be reduced for a specified load condition. This is evident, for example, from $F = Kx$, where F = applied static or dynamic load, K = stiffness, and x = displacement.

A plot of displacement versus load for a CH-47C forward transmission housing fabricated from various materials is shown in Figure 1 and indicates that the magnitude of the housing displacements can be reduced substantially by the use of stiffer metal-matrix materials. Steel is shown in the figure as a point of reference. Since the amplitude of the vibration and resulting sound waves is proportional to the magnitude of the displacement of the structure, the overall effect of increased stiffness would be to reduce the vibration and noise level. In addition, substantial weight savings can be achieved through the use of metal-matrix materials to achieve a desired stiffness. If the standard magnesium housing was replaced with a steel housing of the same dimensions, a weight increase of 182 pounds would result. If the housing were fabricated with 100-percent metal-matrix material to achieve a stiffness close to that of steel, a weight increase of approximately 30 pounds would result. It is anticipated that only local stiffening of the housing will be required to achieve a significant reduction in deflections and therefore the weight will increase by much less than 30 pounds. This increase in housing weight will be offset by a significant reduction in the weight of various acoustical treatment materials required to achieve the same results.

A further benefit of the metal-matrix configuration is that it is much better suited for detuning of the housing than the conventional monolithic cast structure. A typical transmission frequency spectrum is presented in Figure 2. Because of the multiple forcing frequencies and the many natural frequencies of the structure which occur, detuning of this housing is extremely difficult. Although the natural frequencies can be shifted by modifying the wall thickness, the multitude of closely packed frequencies generally will cause the tuning process to be only minimally effective. The new frequency spectrum which results after substituting a typical metal-matrix material for monolithic magnesium is also presented in Figure 2. It is significant that the natural frequencies have been shifted toward the high end of the spectrum and that

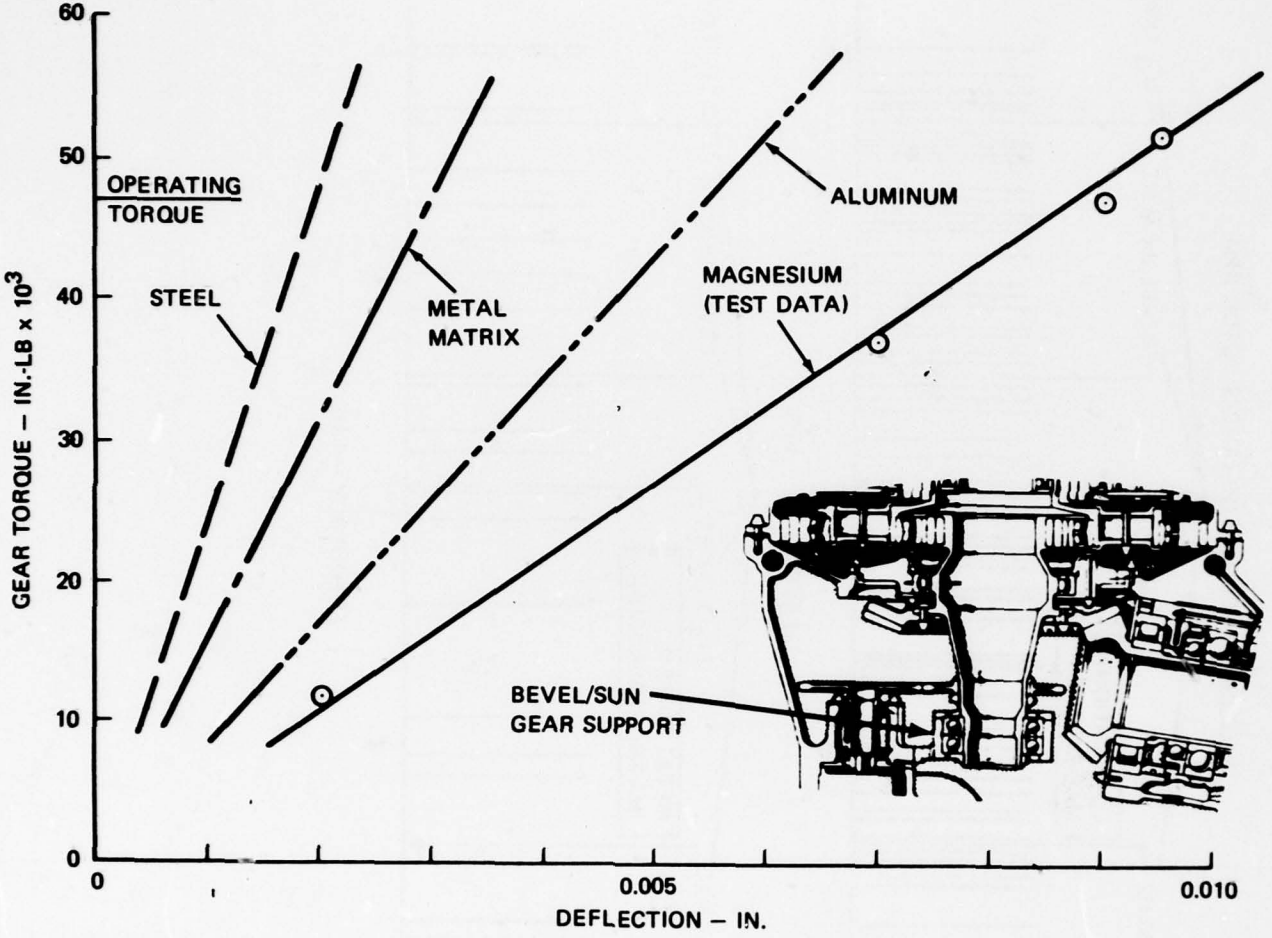

Figure 1. CH-47C Forward Transmission Dynamic Housing Deflection at Operating Speed.

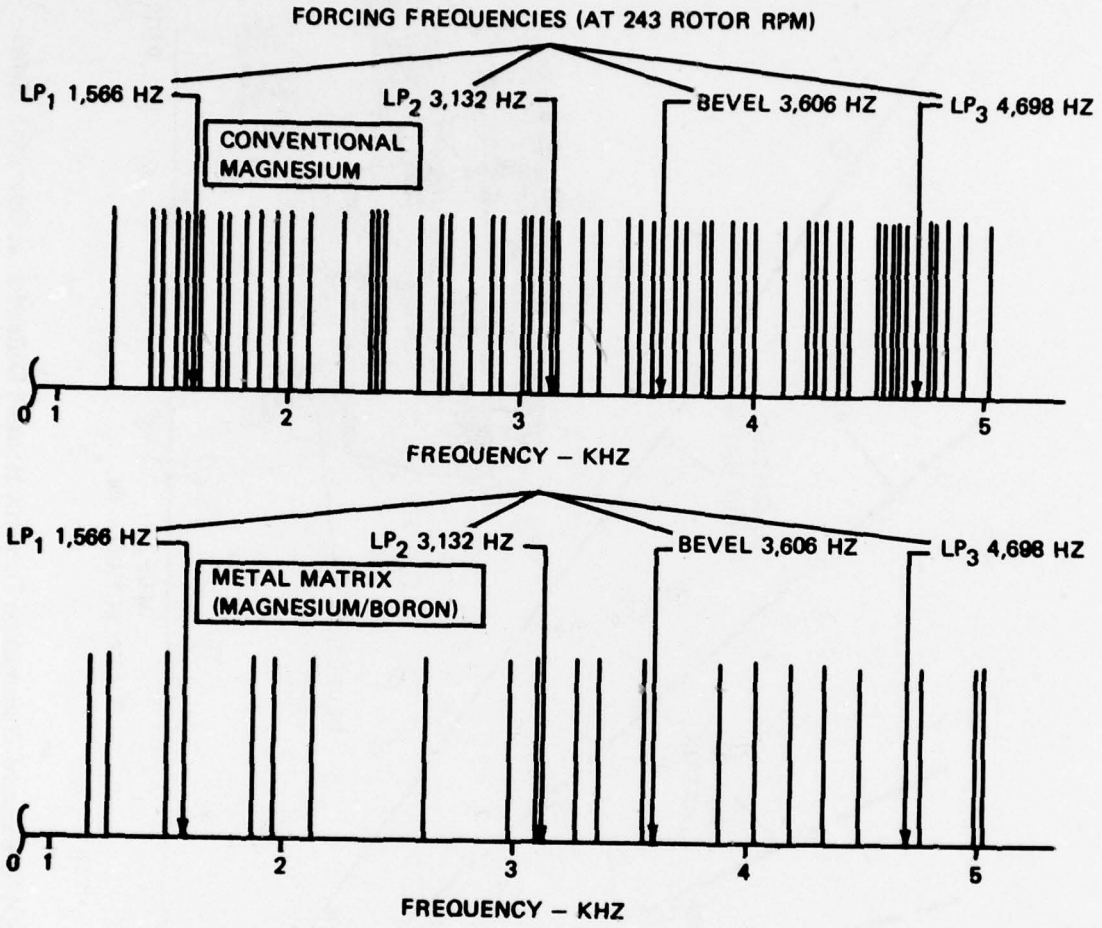

Figure 2. Typical Spectrum of Forcing Frequencies Versus Natural Frequencies.

only about 40 percent of the frequencies remain in the range of interest (below approximately 5,000 Hz) as compared to the solid magnesium configuration. Those natural frequencies remaining in the range of interest also have been dispersed and are thus much more amenable to the detuning process. Using the selective stiffening capability provided by the metal-matrix design, the housing can be tuned to reduce the vibration and noise levels. Further areas of potential vibration and noise improvement for the metal-matrix structure include structural damping and acoustic transmission loss (TL). Little data is available on these aspects, and therefore they must be investigated fully.

Boeing Vertol has worked with various casting concerns in an attempt to find a firm with the technical capability necessary to produce fiber-filled aluminum and magnesium cast components. Some firms have attempted to fabricate test specimens with little success.

During the past several years, the Du Pont Pioneering Research Laboratory has been conducting experimental fabrication using FP aluminum filaments in a magnesium matrix. In addition, Du Pont has also been working with Boeing Vertol on a series of developmental steps necessary to develop full-scale test hardware. To further explore the use of FP/magnesium matrix, Boeing Vertol and Du Pont have fabricated several typical test specimens containing the high-modulus reinforcing fibers. This work and hardware fabrication were used to supplement the work conducted under a modification to contract DAAJ02-74-C-0040 to fabricate and test transmission housing specimens.

The objective of this program was to assess the potential applicability of metal-matrix composite materials for the selective stiffening of a helicopter transmission. Previous analysis and testing of a CH-47C forward transmission housing by the application of strain-energy methods in conjunction with finite-element modeling have defined the most effective portions of the housing to be reinforced. The work conducted in this program has been directed to the area of the bevel gear support structure of the forward transmission. Several basic shapes representing this area were fabricated with FP fibers in a magnesium matrix to demonstrate the selective reinforcement of a magnesium structure via casting technology. These specimens, which are also representative of typical cross-section elements of a transmission housing, were analyzed, fabricated, and tested to determine material properties and to develop the technology for the application of selective reinforcement to a full-scale helicopter transmission housing

DESIGN SELECTION

TEST SPECIMEN CONFIGURATIONS

To provide a better understanding of the configuration, functional requirements,and design criteria of a typical helicopter transmission, a brief description and background for the selection of the test specimens used in this program will be provided. The CH-47C forward rotor transmission shown in Figure 3 will be considered as a typical baseline transmission and is composed of three major parts with essentially separate functions: the upper cover, the ring gear, and the case. The upper cover supports the rotor shaft and provides lugs for mounting the transmission to the airframe. Hence, the rotor system loads are transmitted through the upper cover into the airframe structure. The case contains and supports the main bevel gears and may also include a tail-rotor or synchronizing shaft drive, lubrication pump, or other accessory drives. The transmission case may also have a separate sump for containment of the lubricant. The stationary ring gear, which connects the upper cover and case, contains the planetary gear system. The entire transmission housing also performs the functions of sealing in the lubricant, providing passages for lubricant delivery, protecting critical transmission components, and dissipating heat by conduction and radiation. Figure 4 shows the CH-47C forward transmission case in detail.

Because of the complex geometry, large size, and the many functions that a typical helicopter transmission housing must perform, a simplified housing specimen was designed to simulate the major structural elements of the housing. The critical areas to be considered in this design were the outer shell, the inner support of the bevel gear, and the support webs that transfer loads from the inner ring to the outer shell. The simulated housing specimen of the CH-47C forward transmission is shown in Figure 5. A wood and plaster model of this specimen was made and is shown in Figure 6.

A typical transmission housing has evolved as a generally thick-walled magnesium casting. A weight breakdown shows that the housing weight represents approximately 24 percent of the total transmission weight. It is recognized that minimum wall thickness in nonstructural areas is limited by the casting process. With the methodology developed under contract DAAJ02-74-C-0040 and reported in USARTL-TR-78-2A, significant application of load path analysis can be used to optimize the structure of advanced transmission concepts employing fabricated housings, composite materials, and other advanced concepts that will permit greater design flexibility. For example, major load paths could be selectively reinforced to decrease deflections and minimize the noise and vibration emanating from the housing.

To further simplify the housing specimen, several smaller, less complex shapes were designed to represent the three major areas of a typical transmission housing: the outer shell cross section, the outer rim/web/inner rim cross section, and cylindrical shapes representing the outer wall and bearing support areas. The outer shell was represented as a flat section with increased thickness at each end as shown in Figure 7. This specimen was used to demonstrate fiber reinforcement of the thin outer shell wall and fiber transition into the heavier sections

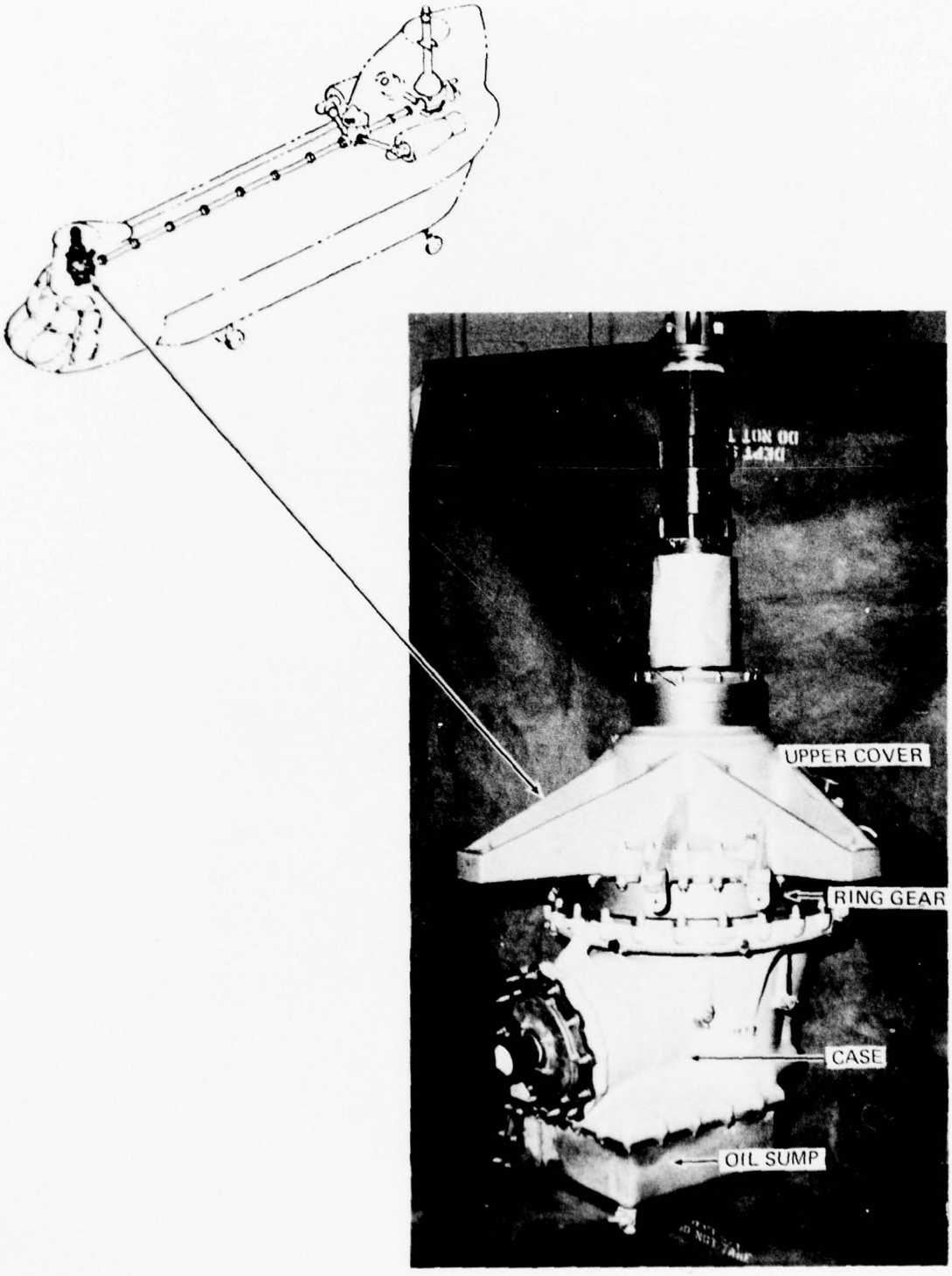

Figure 3. CH-47C Forward Rotor Transmission.

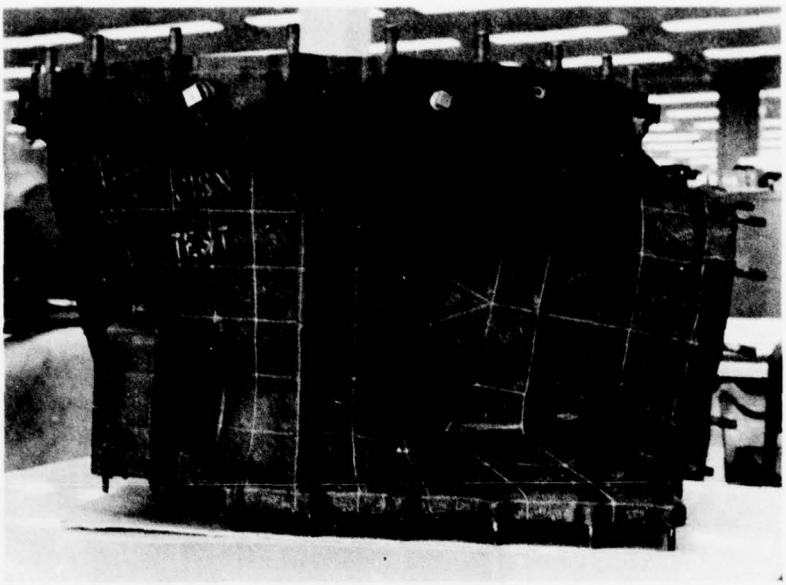

LEFT SIDE VIEW

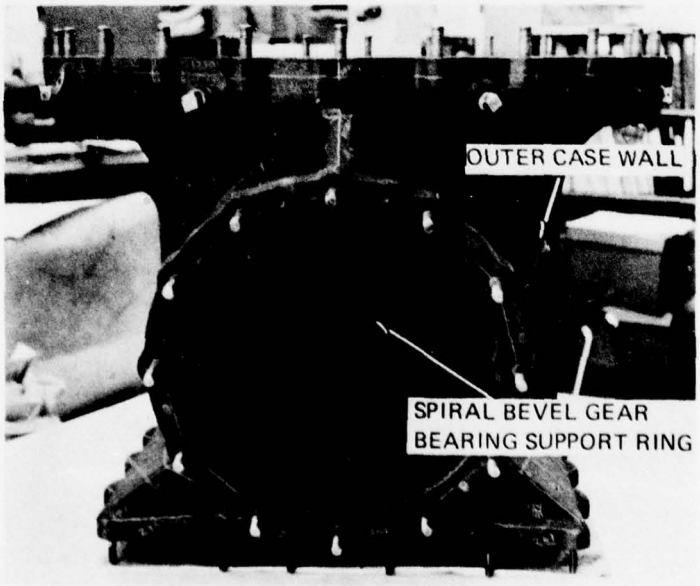

AFT VIEW

Figure 4. CH-47C Forward Rotor Transmission Case (Sheet 1 of 2).

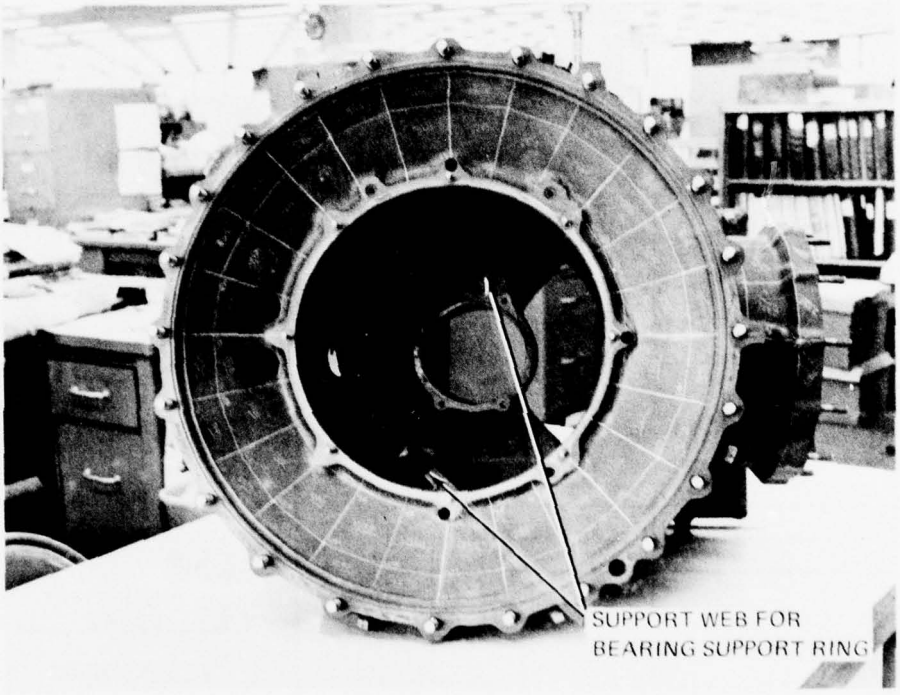

Figure 4. CH-47C Forward Rotor Transmission Case (Sheet 2 of 2).

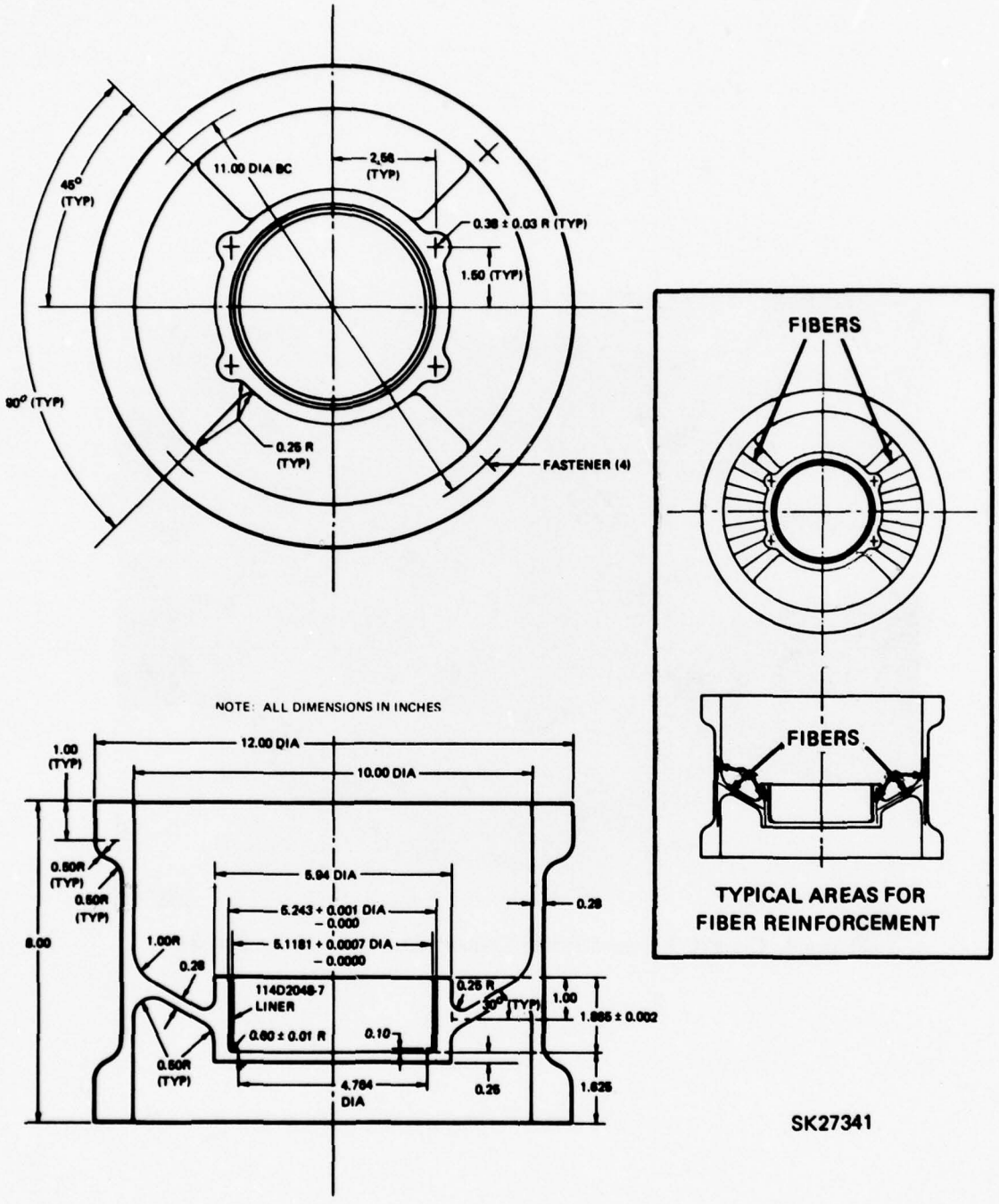

Figure 5. Simulated Bevel Gear Support Housing Specimen.

Figure 6. Model of Simulated Housing Specimen.

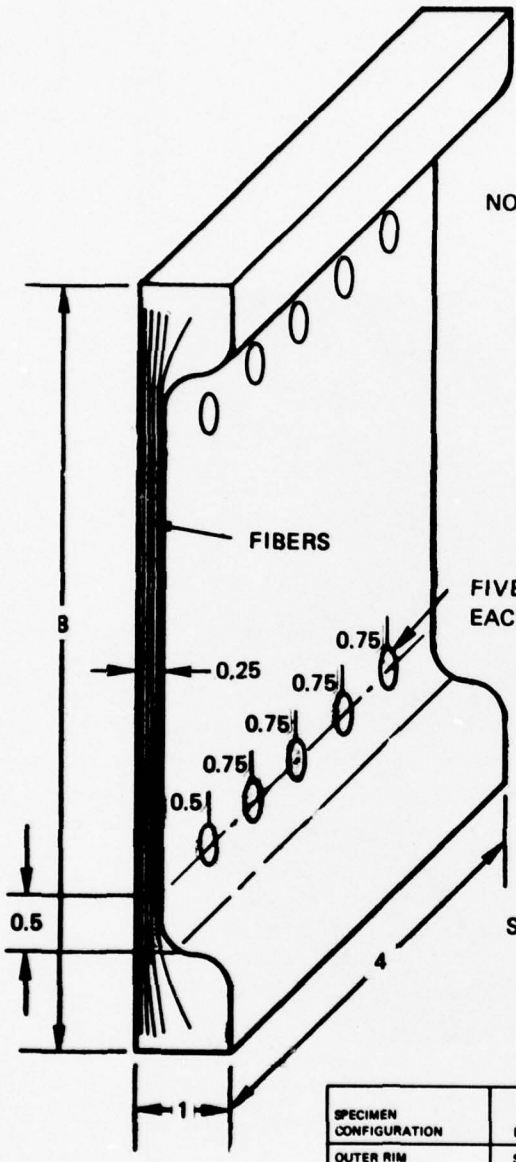

SPECIMEN CONFIGURATION	DRAWING	FIBER ORIENTATION AND VOLUME, %	MATERIAL
OUTER RIM CROSS SECTION, FIBER REINFORCED	SK27376-1	$\pm 60^{\circ}-0^{\circ}-\pm 60^{\circ}$ 56	FIBER – DU PONT FP, 20-MICRON NOMINAL DIAMETER, 200-KSI UTS MINIMUM MATRIX – MAGNESIUM ALLOY
OUTER RIM CROSS SECTION (BASELINE SPECIMEN)	SAME AS SK27376-1 EXCEPT NO FIBERS SK27376-2	NONE	AZ91C MAGNESIUM ALLOY

Figure 7. Outer Rim Cross Section.

where studs will be placed. The dimensions of this specimen represent typical thin-wall casting capabilities.

The outer rim/web/inner rim cross-section specimen (Figure 8) represents a major support member of a spiral bevel gear. The aim of this specimen was to demonstrate that fibers can be cast into a specimen to provide continuous fiber flow from an inner member (bearing support) through a web and into the outer member (housing outer shell). A continuous flow of fiber is essential to provide adequate stiffness and strength. Finally, the last specimens to be fabricated as part of this program are shown in Figure 9. These specimens represent large cylindrical shapes containing oriented fibers which represent the outer shell and bearing support areas of a helicopter transmission housing.

REINFORCEMENT FIBER SELECTION

Description

Fiber FP is an experimental continuous aluminum oxide fiber currently under development by the Du Pont Company (Reference 4). In contrast to existing high-alumina insulation fibers on the market, Fiber FP is essentially 100-percent polycrystalline α-alumina at a purity of greater than 99 percent Al_2O_3, fired to a density of 98 percent of theoretical. The fiber is therefore inherently stable at elevated temperatures and is compatible with a variety of metal systems. Fiber FP is a multifilament yarn which offers flexibility and relative ease of handling. In addition, the projected cost of the fiber is competitive with graphite and is substantially below that of large-diameter monofilaments of boron and silicon carbide. These features make Fiber FP an excellent candidate for metal-matrix composite reinforcement. A typical 500-gram bobbin of Fiber FP is shown in Figure 10.

A technique based on molten-metal infiltration has been developed for fabricating metal-matrix composites with Fiber FP. The infiltration technique offers the potential for low cost and can be extended to making large reinforced castings.

Room-Temperature Properties

Fiber FP is experimentally produced as a continuous, polycrystalline α-Al_20_3 yarn containing 210 filaments. Each filament is round in cross section with an average diameter of 20 microns. The fiber purity is greater than 99-percent alumina and the density is 98 percent of theoretical. Properties are summarized in Table 1. The tensile modulus of 345-379 GPa (50-55 x 10^6 psi) is considerably greater than alumina fibers which contain large amounts of silica or other metal oxides.

4. Champion, A. R., Krueger, W. H., Hartmann, H. S., and Dhingra, A. K., FIBER FP REINFORCED METAL MATRIX COMPOSITES, Second International Conference on Composite Materials, Toronto, Canada, April 1978.

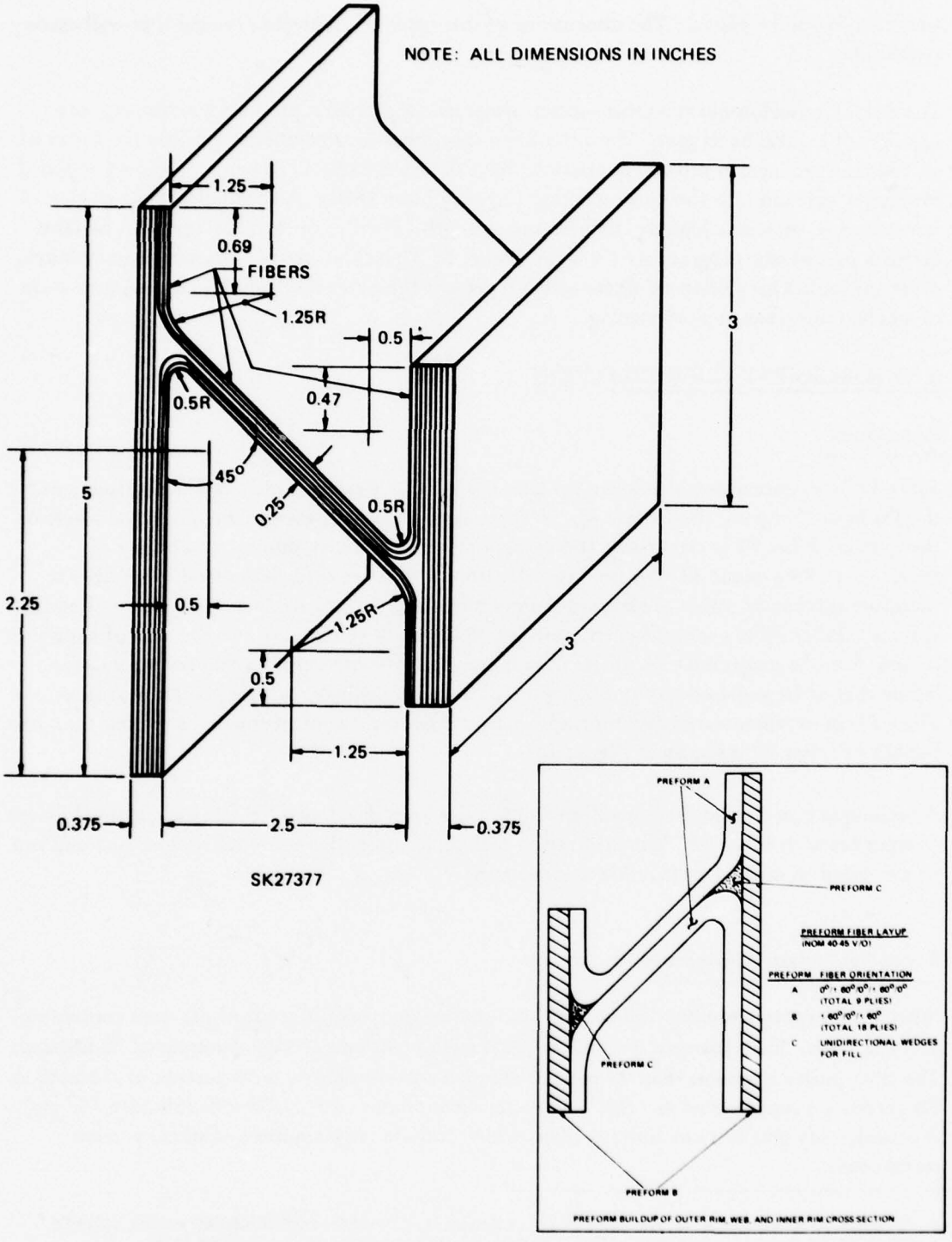

Figure 8. Details of Outer Rim, Web, and Inner Rim Cross Section.

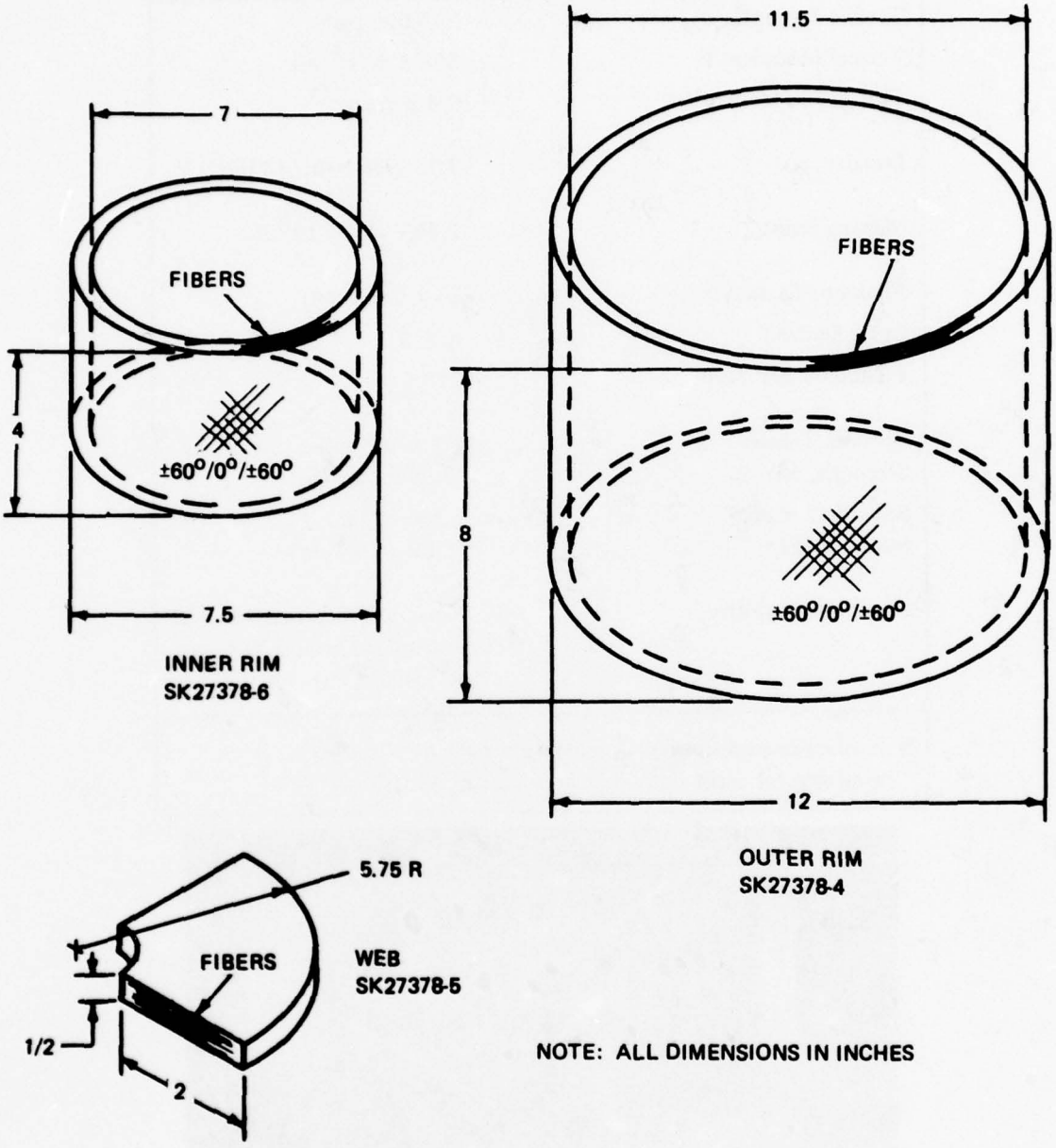

Figure 9. Outer Rim, Web, and Inner Rim Components.

TABLE 1. FP FILAMENT PROPERTIES

Tensile Strength, σ	200,000 psi*
Tensile Modulus, E	50-55 x 10^6 psi
Elongation to Break	0.4 percent
Density, ρ	3.95 gm/cc (0.143 lb/in.^{3})
Melting Point	2,045°C (3,713°F)
Filament Diameter	20 ± 5 microns
Cross Section	round
Filaments per Yarn	210
Specific Tensile Strength, σ/ρ	1.4 x 10^6 in. (3.56 x 10^6 cm)
Specific Tensile Modulus, E/ρ	3.5 x 10^8 in. (8.89 x 10^8 cm)
Oxidative Stability	Room temperature strength unchanged after 300 hours at 1,000°C.

* A silica-coated fiber with tensile strength of 275,000 psi is available for resin and other nonmetal applications.

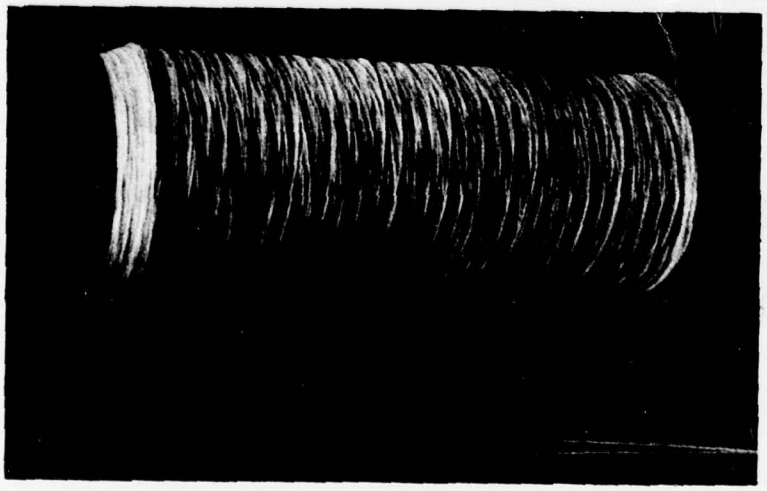

Figure 10. Bobbin of Fiber FP Continuous Alumina Yarn.

Fiber FP was primarily developed for metal reinforcement applications. In processing the fibers, a small amount of silica coating is applied to the fiber primarily to aid in wetting by molten metal during composite fabrication. Coating levels are of the order of 0.20-0.25-percent silicon as determined by atomic adsorption of an extract of the fiber. Using secondary ion mass spectrometry (SIMS) techniques, Prewo (Reference 5) estimates the thickness of the silica coating to be approximately 50 angstroms. Typical filament strengths measured at 6.4-mm (0.25-in.) gage length average 1380-1500 MPa (200-220 ksi) prior to silica coating. Coating with silica typically raises the strength level by 275-350 MPa (40-50 ksi). The exact mechanism of the strengthening effect is not known. Du Pont believes that a partial healing of surface flaws takes place through rounding off of crack tips. This strength increase, however, is of practical usefulness only for resin applications of the fiber, since the silica coating generally reacts with molten metals and the strength of the fiber drops back to its uncoated level. For this reason, Fiber FP strength is quoted in the uncoated condition. Typical stress-strain behavior of FP fibers versus other commonly used reinforcing fibers is shown in Figure 11. In addition, the fiber strength at elevated temperatures compared to other materials is shown in Figure 12.

Microstructure

The surface texture of Fiber FP shows the typical cobblestone appearance of glass-free polycrystalline alumina (Figure 13). There is no visual difference between silica-coated and uncoated fiber, even at a magnification of 12,000 times. Fracture surfaces show typically transgranular failure and it is difficult to locate fracture origins or to determine grain size accurately. Grain size determination is improved by thermal etching of the fracture surface, but it is more accurate when fiber ends are first polished and then thermally etched to reveal grain boundaries (Figure 14).

Recent Developments

Fiber FP has the potential for higher strength than the current 1380 MPa (200 ksi) level used in this program. Recently, fibers with an average tensile strength of 2000 MPa (300 ksi) prior to silica coating have been demonstrated on a laboratory scale. This strength increase was achieved without any sacrifice in modulus.

It also has been demonstrated that Fiber FP can be woven into two-dimensional fabrics. Since the yarn is brittle it is necessary to overwrap the fiber with three to four wraps per inch of 50-denier rayon prior to weaving. Plain weaves, 8-, and 12-harness satin constructions have been made.

Woven fabric was not used in this program. Because of the variation of fiber orientations, the fiber was used in sheet form consisting of unidirectional fibers. These sheets are used to obtain the desired fiber orientation and percent fiber volume for each specimen fabricated for this program.

---

5. Prewo, K. M., Report R77-912245-3, United Technologies Research Center, East Hartford, Connecticut, May 1977.

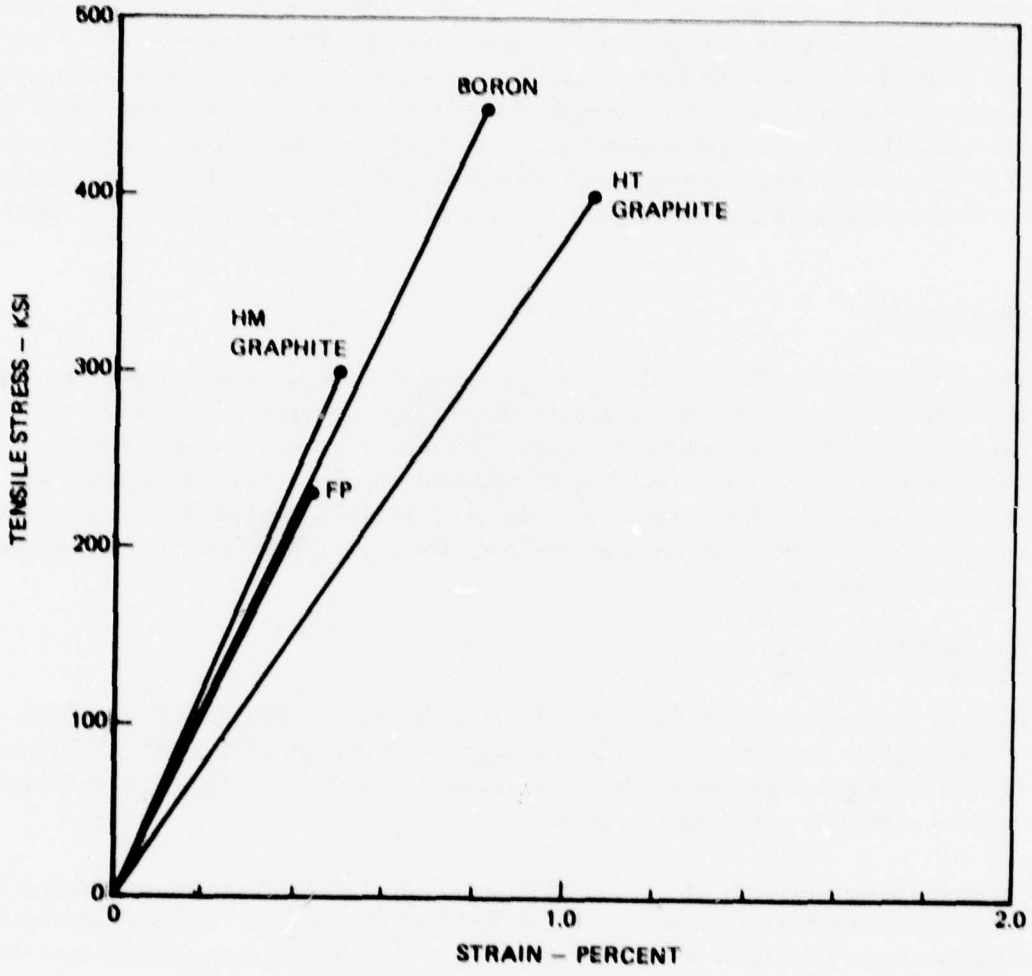

Figure 11. Stress-Strain Behavior of Reinforcing Fibers.

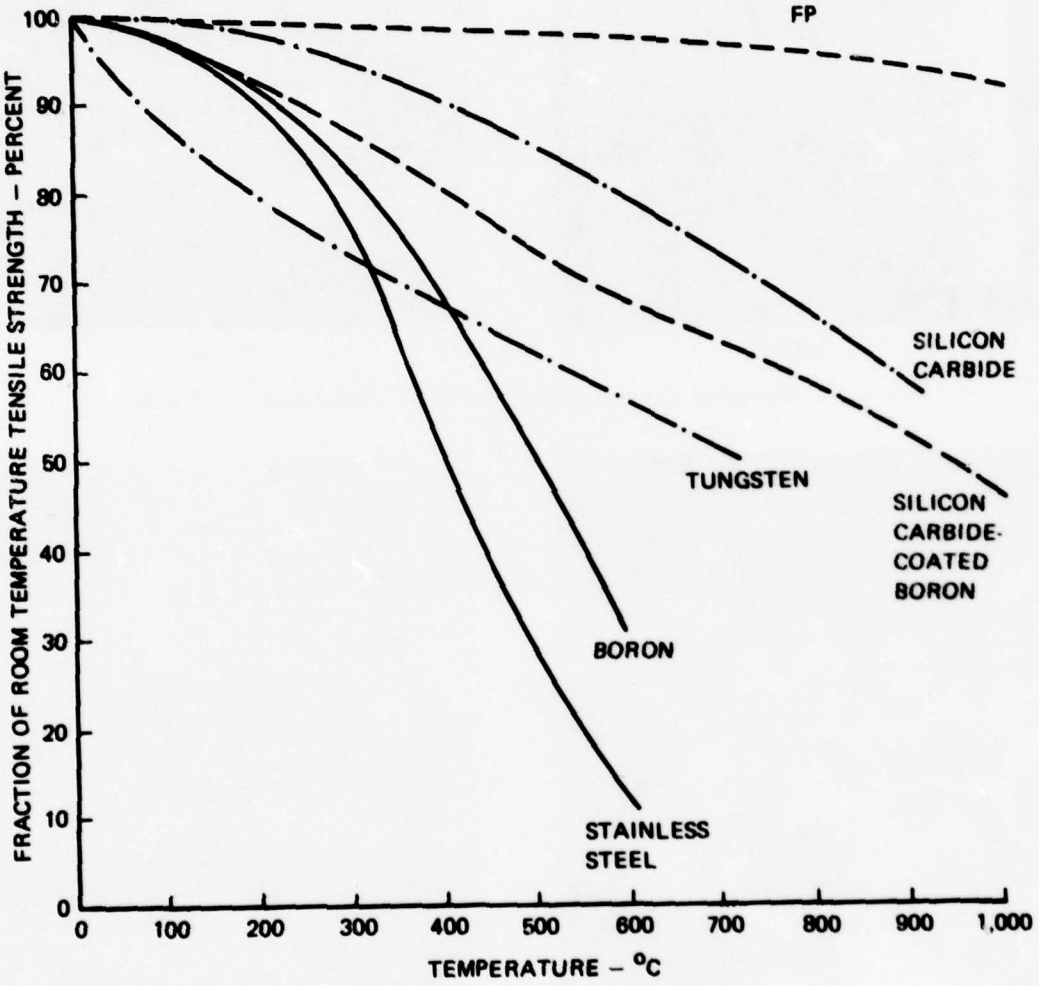

Figure 12. Fiber Strength at High Temperature.

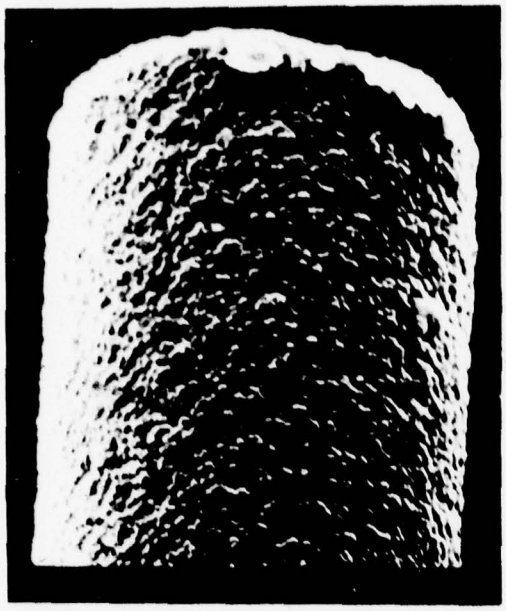

3,000X

12,000X

Figure 13. Scanning Electron Micrographs of Typical Fiber FP Surface.

THERMALLY ETCHED FRACTURE SURFACE
12,000X

POLISHED AND THERMALLY ETCHED
FIBER END TO REVEAL GRAIN SIZE
12,000X

Figure 14. Fiber FP Grain Size.

TEST SPECIMEN ANALYSIS

A significant portion of the work completed in the early phases of this contract was aimed at identifying by analysis those areas of a transmission housing which, when selectively stiffened, would result in a reduced audible transmission noise level. This capability has been demonstrated and substantiated by test and is documented in References 1 and 2. In order to fully utilize this technology, it is necessary not only to develop the high-modulus materials and fabrication techniques, but also to demonstrate the applicability of available analytical methods to these materials. Analytical techniques to characterize the structural behavior of these materials are necessary to assist the engineer in designing a future helicopter transmission which incorporates the advantages of selective stiffening.

The major objectives of the analytical portion of this program were as follows:

1. To investigate the applicability of available analytical methods to predict the behavior of Fiber FP/magnesium matrix laminates.

2. To analytically compare the strength and stiffness characteristics of the Fiber FP/magnesium composite specimens to the same characteristics of specimens made entirely of magnesium.

3. To verify the results of the analytical investigation by comparison with experimental test data and to identify areas where the analysis may require improvement or special techniques to adequately model Fiber FP/magnesium composite behavior.

These objectives were met during the course of this program. The methodology used in the analyses is identical to that documented in References 1 and 2, except that static-loading conditions only were considered in this program.

The analyses of the various test specimens were approached in the following manner:

1. Employ existing analytical methods to calculate material properties for each of the Fiber FP/magnesium laminates comprising the composite test specimens.

2. Model and analyze the test specimens using the finite-element technique. Input material property data calculated in first step. The finite-element model should endeavor to simulate the loading conditions and fixity of the specimen experimental test configuration.

3. Model and analyze baseline AZ91C-T6 magnesium specimens for comparison of strength and stiffness characteristics with Fiber FP/magnesium specimens.

All housing component specimens were analyzed using the same general computer approach. First, the material properties for the Fiber FP/magnesium laminates comprising the various sections of the composite specimens were computed using the Point-Stress Laminate Analysis

(PSLA) computer program, Reference 6. This program accounts for the anisotropic characteristics of the composite by using the basic single-ply (lamina) material properties (Figure 15) to calculate the equivalent pseudo-orthotropic material properties of the laminate. These anisotropic material properties are then used in the NASTRAN analysis. Figure 16 illustrates the lamina or layer coordinate system (1-2) which is transformed to the laminate (X-Y) axis system. The angle θ shown is the angle defining the orientation of the lamina material coordinate system with respect to the laminate coordinate system. The resultant forces and moments, representing a force system which is statically equivalent to the stress system acting on the laminate, are also shown. This computer program may be used after the NASTRAN analysis as a post processor to obtain interlaminar and laminar stresses.

The NASTRAN analysis of the test specimens considered only static loading conditions. Models of each specimen were developed with quadrilateral elements. Material properties from the PSLA computer program were input for the Fiber FP/magnesium specimens while AZ91C-T6 material properties (Table 2)were input for the magnesium specimens (Reference 7).

The NASTRAN finite-element model of the outer-rim cross-section test specimen (SK27376) is shown in Figure 17. The model consisted of 169 quadrilateral plate elements joined at 207 grid points. In developing the model, advantage was taken of the geometric symmetry of the specimen. Due to reflective symmetry about the horizontal and vertical centerlines of the specimen, only one quadrant of the specimen (with appropriate boundary conditions) need be modeled. The stresses and displacements in the other three quadrants are reflections or mirror images of the single-quadrant model. This modeling technique reduces the number of elements required in the finite-element idealization, and hence decreases computing time. The boundary conditions compatible with the 1/4-symmetry model are shown in Figure 18. NASTRAN analyses were performed with this model for both the magnesium and FP fiber-reinforced magnesium specimens. The composite material properties of the Fiber FP/magnesium laminate ($\pm 60^{o}/0^{o}/\pm 60^{o}$ fiber orientation) were developed with the PSLA computer program and subsequently input into NASTRAN for the Fiber FP/magnesium finite-element analysis. Material properties of the AZ91C-T6 magnesium alloy were input for the finite-element analysis of the plain magnesium specimen. Figure 19 is a plot of the typical deformed shape due to load of the outer-rim cross-section test specimen. Note that, for purposes of visualization, the deformations on the plot are shown to a greatly exaggerated scale.

The finite-element model of the outer rim/web/inner rim test specimen (SK27377) is shown in Figure 20. The model consists of 167 quadrilateral plate-bending/membrane elements connected at 175 grid points. This model was employed in the NASTRAN analysis for both the single-specimen test configuration and the back-to-back test configuration; the back-to-back configuration used two specimen models. Both analyses assume that the test specimens are rigidly fixed to the test fixture members at the fixture mounting points. Loads were applied through a rigid coupling analogous to the test fixture center section. Stress and deflection data

6. Reed, D.L., POINT STRESS LAMINATE ANALYSIS, Document FZM-5494, Advanced Composite Division, U.S. Air Force Materials Laboratory, Wright-Patterson Air Force Base, Ohio, April 1970.

7. MIL-HDBK-5C, MILITARY STANDARDIZATION HANDBOOK, METALLIC MATERIALS AND ELEMENTS FOR AEROSPACE VEHICLE STRUCTURES, FSC1560, Department of Defense, Washington, D.C., September 1976.

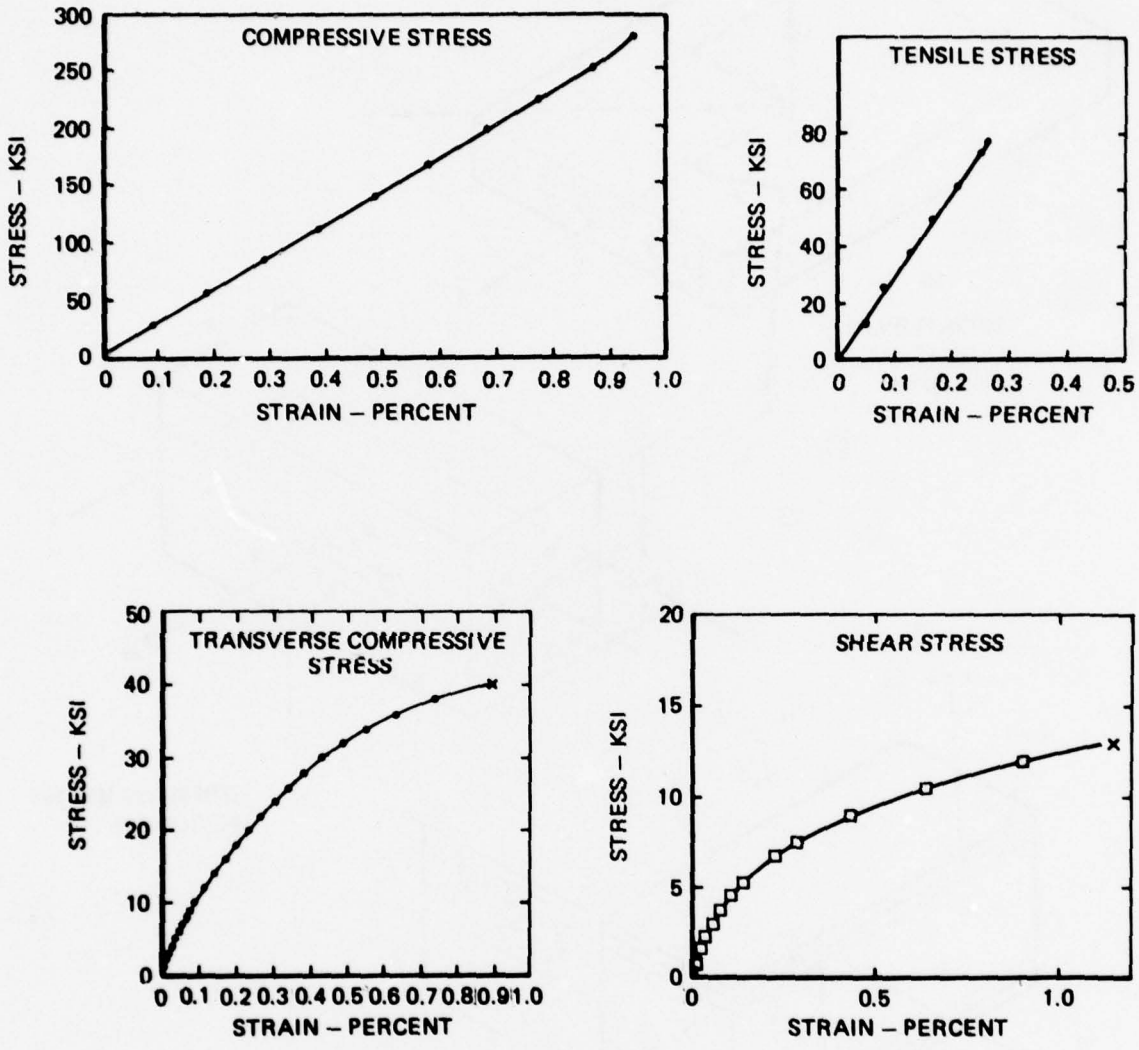

Figure 15. Properties of FP/Magnesium Composites.

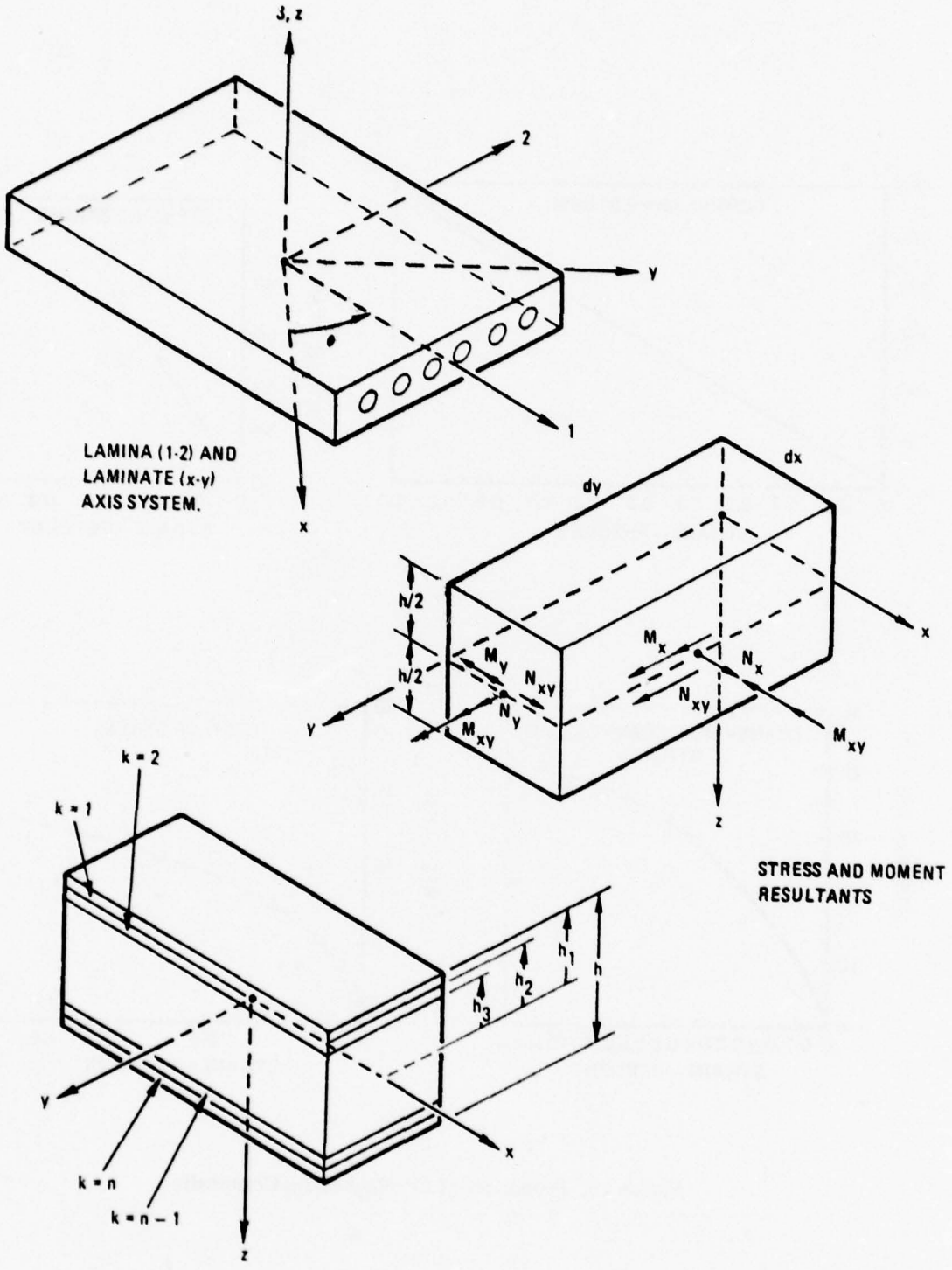

Figure 16. Lamina Notation.

TABLE 2. MATERIAL PROPERTIES OF FIBER FP/MAGNESIUM MATRIX AND AZ91C-T6 MAGNESIUM

Property	Fiber FP	Commercially Pure Magnesium Matrix*	Unidirectional Single-Ply FP/Magnesium	Cast AZ91C-T6 Magnesium**
Modulus of Elasticity (longitudinal, psi)	55×10^6	6.4×10^6	29×10^6	6.5×10^6
Modulus of Elasticity (transverse, psi)	–	6.4×10^6	15.5×10^6	6.5×10^6
Poisson's Ratio	–	0.35	0.23	0.35
Shear Modulus (psi)	–	–	5.9×10^6	2.4×10^6
Density ($lb/in.^3$)	0.143	0.063	0.101	0.065
Fiber Volume Fraction (%)	–	–	50	–
Thermal Expansion Coefficient (longitudinal, in./in./°F)	–	26×10^{-6}	3.78×10^{-6}	14×10^{-6}
Thermal Expansion Coefficient (transverse, in./in./°F)	–	26×10^{-6}	7.56×10^{-6}	14×10^{-6}
Ultimate Strength, Tension (longitudinal, ksi)	200	9.2–22	77	17–34
Ultimate Strength, Tension (transverse, ksi)	–	–	9.5	17–34

*Reference 8, Emley, E. F., PRINCIPLES OF MAGNESIUM TECHNOLOGY, London, England, Pergamon Press, 1966.
**Reference 7, Table 4.3.3.0(6), Page 4–62.

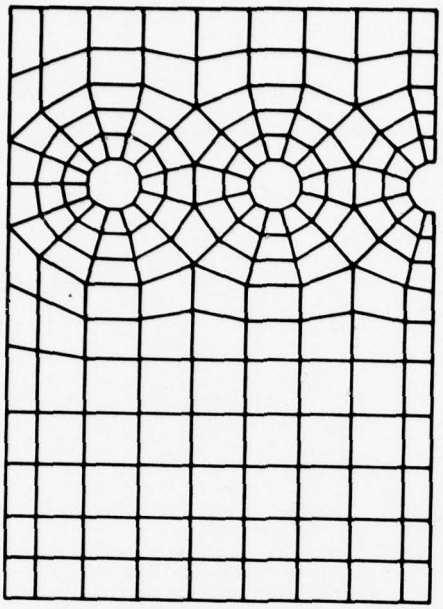

Figure 17. Computer Model of Specimen SK27376.

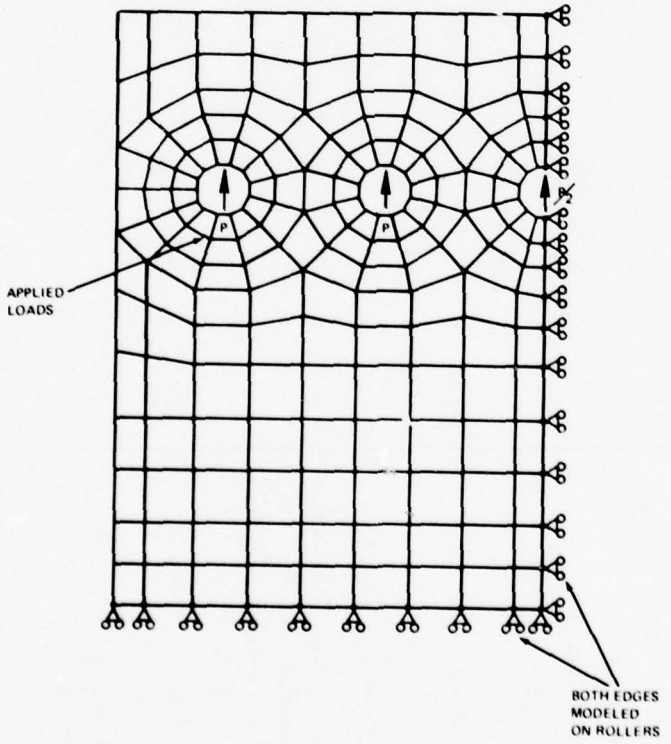

Figure 18. Boundary Conditions for 1/4-Symmetry Computer Model.

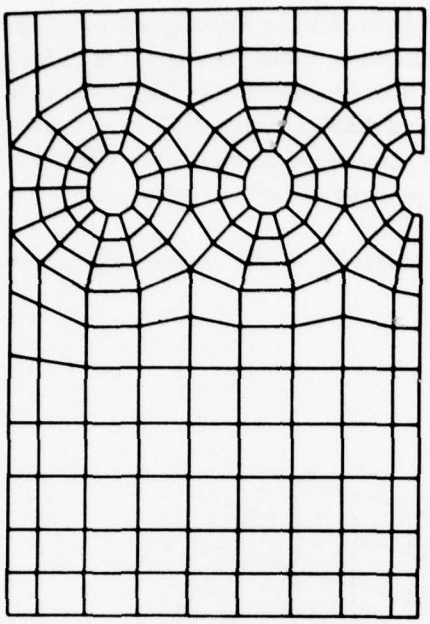

Figure 19. Elastic Deformation of Simulated Specimen SK27376 Under Load.

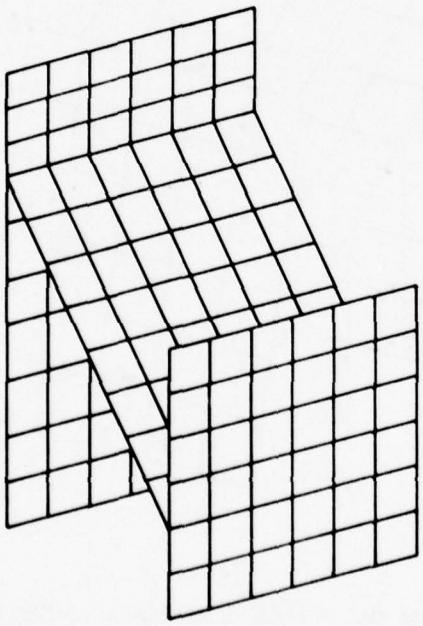

Figure 20. Undeformed Plot of NASTRAN Model of Test Specimen SK27377.

was obtained for specimens made from Fiber FP/magnesium composite and AZ91C-T6 magnesium for the two test configurations, although only Fiber FP/magnesium specimens were actually fabricated and tested. This provides for a comparison based on analytical data between the FP/magnesium composite and AZ91C-T6 magnesium test specimens. Figure 21 shows a typical deformed-shape plot of the single-specimen test configuration. Figure 22 shows typical undeformed and deformed-shape plots of the two test specimen models in the back-to-back test.

The results and experimental comparison of the analysis will be discussed in a subsequent section of this report.

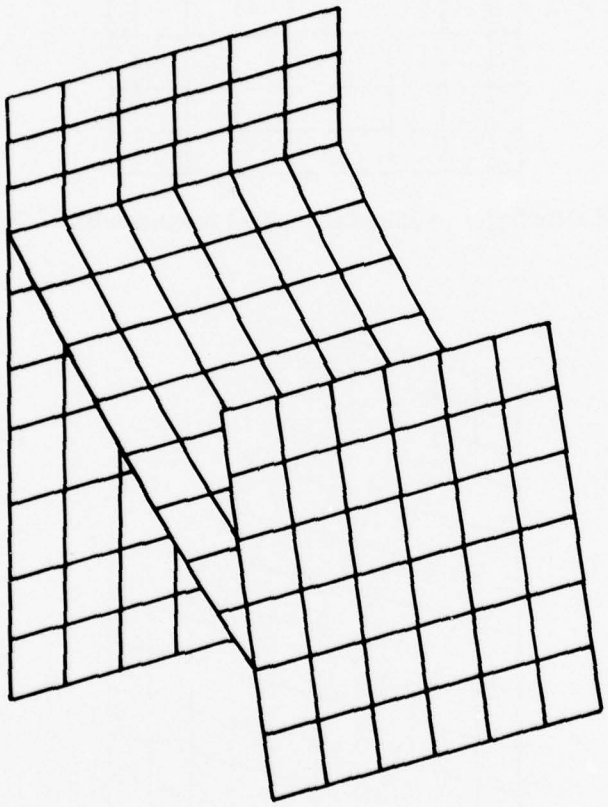

Figure 21. Deformed Plot of NASTRAN Model of Test Specimen SK27377.

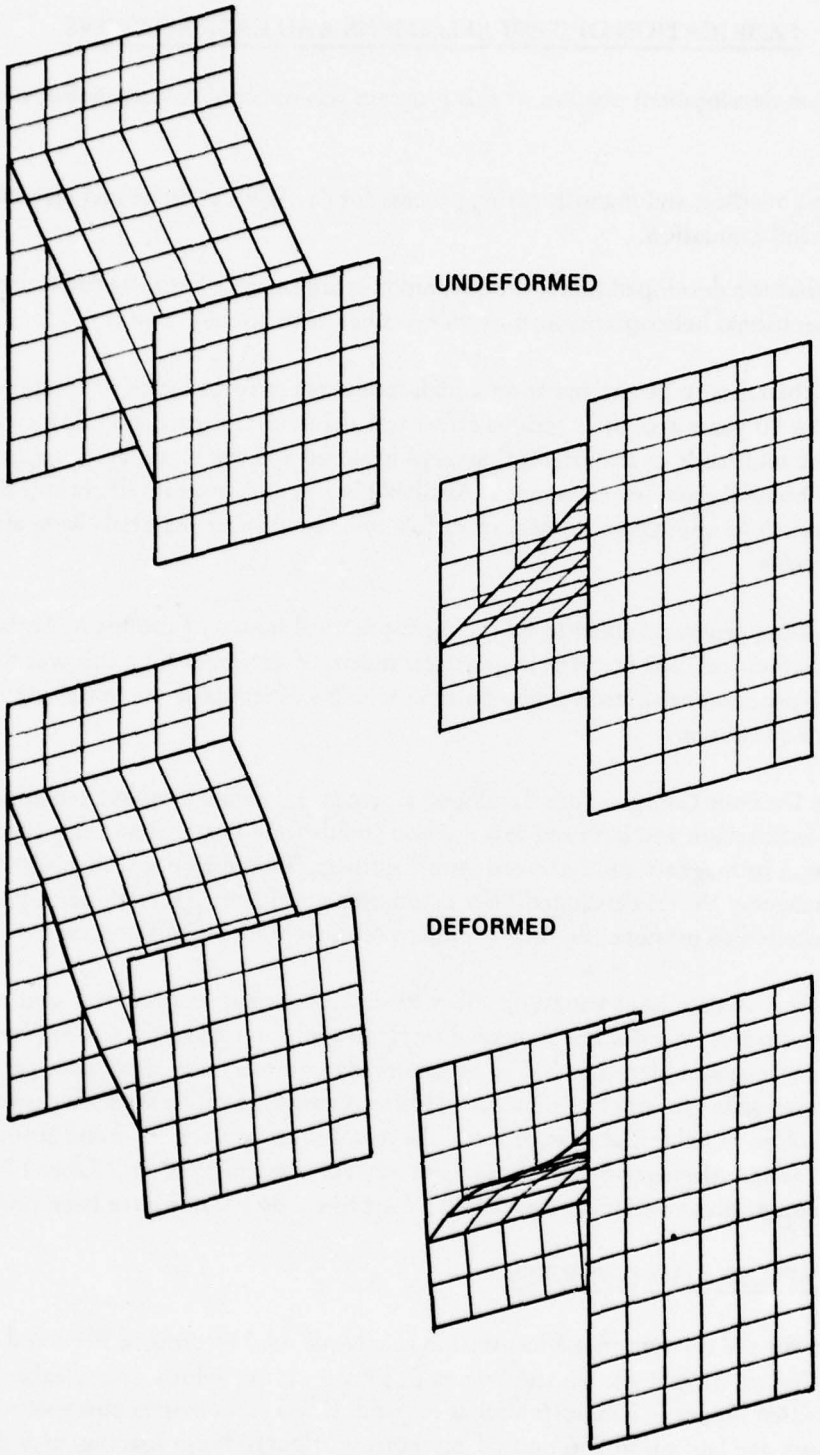

Figure 22. Composite Specimens SK27377 Shown in the Back-to-Back Configuration.

FABRICATION OF TEST SPECIMENS AND CASE SECTIONS

The fabrication development portion of this program was directed to accomplish two major goals:

1. Develop a method and manufacturing process for the fabrication of test elements required for test and evaluation.
2. Insure that the developed fabrication techniques are suitable for the production of full-size, operational helicopter transmission housings at reasonable cost.

Although the benefits to be derived from a high-modulus reinforced case structure were identified more than 10 years ago, little serious effort was made to fabricate monolithic case elements because of the multitude of manufacturing steps involved and the manufacturing costs projected for diffusion-bonded complex structures. Available boron and graphite fibers and their precursor forms such as multifilament wire or diffusion-bonded sheet materials were also investigated with little success.

The direct-casting process seemed to be the most practical means of producing helicopter transmission case structures, but no reliable, practical means of accomplishing this was found. The direct-casting process envisioned required a fiber which was stable at the temperatures of molten magnesium or aluminum.

Recently, the Du Pont Company has developed a process involving a casting technique based on liquid-metal infiltration and has used this method to fabricate test bars and flat specimens made from aluminum or magnesium reinforced with FP fibers. In addition, this concept has been coupled to a Boeing Vertol-developed fiber laminating and forming technique to provide the technology needed to produce the test specimens fabricated under this contract.

The major effort to date has focused on Fiber FP reinforcement of aluminum and magnesium, since fiber incorporation would be expected to greatly improve the stiffness, high-temperature strength, and strength-to-density ratio of these already commercially significant lightweight engineering materials. In order to produce void-free composites with attractive mechanical properties by a molten-metal infiltration process, the metal must wet the fiber and form a strong fiber/matrix bond. Magnesium and its alloys satisfy these conditions with Fiber FP, and FP/magnesium composites containing up to 70 percent fibers by volume have been prepared.

VACUUM INFILTRATION PROCESS

A flow chart for the vacuum metal infiltration technique used to prepare FP/metal composites is shown in Figures 23 and 24. As the first step, FP yarn is made into a handleable FP tape with a fugitive organic binder in a manner similar to producing a resin-matrix composite prepreg. Fiber FP tapes are laid up in the desired orientation, fiber volume loading, and shape, and are then inserted into a casting mold of steel or other suitable material. The fugitive organic binder is burned away, and the mold is infiltrated with molten metal. While there are numerous

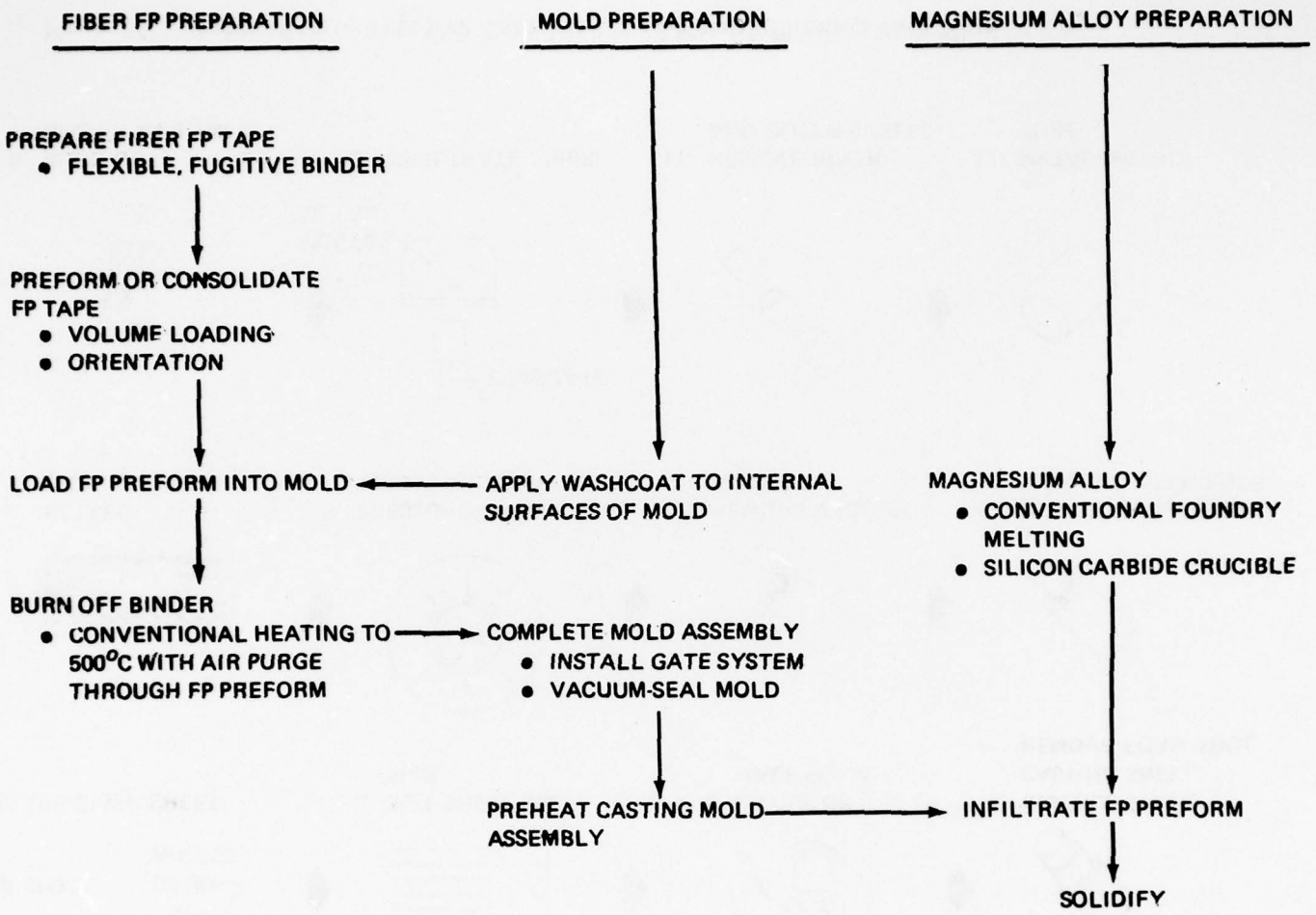

Figure 23. Flow Chart for FP/Magnesium Castings.

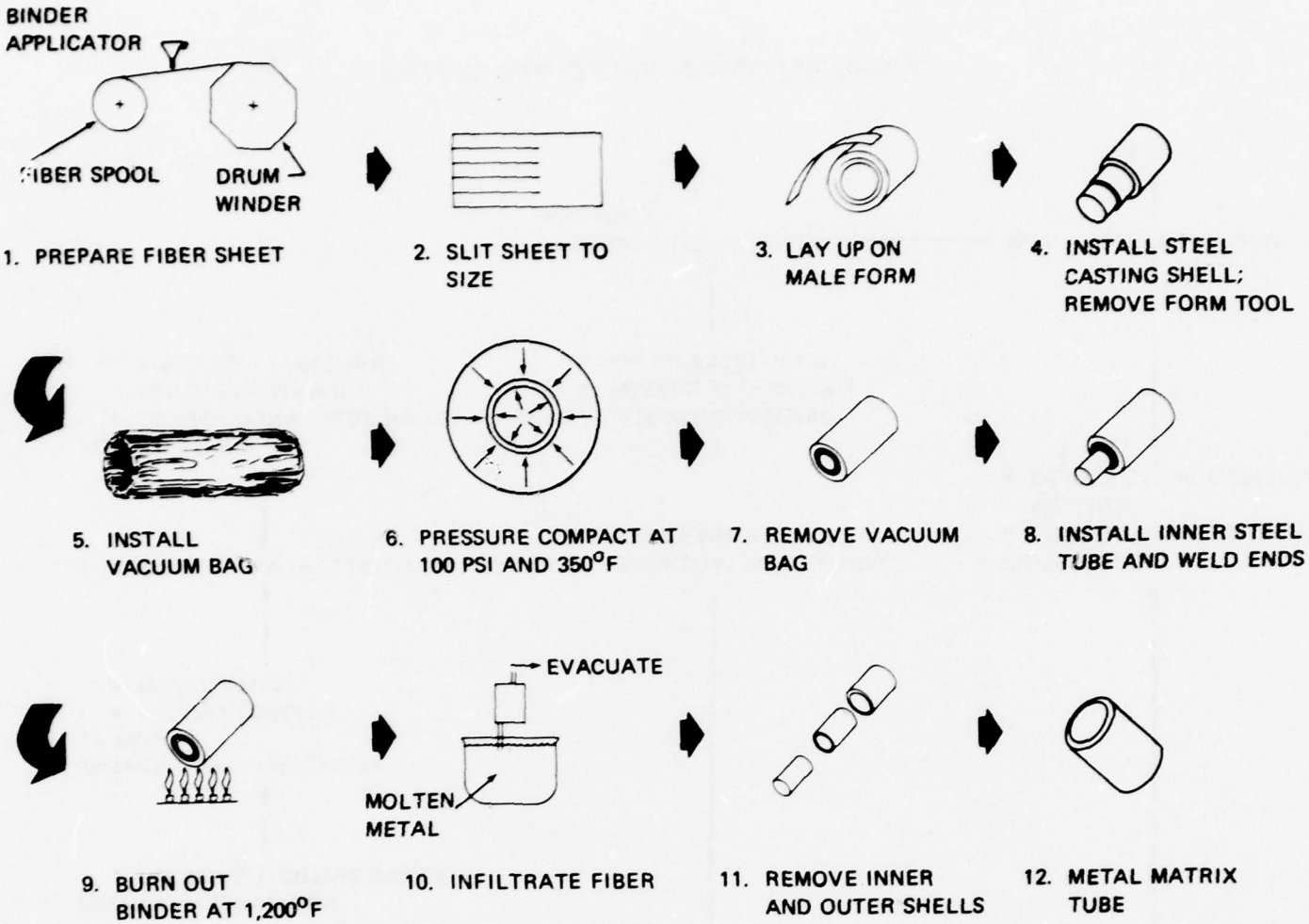

Figure 24. Fabrication of Thin-Wall Tube Via Liquid-Metal Infiltration With Metal Molds.

methods for infiltrating the metal into the FP fiber preform assembly, the best castings in terms of soundness and mechanical properties have been obtained by preevacuating and preheating the mold assembly prior to introducing the molten metal.

PREFORM PREPARATION

Prior to casting the test specimens, a series of steps must be taken in order to prepare a preform of the test specimen which contains the fibers with predetermined orientation. Simple flat sheets or plates are made by cutting, laying up, and hot-press compacting the fibers into preform material in a manner analogous to conventional epoxy laminates. Complex-shape fiber laminates or preforms are fabricated by the techniques shown in Figure 24, steps 1 through 7.

The process used in this program to prepare the preforms for casting involves the modification of the FP fiber sheet material made in step 1 by the addition of a volatile, ash-free organic material to improve the flexibility and adhesive tack of the fiber sheet. These sheets can be cut into tape and various ply patterns can be developed and preshaped to fit the test specimen shape and then tacked in place using moderate heat and pressure, in a manner again similar to that used for the fabrication of organic resin components (step 3). For simple shapes such as a cylinder, the completed preform is then installed into the outer shell of the casting mold, as shown in step 4. A vacuum bleeder bag is then installed and the preform is compacted and adhesively tacked together, as shown in steps 5 and 6. After the completion of step 6, the preform may be stored or moved directly to the casting area. At the casting area, the preform is inserted into the casting mold (step 8) where the binder is burned out (step 9) and the casting operation is conducted (step 10). After casting and cooling, the mold is removed and the test specimen is complete except for the removal of excess material.

Some of the key steps in the preparation of the FP fiber preforms for a cylindrical shape are shown in the following photographs. The step numbers refer to Figure 24.

- Step 2 – Sheet material is slit to size (Figure 25).
- Step 3 – Preform pattern is developed and a binder added to improve sheet flexibility and tack.
- Step 4 – The preform is installed into the casting mold (outer shell only) prior to pressure compaction (100 psi) at elevated temperatures (350°F) (Figure 26).
- Step 7 – The vacuum bag is removed and the preform is complete and ready for casting. The completed stable outer cylinder preform is shown in Figure 27.

The most complex preform developed in the program was the preform for the outer rim/web/inner rim cross section composite (SK27377). The final preform which was used to cast this specimen was composed of six individual preforms. Figure 28 shows the various steps required to prepare the preform. Shown in this figure are the preform dies which are used to lay up the fiber into desired shapes, the individual preforms, and the casting mold into which the preforms are inserted to form the final shape of the test specimen. Figure 29 shows a polished cross section at the flange/web joint of a final cast specimen.

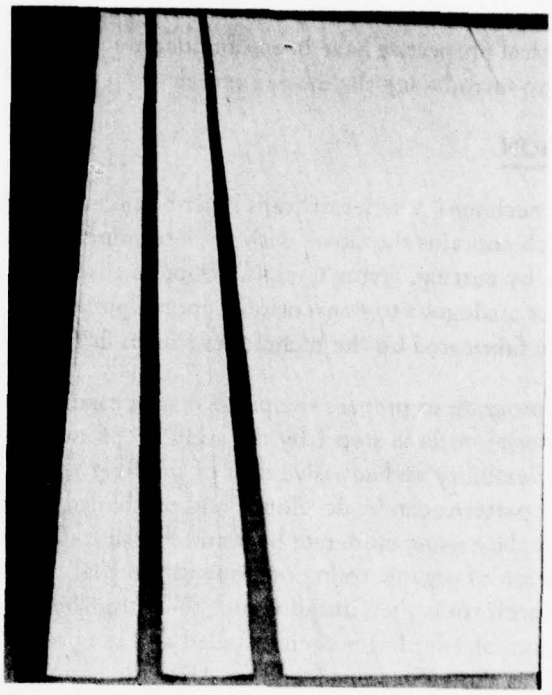

Figure 25. Sheet Material of Fiber FP Slit to Size.

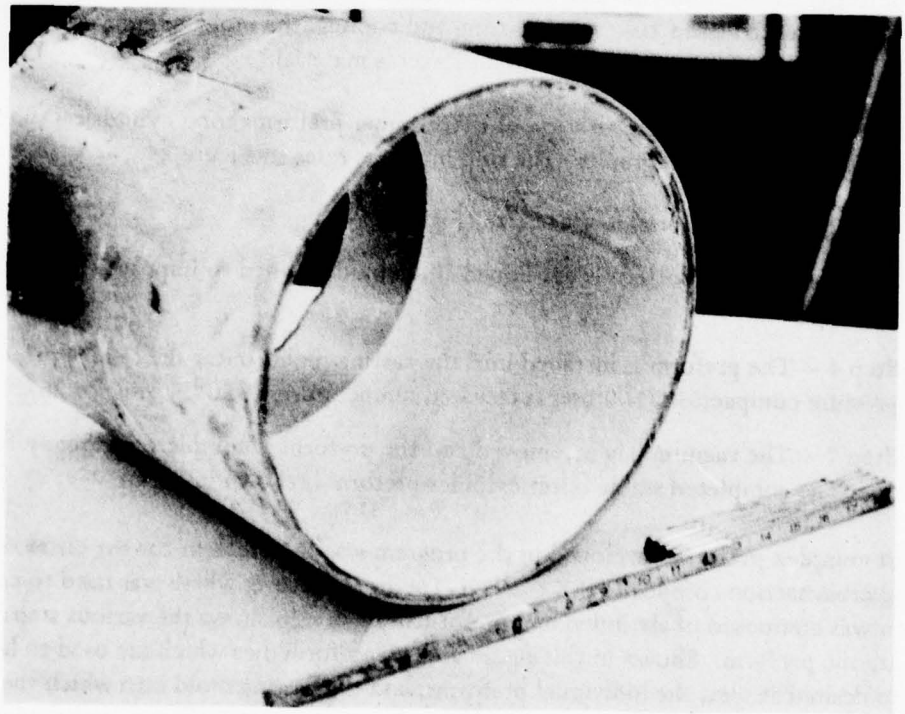

Figure 26. Preform Installed Into Casting Mold.

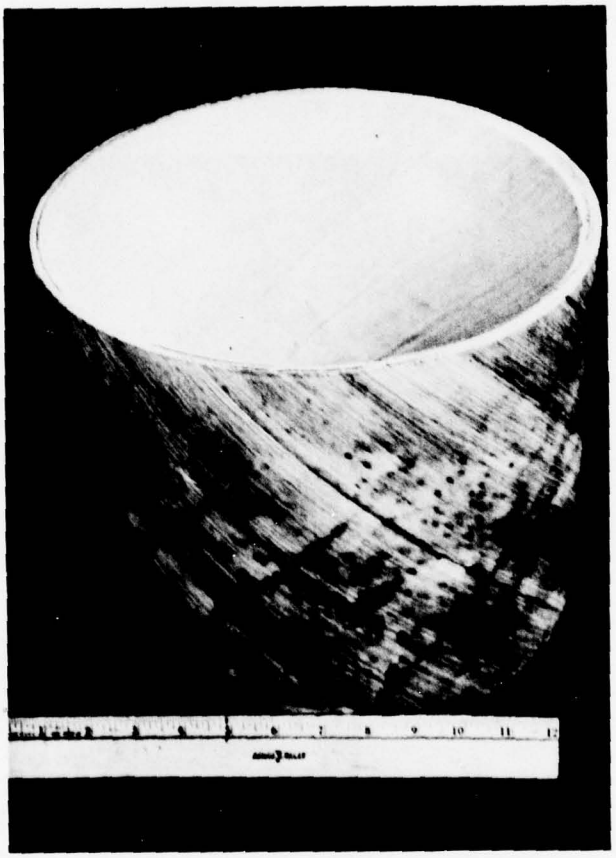

Figure 27. Fiber FP/Rhoplex Binder Preform for Outer Shell Composite Component.

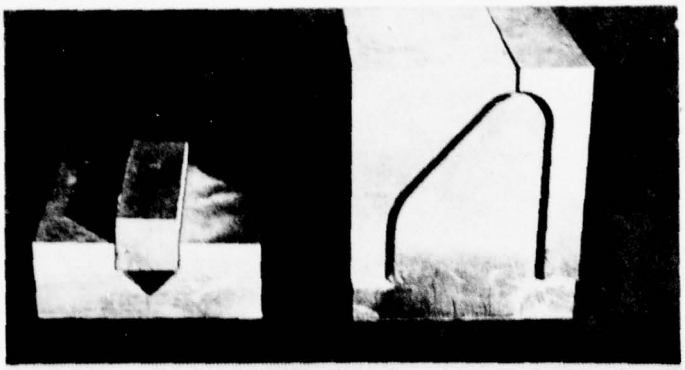

PREFORM DIES

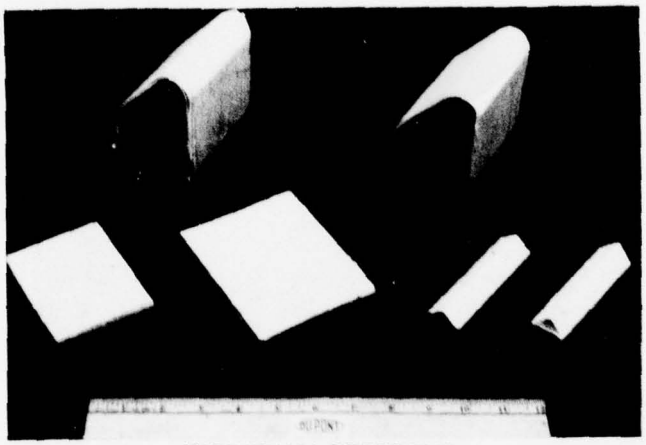

INDIVIDUAL PREFORMS

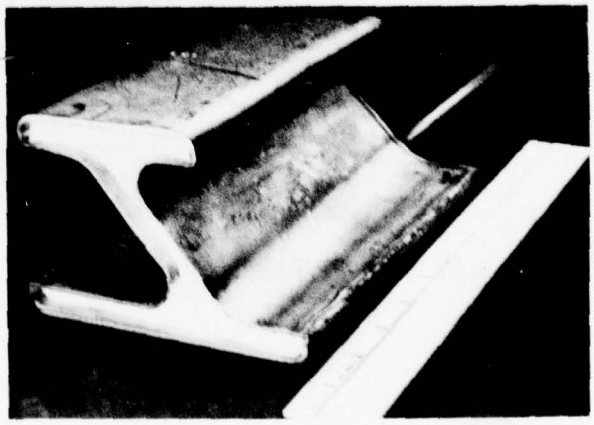

CASTING MOLD

Figure 28. Preform for Outer Rim/Web/Inner Rim Specimen.

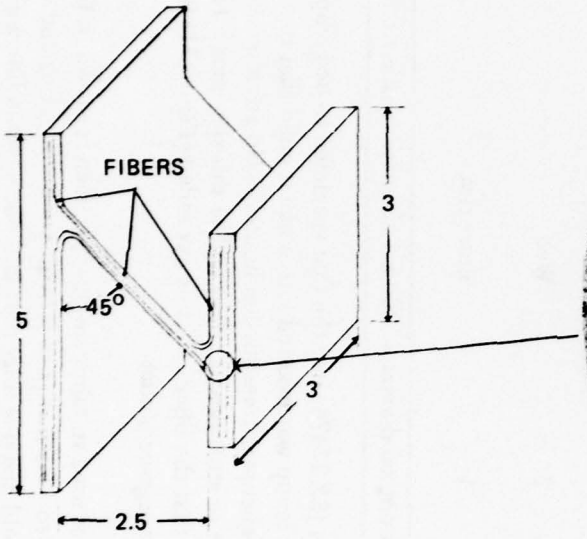

FIBER FP PLY LAYUP

FLANGES: EIGHTEEN PLIES $\pm 60^{\circ}(6)/0^{\circ}(6)/\pm 60^{\circ}(6)$
WEB: NINE PLIES $0^{\circ}(1)/\pm 60^{\circ}(2)/0^{\circ}(3)/\pm 60^{\circ}(2)/0^{\circ}(1)$

MAGNIFICATION
20X

NOTE: ALL DIMENSIONS IN INCHES

Figure 29. Polished Cross Section at Flange/Web Joint of Specimen SK27377.

TEST SPECIMEN FABRICATION – METAL INFILTRATION

The test specimens fabricated for this program have been identified as SK27376, outer rim cross section; SK27377, outer rim/web/inner rim cross section; and SK27378, outer rim, web, and inner rim components. Table 3 provides a summary of the components and materials used to fabricate the test specimens. The test specimens and their relationship to the end item case are shown in Figure 30.

TABLE 3. PROGRAM TEST SPECIMENS

Drawing Number	Number of Specimens	Description	Material
SK27376-1	1	Outer rim cross section	Magnesium alloy plus FP fibers*
SK27376-2	1	Outer rim cross section	AZ91C magnesium alloy, T6 heat treatment
SK27377-2	2	Outer rim/web/ inner rim cross section composite	Magnesium alloy plus FP fibers*
SK27378-4	1	Outer rim	Magnesium alloy plus FP fibers*
SK27378-5	2	Web	Magnesium alloy plus FP fibers*
SK27378-6	1	Inner rim	Magnesium alloy plus FP fibers*

*FP fiber – 20-micron nominal diameter, 200 ksi ultimate tensile strength minimum

The outer rim cross section (SK27376) was the first specimen to be completed. A flat preform of the $\pm 60^{o}/0^{o}/\pm 60^{o}$ fiber layup was inserted into a metal mold that represented the outer rim cross section of a typical helicopter transmission housing. No attempt was made to add additional fibers in the flange or stud area at either end of this specimen. The first test specimen to be fabricated indicated that the fiber's volume expanded (Figure 31) in the end areas during the burnout of the fugitive organic binder.

The casting mold which was used to fabricate this specimen is shown in Figure 32. The length of the mold was increased to 11.5 inches to provide room for gating and a material reservoir (riser) for cooling. The mold had one inlet port and one vacuum line with a compression fitting on either end of the specimen. This procedure had been previously used to fabricate standard flat-plate specimens. A schematic diagram of the molten-metal infiltration process used to fabricate all test specimens is shown in Figure 33.

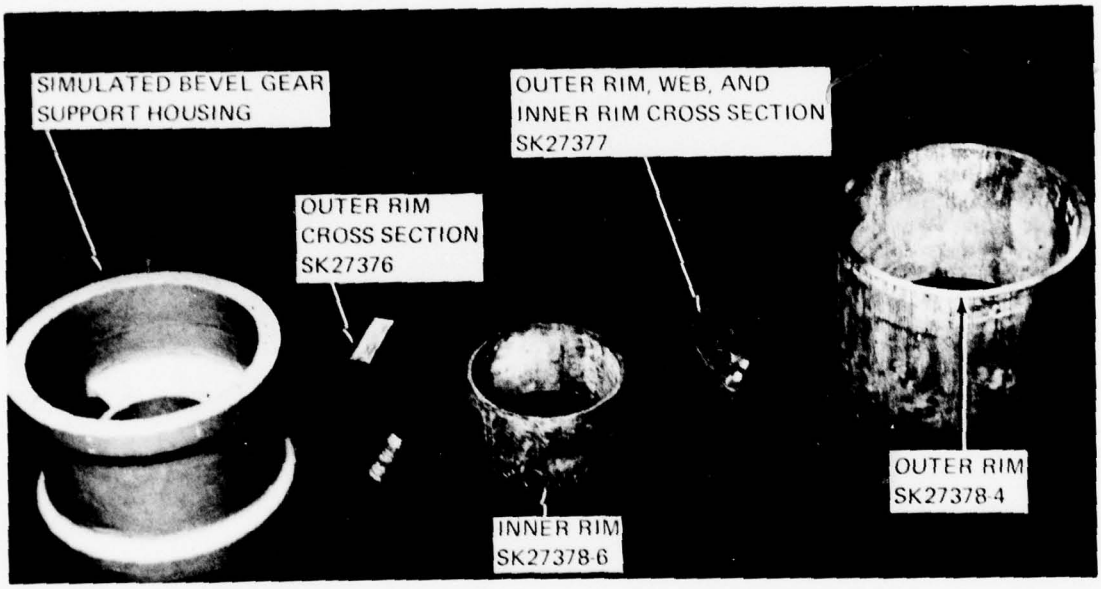

Figure 30. Fiber FP/Magnesium Component Test Specimens and Case Assembly.

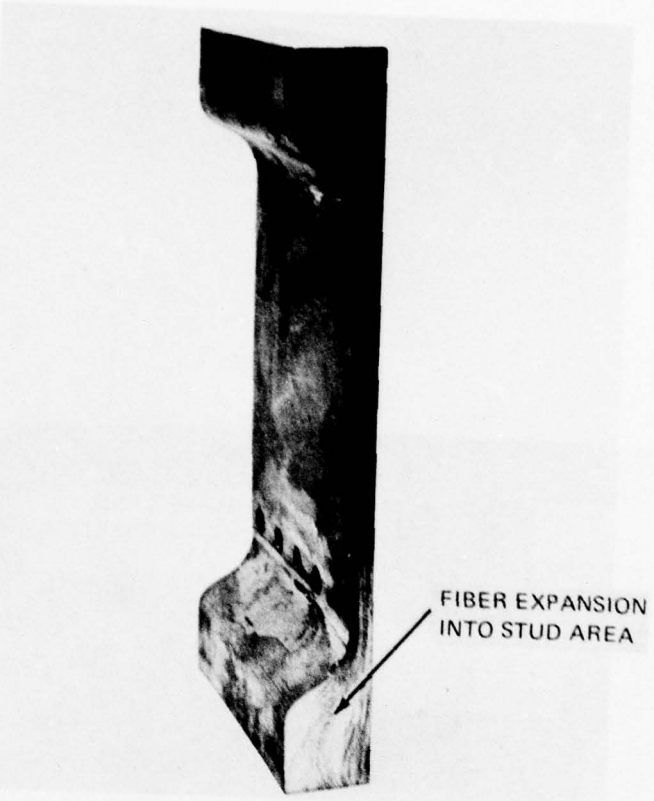

Figure 31. Fiber FP/Magnesium Outer-Rim Cross-Section Specimen.

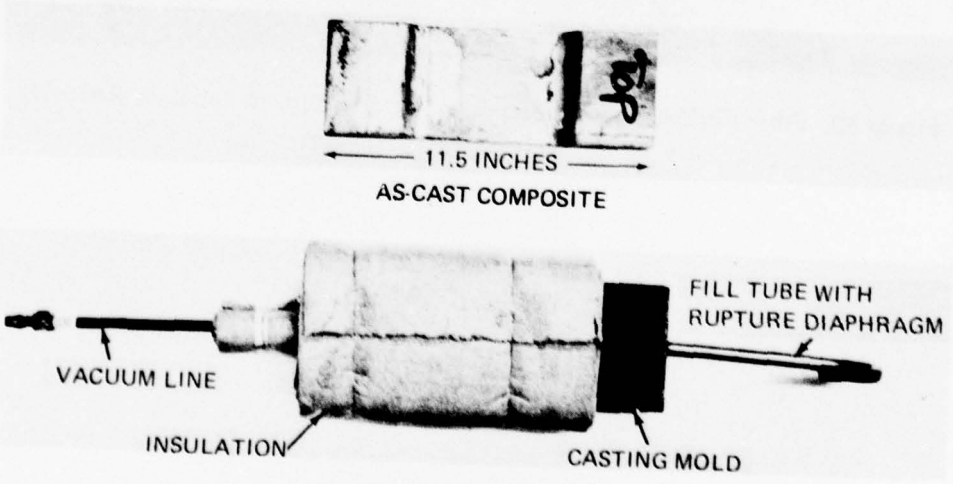

Figure 32. Mold Design and Insulation Technique for Preparation of Outer-Rim Cross-Section Specimen and Composite as Cast.

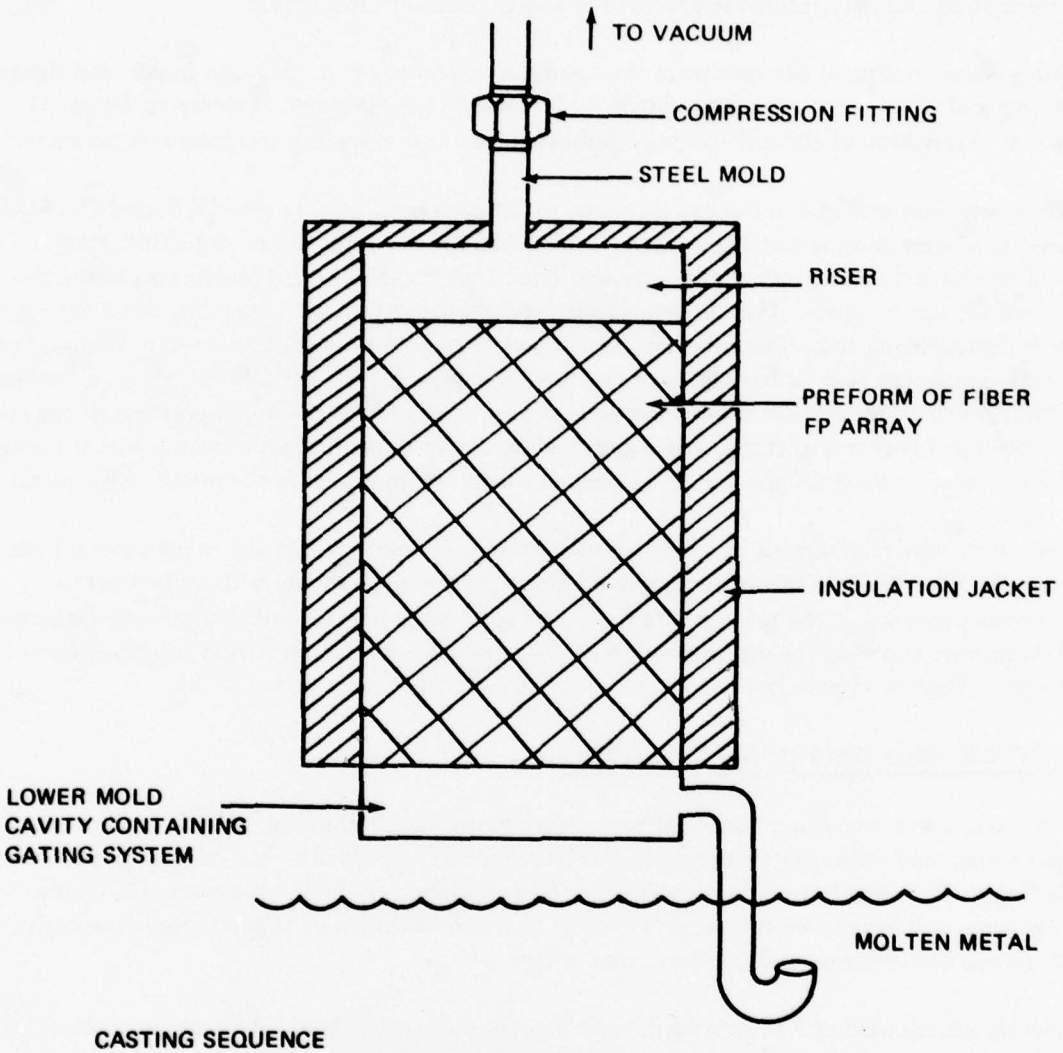

CASTING SEQUENCE

- PREHEATING OF MOLD (STEP 9, FIGURE 24)
- CASTING/INFILTRATION OF MOLTEN METAL (STEP 10, FIGURE 24)
- PROGRESSIVE SOLIDIFICATION

Figure 33. Fabrication of Fiber-Reinforced Metal Castings Via Molten-Metal Infiltration Technique.

It should be noted that the casting mold should be properly designed with an adequate gating system and riser in order to prevent fiber damage or distortion during casting. Results of the testing and visual examination of the first test specimen after test revealed that the gating procedure used to fabricate the outer rim cross section (SK27376) may have resulted in distortion of the fiber in the center portion of the specimen during the metal infiltration process. Further information and description are provided in a later section of this report.

After water cooling of the specimen, the casting was removed from the steel mold and the ends (gating and risers) were cut off to obtain an 8-inch-long test specimen as shown in Figure 31. Visual observation of the test specimen indicated that a good quality test item was obtained.

The operations involved in the molten-metal infiltration are shown as steps 8, 9, and 10 in the process schematic shown in Figure 24. As described for the outer rim cross section, similar tooling and infiltration techniques were used for the fabrication of all the test specimens required for this program. Two different filling techniques were used, depending upon the type of specimen being cast. The two methods used were remote filling and immersion filling. For simple specimens such as flat plates or the outer rim cross section (SK27376), either technique can be used. In the remote filling technique shown in Figure 33, the upper portions of the mold are insulated with a refractory fiber blanket which serves to maintain the casting area at molten-metal temperature while the gate and inlet tube areas are immersed in the molten filler metal.

The alternative technique is to simply immerse the entire mold within the molten-metal bath after the fiber binder burnout is complete. The remote filling technique described in the previous paragraph is the most practical method for casting larger, more complex configurations. This process was used for the fabrication of the large 12-inch-diameter outer case shell component. Figures 34 and 35 show the molds of two test specimens after casting.

CUTTING AND MACHINING TECHNIQUES

Although a near-net-shape casting process is envisioned for production operations, some cutting, machining, and drilling operations will still be required to produce a final finished part. Gasket sealing surfaces and bearing bores will need to be machined to final dimensions. Gates and riser areas will have to be cut away. Holes will have to be drilled and tapped for oil passages, jet nozzle installations, and accessory mounting.

The aluminum oxide FP fiber is hard, has a high modulus, and should show abrasive characteristics and resulting high tool wear. For this reason it was expected that diamond-edge tools would be required, along with cutting and machining methods previously developed for boron-fiber-reinforced components.

Diamond-coated circular saws were used to cut off heavy or thick gate and riser areas because they were available and known to give a good surface finish.

Figure 34. SK27377 Specimen Mold After Casting.

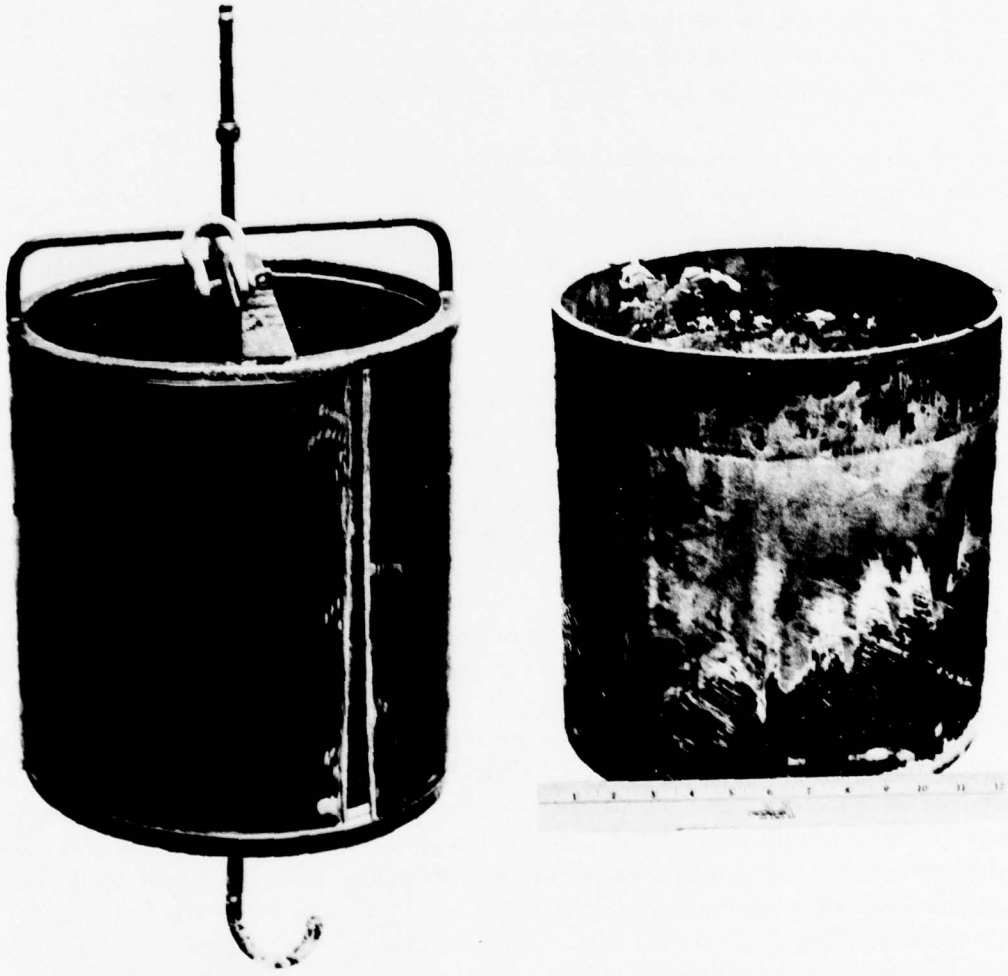

Figure 35. SK27378-4 Specimen Mold After Casting and as-Cast Specimen Removed From Mold.

Drilling was accomplished with carbide-tipped twist drills, with acceptable hole finish. Lathe turn machining was accomplished with carbide-tipped tools, with excellent results. A continuous chip was formed and the material appeared to machine similar to aluminum. The machined surface had a bright, smooth, metallic finish with no visual evidence of fiber fracture or tear-out.

SECONDARY JOINING OF CASE SECTION COMPONENTS

Due to the complexity of casting the simulated bevel gear support structure as a one-piece unit reinforced with Fiber FP, the program was directed toward the fabrication of several major components (outer rim, inner rim, and webs) and the use of secondary joining techniques to form a final assembly as shown in Figure 36. The fabrication of the individual components was successfully completed as stated previously. But before the final joining of the components, several tests were conducted to investigate various secondary joining methods. The results of these tests, which will be briefly discussed later, indicated that additional work would be required before an acceptable and adequate joining procedure could be developed. Therefore the four components which made up the final housing assembly were not joined at this time.

Limited exploratory efforts were made within the cost constraints of this program to determine the feasibility of joining the transmission case components by state-of-the-art welding techniques. Due to fiber discontinuity across such joints, their use as a primary load path was thus precluded. However, the use of welding for attachment of equipment brackets, metallic tubular oil lines or passages, and the repair of porosity or voids in nonstructural areas was a valid reason for pursuing this limited evaluation.

Initial attempts used electron-beam and laser welding equipment to determine the effect of high-energy impingement on aluminum oxide Fiber FP-reinforced magnesium specimens. Penetration of the material was easily achieved, as shown in Figure 37. However, characteristic molten-metal flow and refilling of the area behind the heat zone did not occur as is the case with conventional metal alloys. One theory for this difference in behavior is that the aluminum oxide fiber vaporizes and mechanically blows the molten magnesium out of the weld zone.

These results indicated that structural welds in which melting and fusion of the material to be joined created a deep penetration weld were not practical with the equipment available.

As a result, further efforts were directed at brazing or fillet weld joining with lower-energy heat sources. Initial trials of an aluminum-zinc soldering technique with a conventional oxygen-acetylene torch indicated that the material was amenable to such an approach. T-joints were formed by mechanically scrubbing the solder on the surfaces to be joined at low heat. This technique caused a wetting of the plate surface by the solder and was followed by the buildup of sizable fillets of the solder material. When the specimens were broken by bending, cast magnesium and fiber were torn out of the plate over much of the soldered area. Further work with surface cleaning and fluxing techniques could result in a usable soldering method.

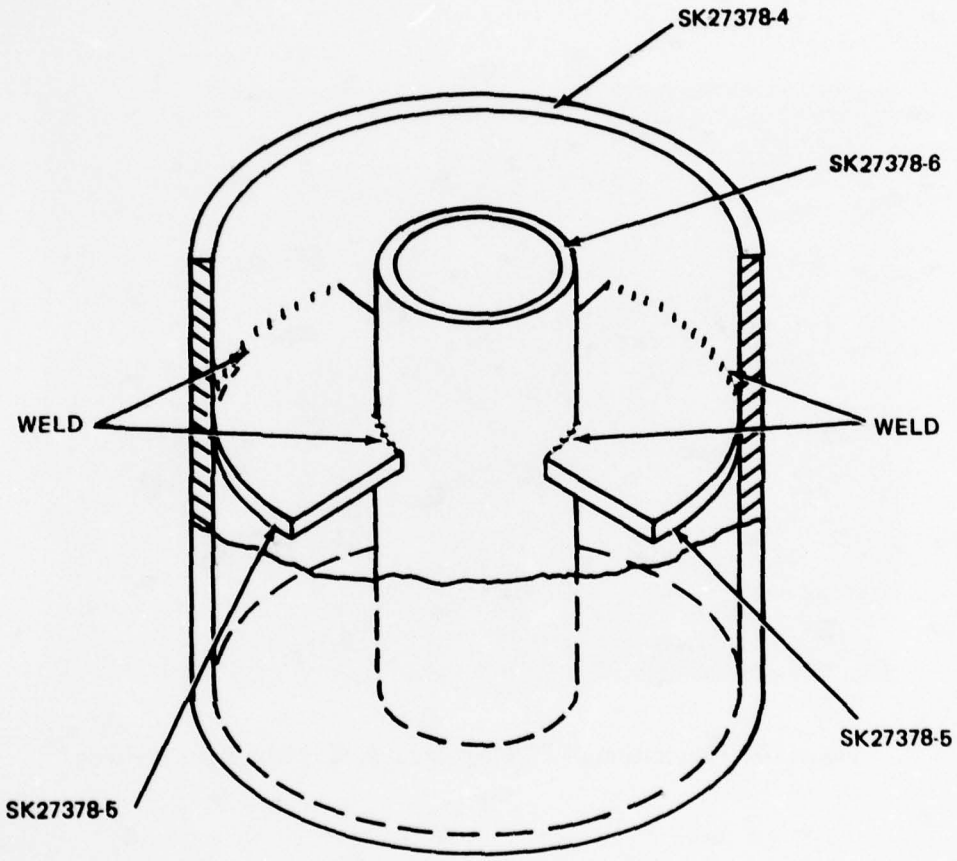

Figure 36. Final Assembly of Outer Rim, Web, and Inner Rim Composite Components.

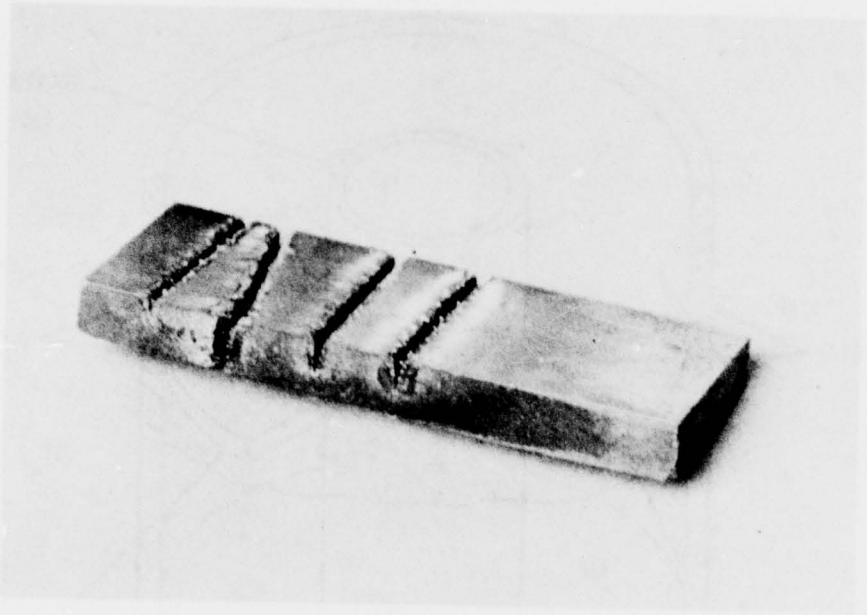

Figure 37. Penetration of FP/Magnesium by Electron-Beam Welding.

Another approach tried was the use of magnesium wire and an inert-gas-shielded arc torch. This technique also produced a suitable fillet joint.

However, none of the techniques described produced any metallurgical joining of the specimens in areas where the fiber ends were exposed, as shown in Figure 38.

To achieve a better metallurgical joint, a plasma-arc metal-spray technique was used to coat the fiber-filled magnesium specimen. It was expected that the deposited aluminum would protect the exposed fiber ends and aid in achieving wetting across the joint surface during the initial torch brazing operation. Figure 39 shows the results of this approach. Partial success was obtained, as can be seen in the photograph, with good adhesion of the flame-sprayed metal to the machined specimen edge and partial fusion of the two flame-sprayed surfaces.

The results of these preliminary tests indicate that welding techniques are feasible and further development should be pursued in order to demonstrate practical secondary structural joining and repair techniques.

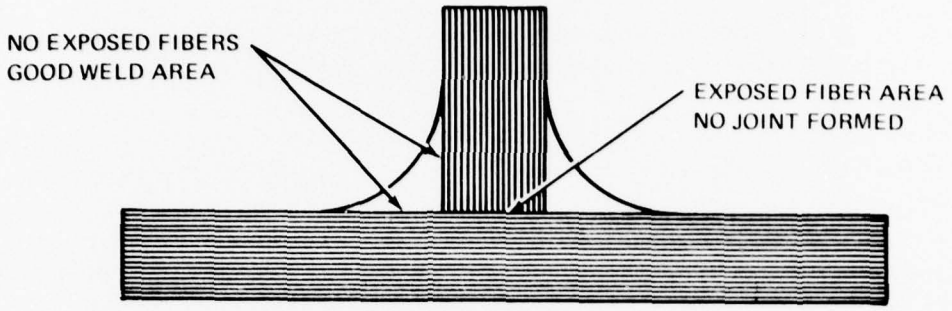

Figure 38. Configuration of Weld Test Specimen.

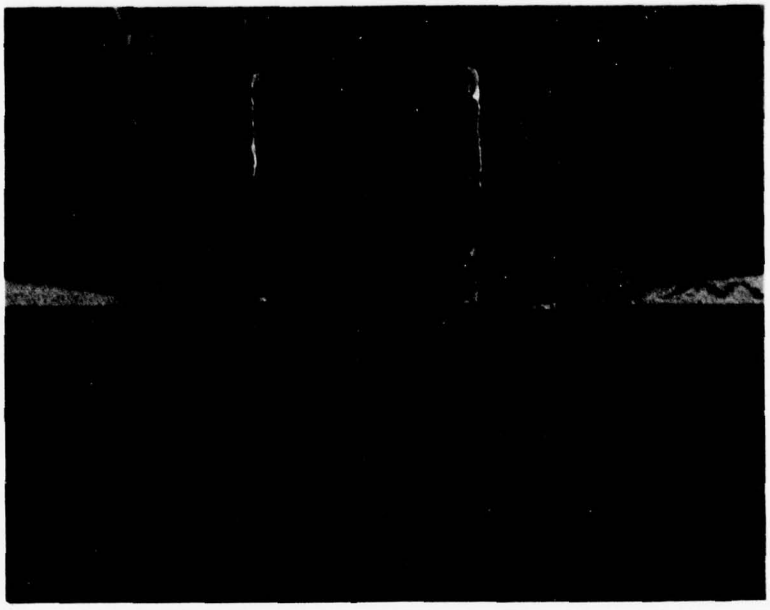

Figure 39. Photograph of Test Weld.

EXPERIMENTAL PROGRAM

A series of five tests was conducted to evaluate the material properties of the FP/magnesium metal matrix and to provide test data to compare with analytical data. Table 4 provides a summary of the tests conducted. All testing was conducted on either a 60-kip or 120-kip universal test machine located in the Boeing Vertol engineering test laboratory.

The first test conducted was that of the SK27376 outer-rim cross-section test specimen. The specimen was mounted in specially designed grips with a filler material to insure uniform contact across the grip area, as shown in Figure 40. These special grips were required because of the thickened ends of the test specimen. This additional material was cast into the specimen to simulate the area of a transmission housing where studs would be installed. Fabrication of the test specimen did prove that the fibers could be dispersed in this area to provide a good material structure for the insertion of studs, but the shape created problems in providing a good grip on the test specimen without causing a moment load.

The specimen was strain-gaged on both sides of the flat section in the center; it was then mounted into the 120-kip universal test machine for tension loading, as shown in Figure 41. Two X-Y plotters were set up to record strain versus load and extension versus load. An extensiometer was mounted along the edge of the test specimen.

Two tests were conducted using this setup. The first test was run with an SK27376-1 test specimen which contained FP fibers in a magnesium matrix. The second test used a similar specimen (SK27376-2) except that it was fabricated from standard AZ91C magnesium alloy with a T6 heat treatment. The standard magnesium specimen represented a baseline for evaluating the FP-reinforced specimens. The results of these first two tests are shown in Table 5. Both specimens failed through a set of five 1/4-inch-diameter holes which were drilled into the specimen for the test grips, as shown in Figures 42 and 43. Because of the holes in the specimen, ultimate failure strains were not obtained for either material. Review of the test data indicates that an elastic modulus of 6.3×10^6 was obtained for the AZ91C-T6 material and an elastic modulus of 20.7×10^6 was obtained for the FP-reinforced magnesium specimen. This represents an increase in modulus of more than three times.

Visual examination of the fracture surface of the fiber-reinforced test specimen indicated a noticeable difference in material appearance from the center of the specimen to either side, as shown in Figure 42. At approximately one-third of the distance in from each side the material showed a distinct layer buildup of the $\pm 60^\circ/0^\circ/60^\circ$ fibers. In the center third of the specimen the layers were not obvious. The specimen was returned to the Du Pont Pioneering and Textile Research Center in Wilmington, Delaware, for a more detailed examination of the material. The results of this examination indicated that the fibers in the center section of this test specimen were disorganized and many of them were broken, as shown in Figure 44. The fibers at the outer third of the specimen appeared normal and were properly aligned. Additional cuts made on this specimen indicated that the fibers in the center were damaged for most of the length of the specimen.

TABLE 4. SUMMARY OF TESTS CONDUCTED

Test No.	Test Specimen Part No. and Size	Material Description	Test Rig	Number of Specimens Tested	Comments
1	SK27376-1 (4 x 0.25 x 8 in.) Outer Rim Cross Section	±60°/0°/±60° 55% volume FP fibers in a magnesium alloy	120-kip universal test machine	1	Figures 40 and 41 show test setup.
2	SK27376-2 (4 x 0.25 x 8 in.) Outer Rim Cross Section	AZ91C magnesium alloy – T6 heat treatment	120-kip universal test machine	1	Figures 40 and 41 show test setup.
3	Du Pont Part No. 7674-4-1 (1 x 0.265 x 8.0 in.) Flat Wall Specimen	±60°/0°/±60° 55% volume FP fibers in a magnesium alloy	60-kip universal test machine	2	
4	SK27377-2 (3 x 3 x 5 in.) Outer Rim/Web/Inner Rim Cross Section	±60°/0°/±60° 45% volume FP fibers in a magnesium alloy	120-kip universal test machine and test fixture ST-31041	2	Tested to a maximum load of 5,000 lb thrust and 5,000 in.-lb moment. Figures 46 and 50 show test setup.
5	SK27377-2 (3 x 3 x 5 in.) Outer Rim/Web/Inner Rim Cross Section	±60°/0°/±60° 45% volume FP fibers in a magnesium alloy	60-kip universal test machine and test fixture ST-31041	1	Tested to ultimate failure. Figures 51 and 52 show test setup.

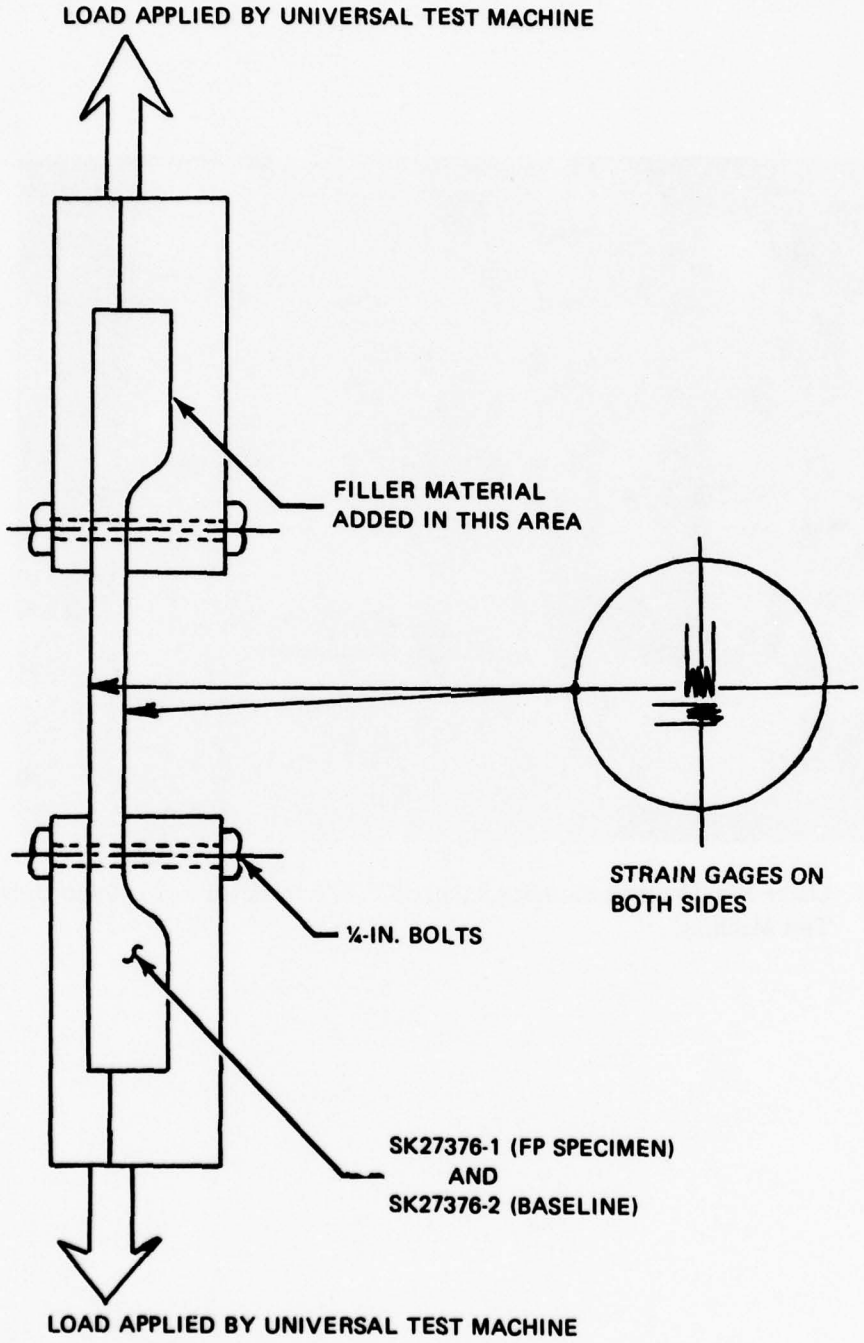

Figure 40. Test Setup for Outer Rim Cross Section.

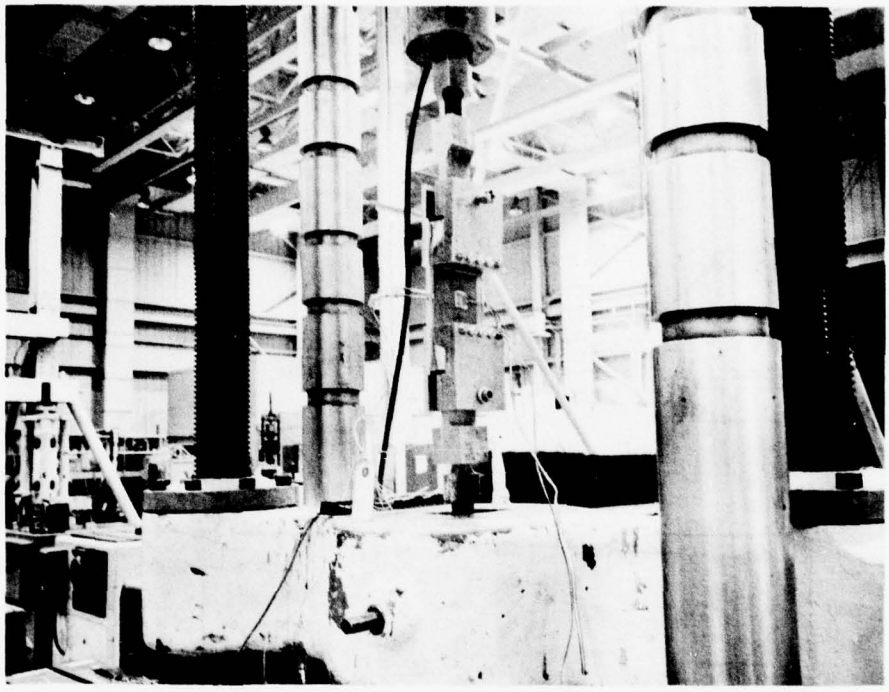

Figure 41. Outer-Rim Cross-Section Specimen SK27376 Installed in a 120-kip Universal Test Machine.

TABLE 5. SUMMARY OF TESTING OF FP/MAGNESIUM SIMULATED OUTER RIM CROSS SECTION (SK27376)

Specimen Identification	Spec No.	Load, Tension (lb)	Strain (μ in./in.)			
			No. 1 Long.	No. 1 Transv	No. 2 Long.	No. 2 Transv
SK27376-1	3	0	0	0	0	0
FP Fibers						
Area = 0.278		2,000	56	−9	101	−20
x 4.01 = 1.1115 in.^{2}						
Fiber Orientation		4,000	121	−20	217	−43
= ± 60°/0°/± 60°		8,000	263	−31	427	−87
		10,400 Failure through bottom row of 1/4-in.-dia boltholes				
SK27376-2	3A	0	0	0	0	0
All Magnesium		2,000	116	−78	428	−68
(AZ91-T6)		4,000	276	−144	789	−139
Area =		6,000	507	−220	1,124	−221
0.3 x 4.0 =		8,000	792	−329	1,503	−366
1.2 in.^{2}		10,000	1,184	−507	2,022	−589
		12,000	1,658	−754	2,600	−819
(Baseline		14,000	2,195	−1,000	3,244	−1,063
specimen)		16,000	2,752	−1,278	3,865	−1,354
		17,500 Ultimate load, failure through ¼-in.-dia boltholes				

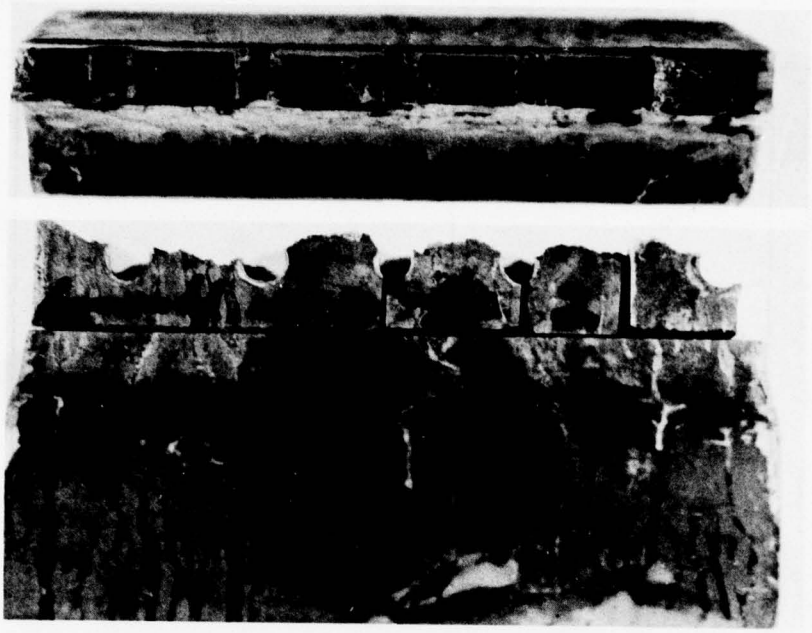

Figure 42. Specimen SK27376-1 After Test.

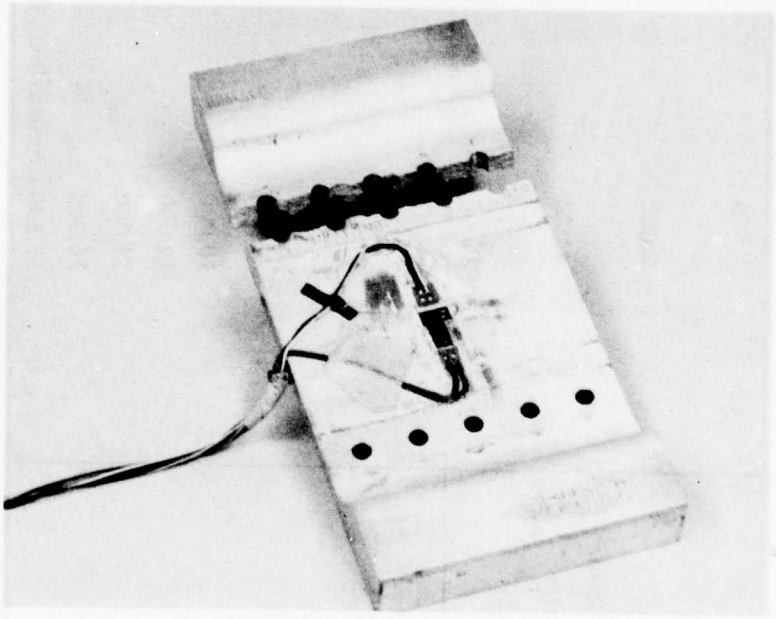

Figure 43. Outer-Rim Cross-Section Baseline Specimen SK27376-2 After Test.

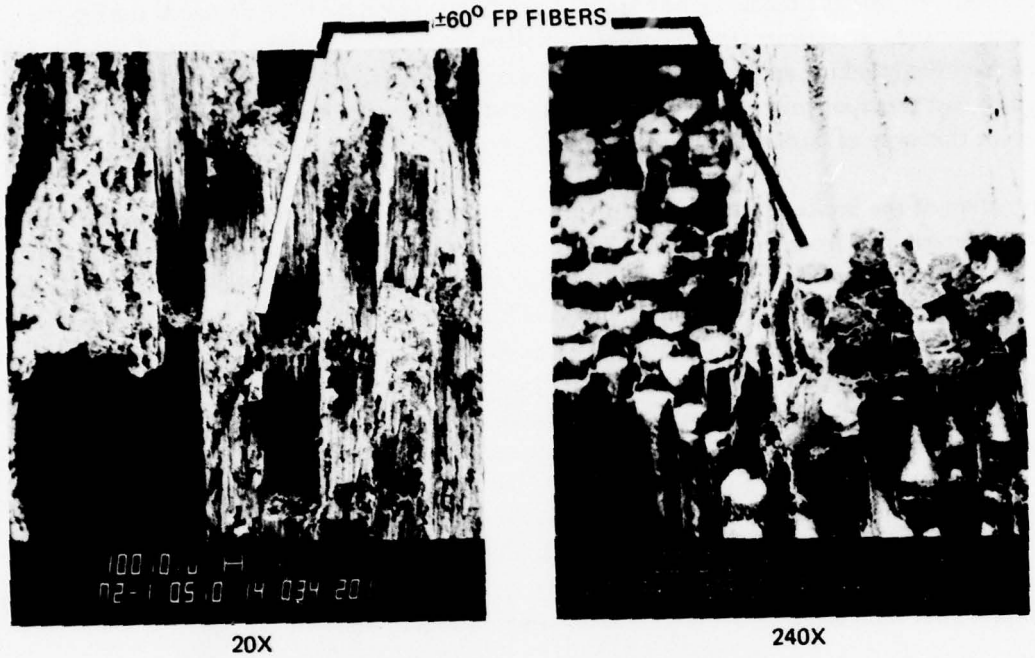

VIEWS SHOWING NORMAL FIBER ORIENTATION
(±60°) AT THE ENDS OF THE TEST SPECIMEN

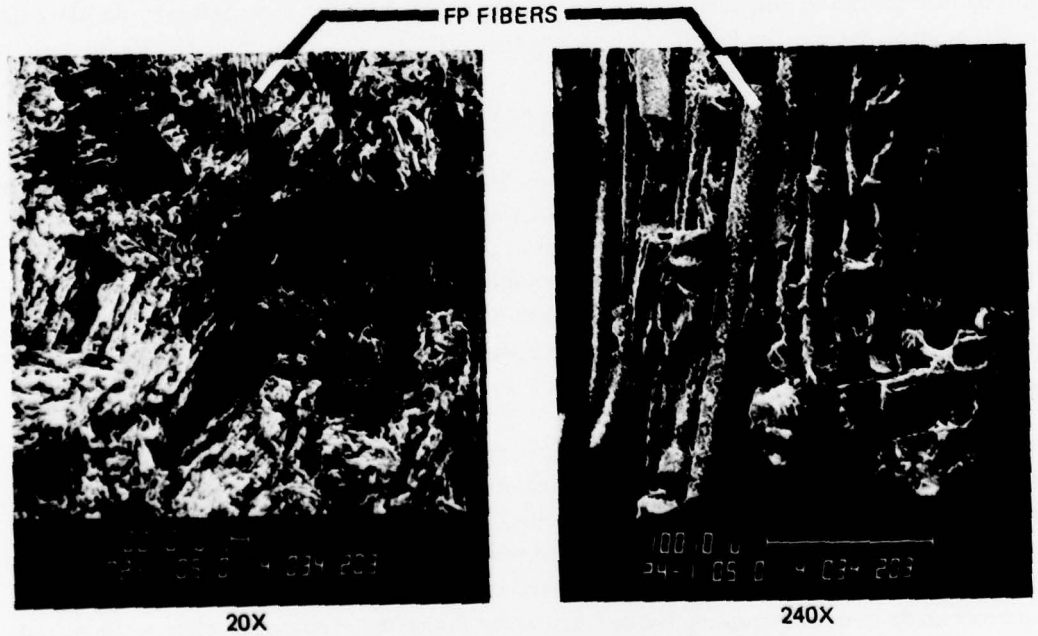

VIEWS SHOWING DISORGANIZED FIBER ORIENTATION
AT THE CENTER OF THE TEST SPECIMEN

Figure 44. Scanning-Electron Micrographs of the Fracture Surface of Specimen SK27376-1.

The results of this examination indicate that the fibers may have been damaged during the casting process. It appears that the flow of molten magnesium into the center of the specimen produced the breaking and disorganizing of the center fibers. It also appears that the gating used to cast this specimen was not adequate to reduce the velocity of the molten magnesium to prevent this type of damage. The outer fibers were not affected by this condition.

The effect of the broken fibers on the material properties of the outer rim test specimen could not be determined from the test data. Therefore, two additional flat specimens were fabricated with a fiber orientation of $\pm 60^{o}/0^{o}/\pm 60^{o}$ and a thickness that represented the flat wall section of the SK27376 specimen. The specimens fabricated were 1 by 0.26 by 8 inches and did not have any holes or other unusual features. The coupons were mounted in standard friction grips in a 60-kip universal test machine for tensile loading. A dial indicator was used to measure the crosshead travel and strain data was recorded incrementally during the loading sequence. A total of two specimens were tested under this condition.

The results of these tests are summarized in Table 6. The mechanical properties determined by test correlated very closely with the predicted values. An elastic modulus of 18.3×10^{6} psi was achieved on these specimens, which is approximately three times that of standard magnesium alloy. The test coupon after test is shown in Figure 45.

The final series of tests conducted involved the use of the outer rim/web/inner rim test specimen. Two tests were conducted, the first using two specimens in a back-to-back setup and the final test incorporating only a single specimen. Figure 46 shows the test setup to simulate the conditions expected for the bearing support of the spiral bevel gear of the CH-47C forward transmission. The load applied to the test specimens was equivalent to a thrust and moment overload produced by the bearing reacting to the gear loads, as shown in Figure 47.

A test fixture was fabricated as shown in Figure 48. The fixture was initially used to support two SK27377 specimens. The large endface of each specimen was mounted to the outboard sides of the fixture representing the outer wall of the housing and the two smaller endfaces of the specimen were clamped together to a simulated bearing supporting the spiral bevel gear. Each specimen was strain-gaged at critical areas and dial indicators were also used to record specimen deflections under load, as shown in Figure 46. A total of 12 strain gages and 6 dial indicators were installed on the specimens.

Initially, the test specimens (SK27377) were supplied in an as-cast condition. First attempts to place the specimens into the test fixture indicated that the uneven face surfaces would result in high induced stresses by clamping the specimen to the fixture. The specimens were removed and the endfaces of each specimen were machined parallel to fit into the test fixture. The specimens were reinstalled in the fixture and clamped. During this operation, extensive effort was made to avoid straining the specimens by shimming each clamp plate while clamping them to the fixture. Many attempts were made until a reasonable zero reading was obtained on all strain gages.

TABLE 6. TEST RESULTS OF SPECIMEN WITH FP FIBERS IN MAGNESIUM MATRIX

Specimen Identification	Tensile Load (lb)	Specimen 1 After Doubler Plates Rebonded					Specimen 2				
		Side A (μ in./in.)		Side B (μ in./in.)		Crosshead	Side A (μ in./in.)		Side B (μ in./in.)		Crosshead
		Long. ϵ	Transv ϵ	Long. ϵ	Transv ϵ	Defl (in.)	Long. ϵ	Transv ϵ	Long. ϵ	Transv ϵ	Defl (in.)
FP/Mg Specimen	0	0	0	0	0	–	0	0	0	0	–
1.0 x 0.265 x 8.0	500	34	−19	166	−27	0	202	−39	−9	−2	0
in. nominal	1,000	127	−47	280	−51	0.019	321	−65	91	−25	0.025
(Ident No. 7674-4-I)	1,500	231	−76	412	−79	0.035	438	−91	227	−54	0.040
	2,000	341	−108	548	−106	0.047	572	−124	360	−84	0.051
	2,500	456	−142	681	−136	0.057	712	−160	510	−112	0.063
	3,000	571	−179	814	−165	0.067	850	−200	651	−144	0.071
	3,200	629	−194	865	−179	0.070	916	−216	709	−156	0.074
	3,400	682	−212	921	−190	0.073	972	−233	770	−170	0.076
	3,600	739	−228	975	−202	0.077	1,034	−250	831	−181	0.079
	3,800	795	−245	1,024	−212	0.080	1,087	−268	887	−194	0.082
	4,000	851	−265	1,072	−224	0.083	1,151	−285	957	−206	0.084
	4,200	916	−284	1,130	−233	0.087	1,213	−303	1,018	−221	0.087
	4,400	988	−305	1,167	−246	0.089	1,274	−321	1,092	−232	0.089
	4,600	1,082	−334	1,197	−250	0.092	1,332	−339	1,145	−246	0.092
	4,800	1,170	−359	1,243	−261	0.094	1,391	−357	1,211	−259	0.094
	5,000	1,253	−386	1,300	−272	0.097	1,457	−374	1,273	−272	0.096
	5,200						1,517	−392	1,350	−286	0.099
	5,400	Ultimate failure at 5,100 pounds					1,522	−393	1,485	−321	0.102
	5,600						1,575	−404	1,566	−335	0.103
	5,800						1,640	−425	1,631	−353	0.106
	6,000						Ultimate failure at 6,000 pounds				

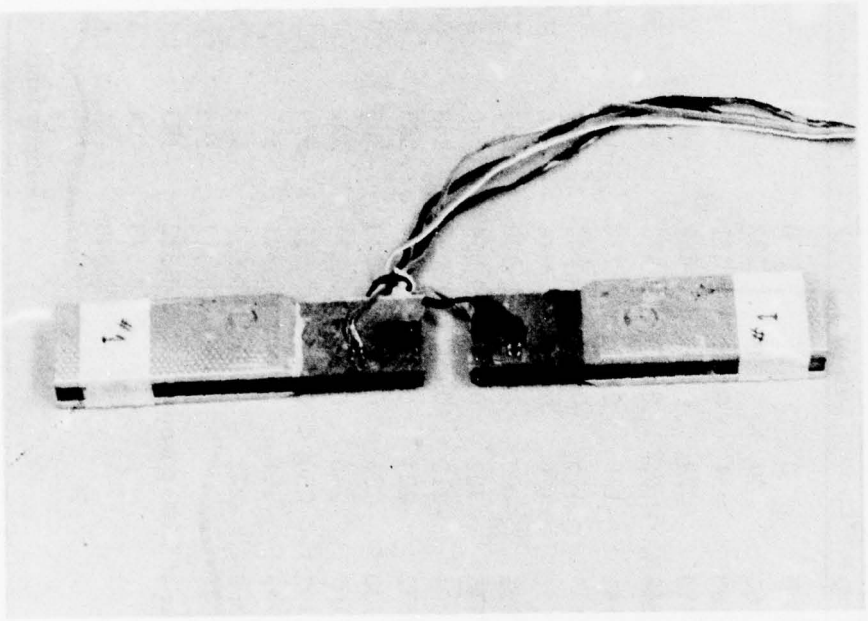

Figure 45. $\pm 60^{\circ}/0^{\circ}/\pm 60^{\circ}$ FP/Magnesium Coupon After Tension Test.

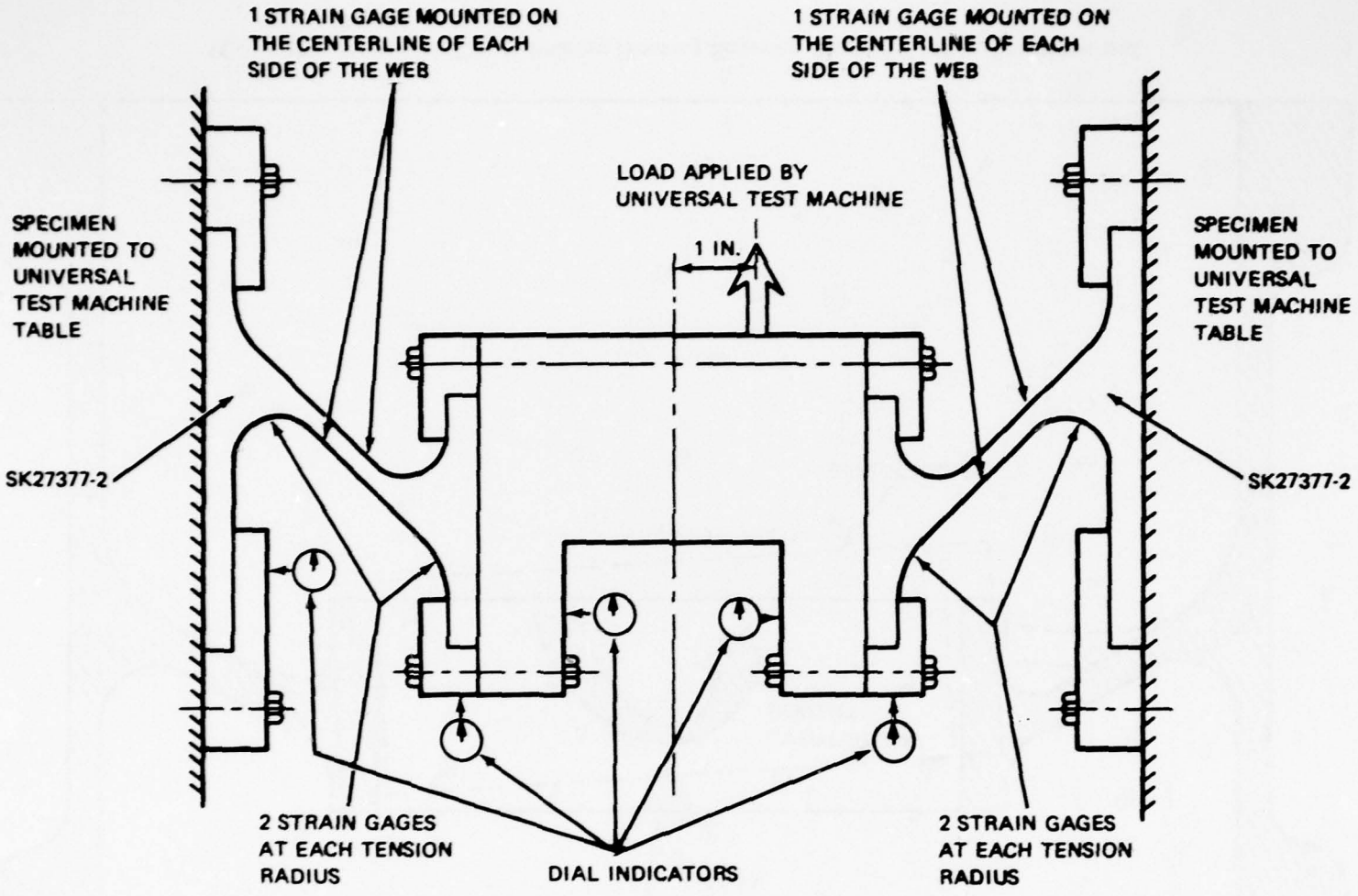

Figure 46. Simulated Test Setup of the Outer Rim, Inner Rim, and Web Component Assembly (SK27378) Using Two SK27377 Components.

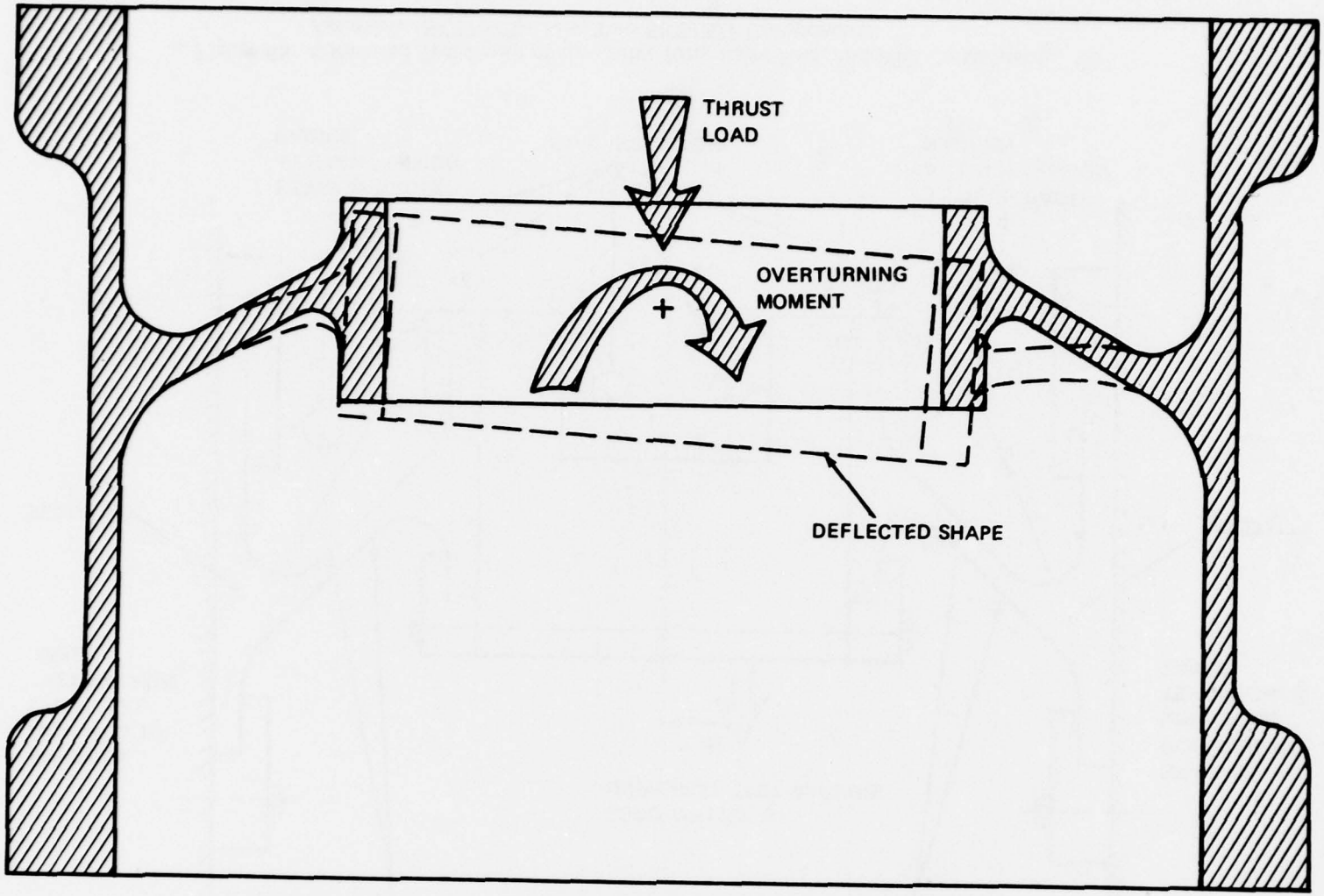

Figure 47. Sketch of Thrust Bearing Housing Showing Applied Bearing Reactions and Deflected Shape.

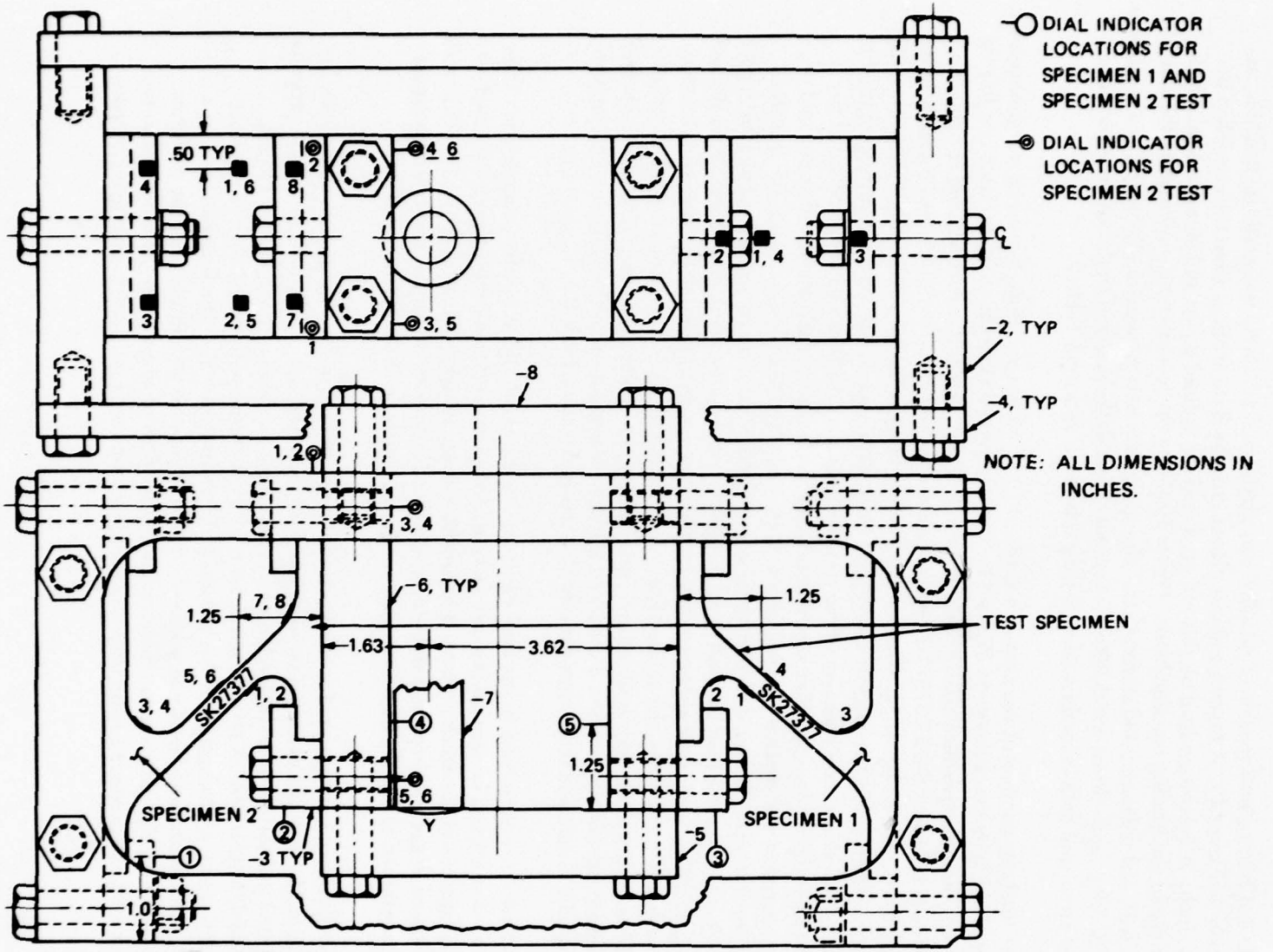

Figure 48. Static Test Fixture for Aluminum Oxide Composite Specimens.

The test fixture with specimens installed was placed into a 120-kip universal test machine, as shown in Figure 49. A loading rod was placed into the fixture offset from the centerline by one inch. A downward load on this rod produced the desired thrust and moment load which simulated the bearing reaction loads. Figure 50 shows the test assembly mounted in the test rig with dial indicators and strain gages. The specimens were incrementally loaded to a maximum of 5,000 pounds thrust and 5,000 in.-lb moment and deflection and strain data was recorded. The strain and deflection data taken during this test is shown in Table 7.

The final test conducted was that of a single SK27377-2 test specimen loaded by a combination shear and moment as shown in Figure 51. The specimen was mounted in the same test fixture except that one specimen was removed from the setup. This test was conducted to achieve an ultimate failure of the SK27377-2 test specimen. The test fixture with the single specimen installed is shown in Figure 52. The test load was to be increased in 100-pound increments until the specimen could not support the applied load. Strain gages and dial indicators were used to record the strain and deflection of the test specimen. As the load was being increased from 300 to 400 pounds, an audible report was heard and a visible crack was noted at one end of the specimen web section (strain gage no. 5, tension side). As a result of this, the next load increments were decreased to 25 pounds and the test was continued. A second audible report was heard when the load was increased to 475 pounds and the crack progressed across the web to gage no. 6. The crack appeared only on the tension side of the web member and the specimen continued to carry the applied load. Application of the load continued until a total of 525 pounds was applied, at which time an ultimate-type failure occurred. The crack appeared on both sides of the web but did not result in a total separation of the specimen. A complete record of strain and deflection data for this test is shown in Table 8.

The two specimens used in the final two tests are shown in Figure 53 after completion of the test. A crack can be seen on the web section of the left specimen in this figure. Detailed photographs of the crack on both sides of the web are shown in Figures 54 and 55. The crack initiated in the area expected and progressed through four strain gages. The failed specimen was returned to the Du Pont Company for further analysis of the fracture surface.

The specimen was separated at the fracture surface and one-half of the specimen is shown in Figure 56. A visual examination of this surface indicated that all the fiber plies were properly aligned and there was no indication of fiber breakage or disorientation as noted in the SK27376 specimen. A section was cut out of the web and polished to observe the fiber distribution; a photograph of this section is shown in Figure 57. The figure shows that a good distribution of fibers was achieved. This examination established that the preforms developed in this program to achieve a continuous flow of fibers from the outer rim to the inner rim can produce a good structure using vacuum-metal-infiltration casting techniques.

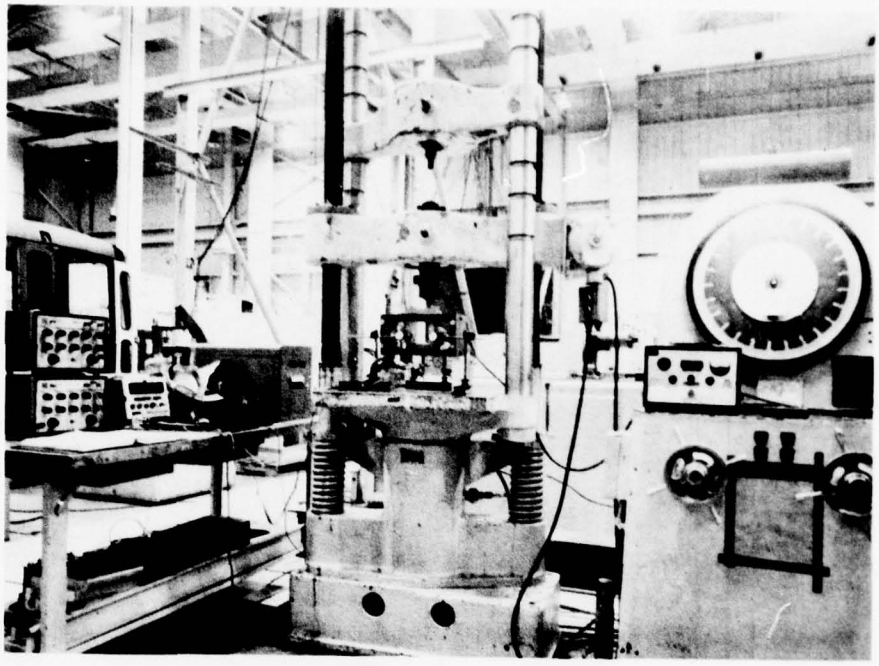

Figure 49. 120-kip Universal Test Machine With Test Fixture Installed.

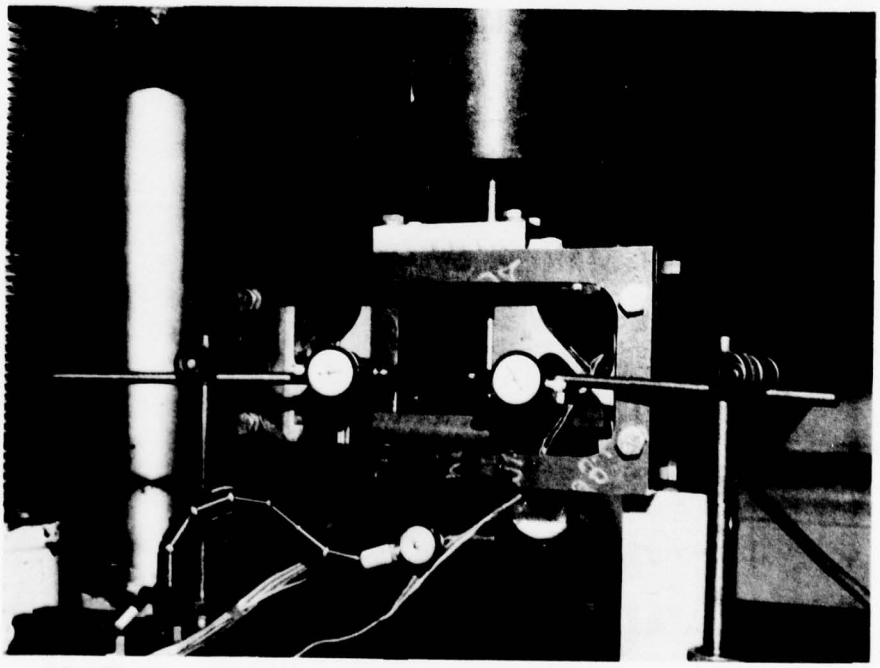

Figure 50. The Test Specimen Instrumented With Strain Gages and Dial Indicators.

TABLE 7. SUMMARY OF TESTING OF SIMULATED OUTER RIM/WEB/INNER RIM CROSS SECTION (SK27377-2)

Specimen Identification	Load (lb)	Specimen 2 ε (μ in./in.)								Specimen 1 ε (μ in./in.)				Dial Ind Defl (in.)						Remarks
		1	2	3	4	5	6	7	8	1	2	3	4	1	2	3	4	5	6	
	0	−3	−57	+47	−126	+60	−8	−4	−54	+189	+68	−52	−129	0	0	0	0	0	0	Best install-
Specimen 1	400	−40	−76	+56	−86	+67	+5	−38	−74	+141	+121	+10	−99	0.0003	0.0007	0.0011	0.0018	0	0.0005	ation zeros
and	800	−80	−92	+56	−31	+65	+22	−72	−97	+97	+161	+69	−76	0.0005	0.0014	0.0021	0.0034	0.0007	0.0012	obtained with
Specimen 2,	1,200	−125	−130	+77	+7	+80	+46	−109	−111	+70	+209	+118	−72	0.0011	0.0019	0.0046	0.0060	0.0017	0.0020	extensive shim-
Ref:	1,600	−255	−207	+108	+142	+162	+140	−124	−133	+105	+270	+133	−145	0.0024	0.0040	0.0130	0.0168	0.0033	0.0035	ming of specimens
Strain Gages	2,000	−312	−248	+130	+200	+188	+168	−152	−148	+87	+324	+173	−158	0.0031	0.0050	0.0163	0.0144	0.0040	0.0042	
Required	2,400	−345	−279	+151	+226	+197	+176	−182	−159	+54	+375	+221	−153	0.0039	0.0059	0.0180	0.0219	0.0047	0.0050	
(Specimen 2	2,800	−346	−297	+164	+234	+183	+162	−210	−170	+8	+424	+281	−129	0.0061	0.0090	0.0200	0.0252	0.0054	0.0055	
has	3,200	−380	−323	+180	+264	+187	+166	−230	−180	−25	+477	+330	−126	0.0073	0.0103	0.0218	0.0283	0.0064	0.0063	
8 strain	3,600	−417	−335	+177	+317	+180	+173	−244	−193	−60	+527	+381	−122	0.0098	0.0138	0.0244	0.0328	0.0071	0.0069	
gages,	4,000	−469	−371	+194	+368	+192	+191	−257	−205	−82	+582	+424	−127	0.0107	0.0151	0.0266	0.0379	0.0081	0.0077	
Specimen 1	4,400	−437	−358	+194	+348	+137	+144	−275	−216	−155	+631	+504	−75	0.0160	0.0208	0.0294	0.0416	0.0089	0.0080	
has	4,800	−447	−371	+206	+348	+118	+125	−290	−232	−201	+680	+567	−51	0.0185	0.0233	0.0317	0.0444	0.0095	0.0088	
4 strain	5,000	−459	−380	+216	+357	+120	+128	−295	−238	−215	+709	+594	−50	0.0190	0.0234	0.0326	0.0456	0.0099	0.0090	
gages)	0	−107	−144	−134	+42	+173	+140	−34	−14	+233	+98	−9	−162	0.0161	0.0190	0.0200	0.0302	0.0030	0.0027	←Indicates slippage
	1,000	−202	−197	+150	+142	+175	+165	−61	−73	+112	+204	+136	−98	0.0166	0.0207	0.0220	0.0337	0.0038	0.0038	occurring during
	2,000	−268	−250	+177	+202	+170	+165	−141	−120	+25	+330	+256	−79	0.0171	0.0213	0.0245	0.0362	0.0055	0.0054	this loading
	3,000	−333	−309	+207	+248	+167	+154	−212	−162	−60	+460	+371	−67	0.0179	0.0221	0.0274	0.0392	0.0071	0.0068	
	4,000	−394	−360	+233	+286	+158	+139	−262	−203	−140	+580	+484	−57	0.0186	0.0227	0.0303	0.0424	0.0088	0.0081	
	5,000	−448	−405	+251	+324	+136	+121	−302	−243	−219	+708	+597	−49	0.0194	0.0235	0.0332	0.0458	0.0103	0.0096	
	0	5	−58	+110	−56	+53	+23	+8	−19	+121	+83	+95	−39	–	–	–	–	–	–	←Specimen bumped after unloading

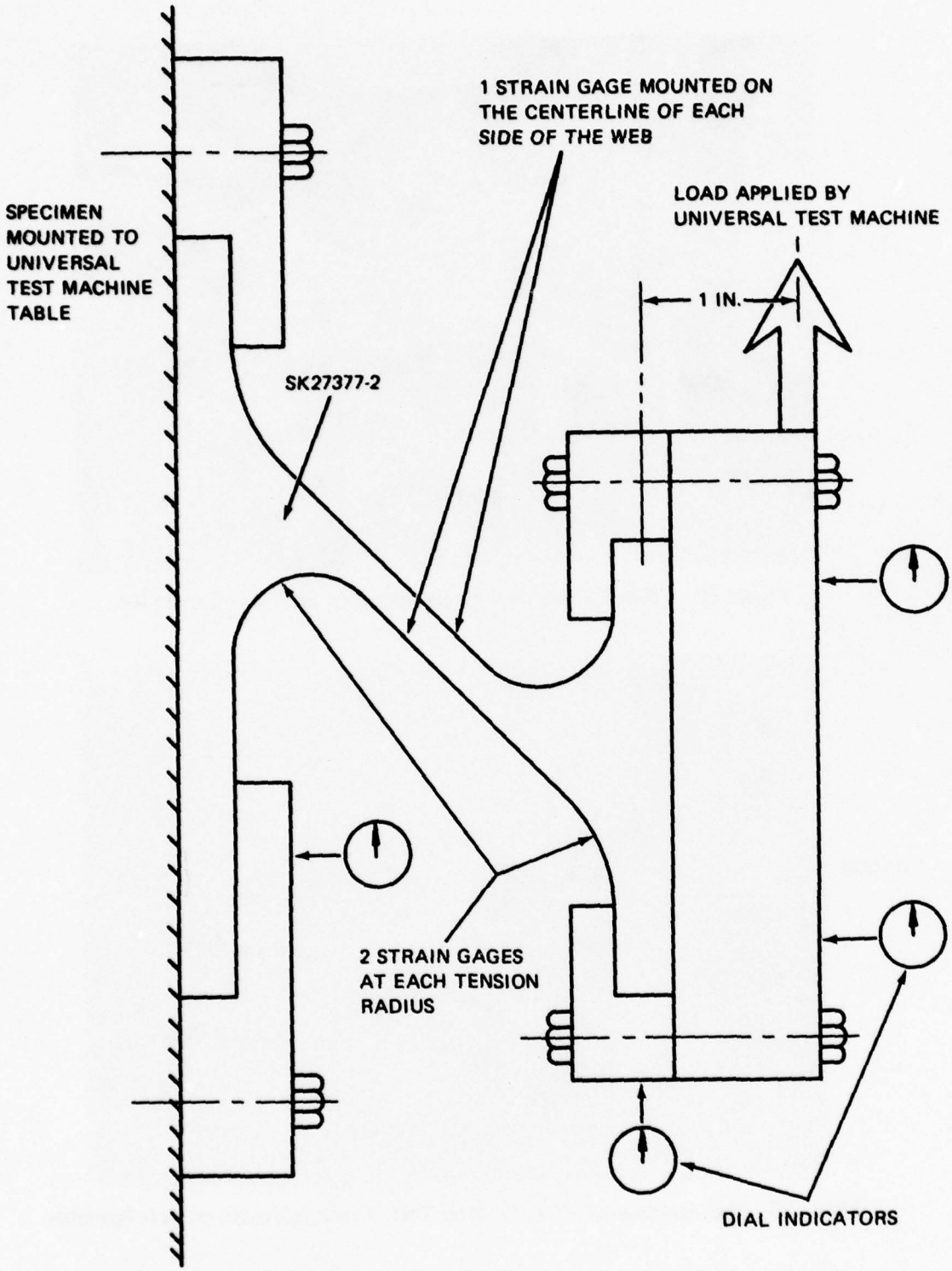

Figure 51. Test Setup for the Outer Rim, Web, and Inner Rim Cross Section.

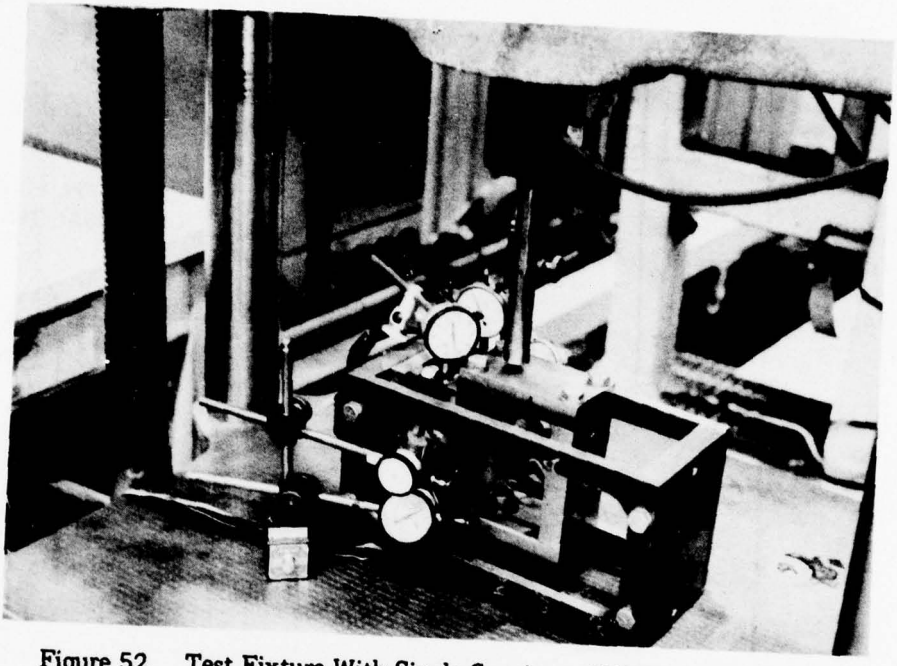

Figure 52. Test Fixture With Single Specimen SK27377-2 Installed.

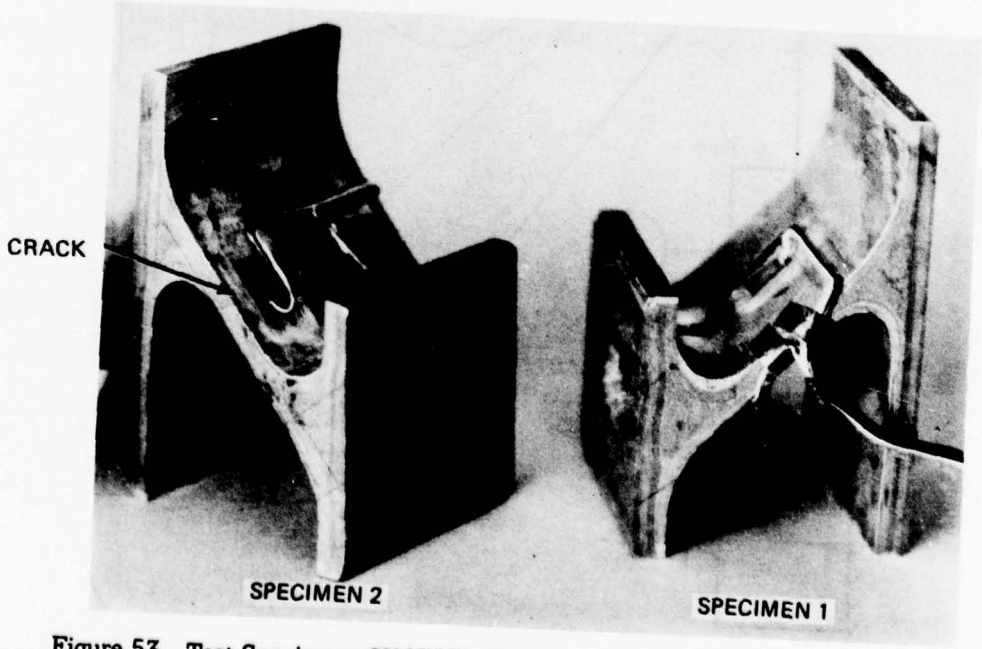

Figure 53. Test Specimens SK27377 After Test. Crack Is Visible on Left Specimen.

TABLE 8. SUMMARY OF TESTING OF NUMBER 2 SPECIMEN OF SIMULATED OUTER RIM/WEB/INNER RIM CROSS SECTION (SK27377-2)

Specimen Identification	Load (lb)	Specimen 2 (μ in./in.)								Dial Ind Defl (in.)					
		1	2	3	4	5	6	7	8	1	2	3	4	5	6
	0	+49	+20	+137	−9	+55	−41	−54	−61						
Specimen 2	0	−73	−92	+191	+108	+168	+94	−41	−16	0	0	0	0	0	0
	100	−523	−558	+568	+519	+692	+620	−31	+9	0.0075	0.0067	0.0094	0.0110	0.0085	0.0065
	200	−786	−824	+759	+756	+996	+927	−28	+14	0.0110	0.0110	0.0150	0.0150	0.0125	0.0100
	300	−1,186	−1,225	+1,093	+1,180	+1,471	+1,388	−18	+22	0.0170	0.0180	0.0130	0.0150	0.0320	0.0290
		Audible report, visible crack across gage 5													
	400	−1,756	−1,761	+1,311	+1,801	–	+2,095	−4	+27	0.0270	0.0270	0.0050	0.0060	0.0650	0.0410
	425	−1,860	−1,855	+346	+1,911	–	+2,211	−5	+29	0.0290	0.0290	0.0060	0.0060	0.0680	0.0620
	450	−1,964	−1,957	+1,430	+2,034	–	+2,357	−6	+33	0.0310	0.0310	0.0070	0.0060	0.0720	0.0660
		Audible report, visible crack across gage 6													
Tested	475	−2,110	−2,109	+1,500	+2,069	–	–	−4	+33	0.0340	0.0340	0.0070	0.0070	0.0800	0.0720
as a	500	−2,462	−2,340	+1,614	+2,227	–	–	+5	+37	0.0370	0.0370	0.0030	0.0030	0.0930	0.0850
Canti-	525	−2,660	−2,600	+1,618	+2,500	–	–	+12	+44	0.0450	0.0450	0.0090	0.0090	0.1260	0.1150
lever	525	−3,678	−2,247	+427	+1,344	–	–	−45	−15	–	–	–	–	–	–
	Ultimate failure at 525 pounds through gages 1, 2, 5, and 6.														

Note: Specimen 1 removed from fixture for above test

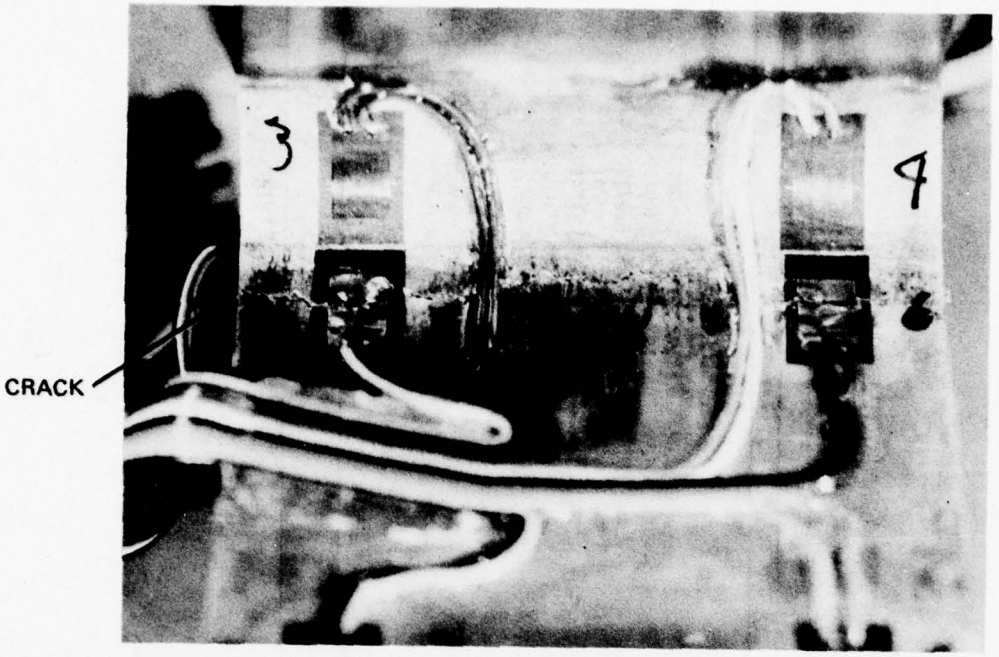

Figure 54. Crack Through Strain Gages 5 and 6 on Tension Side of Web.

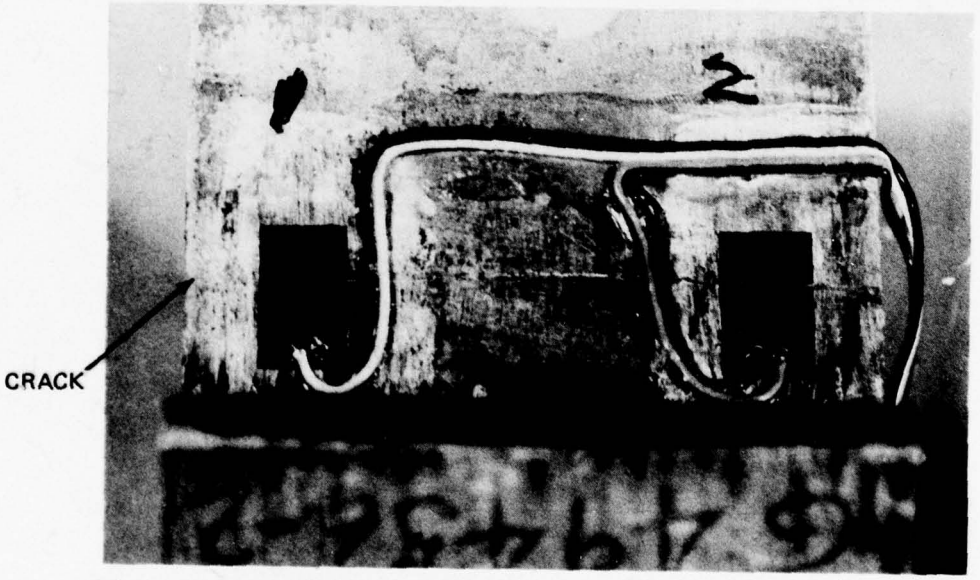

Figure 55. Crack Through Strain Gages 1 and 2 on Compression Side of Web.

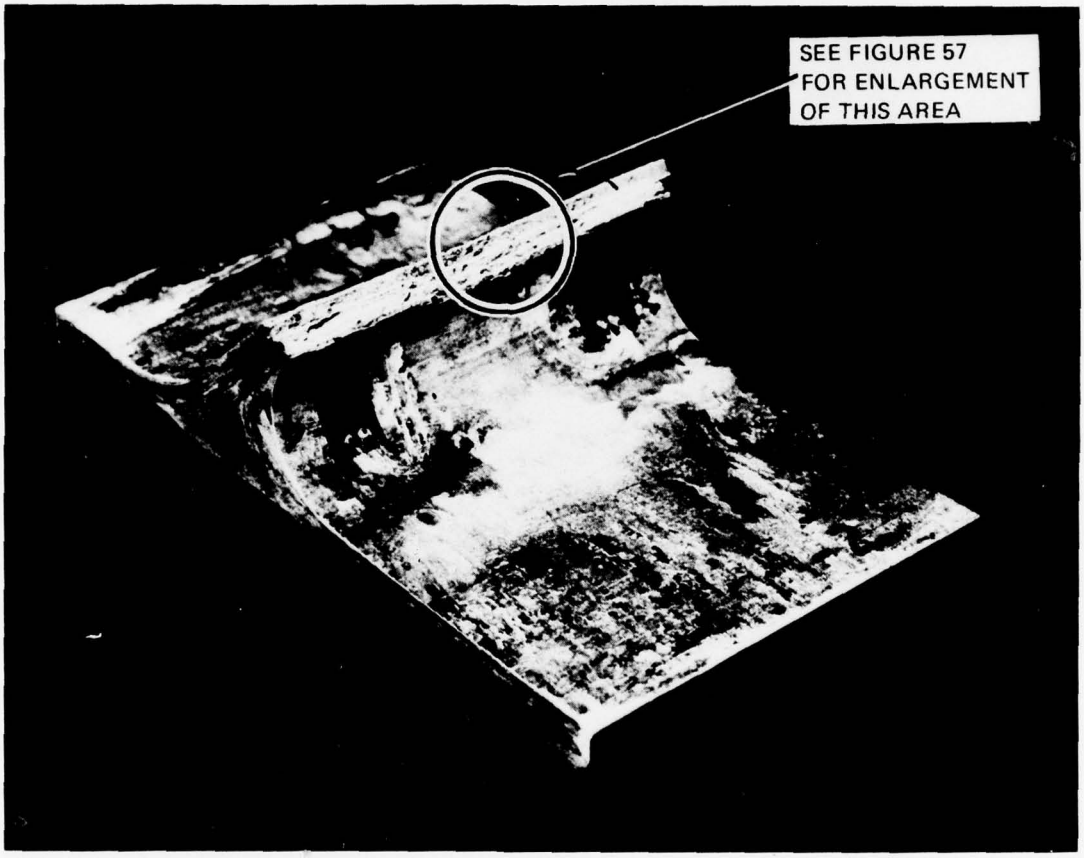

Figure 56. Fracture Surface of Specimen SK27377.

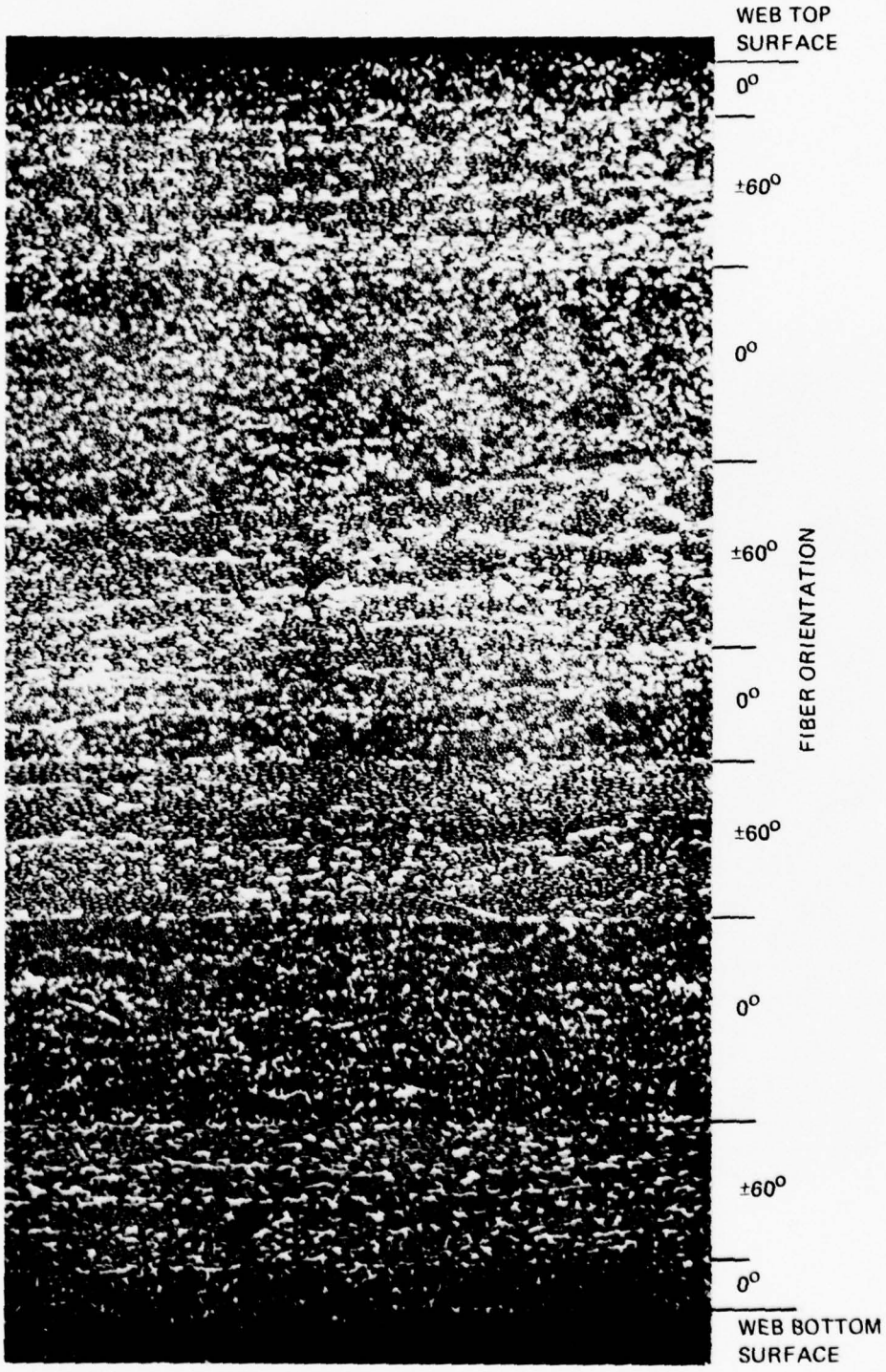

Figure 57. Micrograph of Polished Section of Web Specimen.

TEST RESULTS

This section presents the results of the transmission housing component specimen tests as well as the correlation with the test specimen finite-element analyses. The strength and stiffness characteristics of the Fiber FP/magnesium specimens are compared to those of the AZ91C-T6 magnesium alloy specimens. The results of the test specimen analyses are discussed in relation to the experimental data.

TENSION SPECIMEN TEST AND ANALYTICAL RESULTS

The Fiber FP/magnesium outer-rim cross-section specimen (SK27376-1) was tested to failure in the configuration shown in Figure 40. Failure occurred through the row of 1/4-inch bolt holes; the fracture location and surface are shown in Figure 42. Strain measurements were obtained from four strain gages (two each side) located in the center of the specimen. One gage on each side of the specimen measured longitudinal strain, along the loading axis and colinear with the laminate reference axis. The other gage on each side measured transverse strain, perpendicular to the longitudinal direction. Figure 58 is a plot of the reduced data from this test.

Because the strain-gage readings from the SK27376-1 specimen test do not reflect the strains at the failure location, a second test was run to accurately determine the failure strains. This test specimen (Du Pont 7674-4-1) is a representation of the outer rim wall and is of the same material and layup configuration ($\pm 60^{\circ}/0^{\circ}/\pm 60^{\circ}$) as the thin section of the SK27376-1 specimen. This specimen was strain-gaged (longitudinal and transverse gages each side) and loaded incrementally to failure. The reduced data from this test is presented in Figure 59, where applied load versus average strain is plotted. Load-versus-strain results from the Point Stress Laminate Analysis computer program are shown as dashed lines in Figure 59.

The AZ91C-T6 magnesium alloy outer-rim cross-section specimen (SK27376-2) was tested to failure in a configuration identical to that of the SK27376-1 specimen. The reduced data from this test is presented in Figure 60.

The results of the NASTRAN finite-element analyses for the SK27376-1 and SK27376-2 specimens are shown as dashed lines in Figures 58 and 60. These strain-versus-load relationships represent the strains at the specimen strain-gage locations as derived from the NASTRAN output.

To compare the material behavior on a more unified basis, the test results have been presented as plots of calculated stress at the gage locations versus strain. Figure 61 shows a stress-versus-strain plot for the FP/magnesium $\pm 60^{\circ}/0^{\circ}/\pm 60^{\circ}$ laminate specimens and Figure 62 shows the stress-versus-strain behavior for the AZ91C test specimen. Note that a typical stress-versus-strain curve, as published in Reference 7, has been superimposed on the test data in Figure 62 for comparison with predicted values. Also shown in Figure 61 is the maximum stress level at the failure load and location (1/4-inch-diameter holes) predicted by the NASTRAN analysis for specimen SK27376-1. The Fiber FP/magnesium material properties data for the $\pm 60^{\circ}/0^{\circ}/\pm 60^{\circ}$

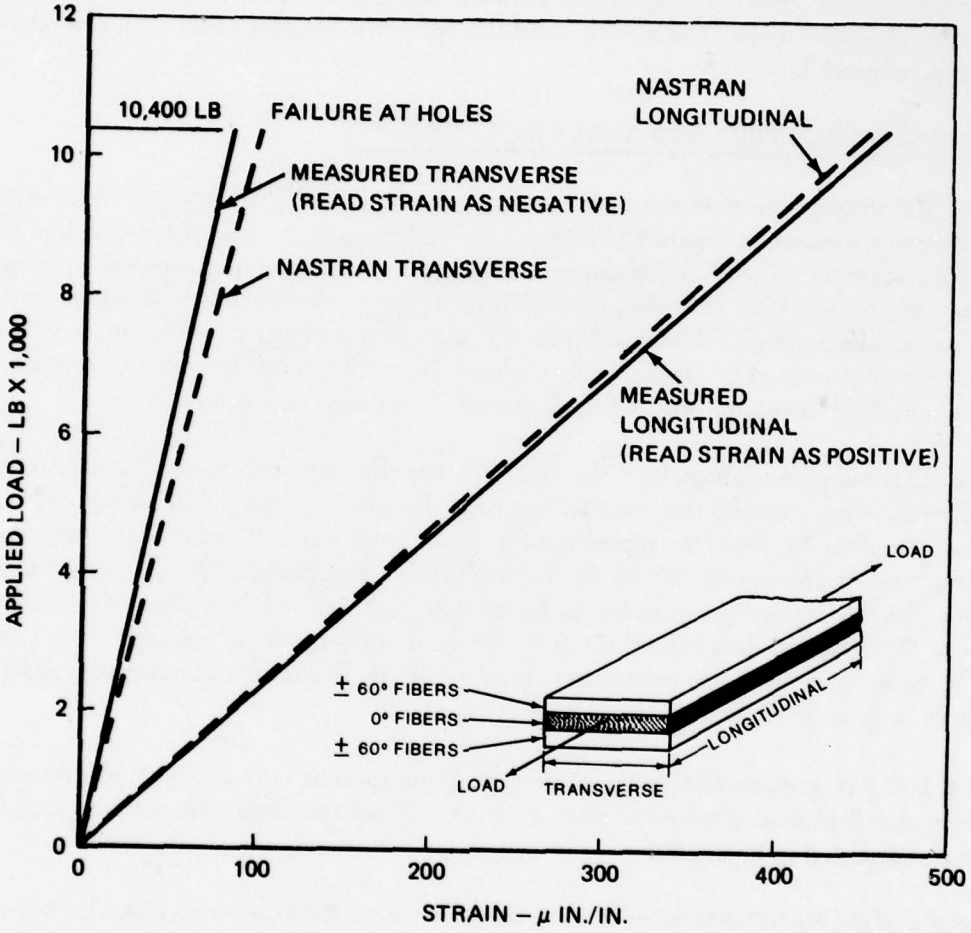

Figure 58. Longitudinal and Transverse Load-Strain Curve of Outer-Rim Cross-Section Specimen SK27376-1 of Fiber FP/Magnesium Composite ($\pm 60^{o}/0^{o}/\pm 60^{o}$).

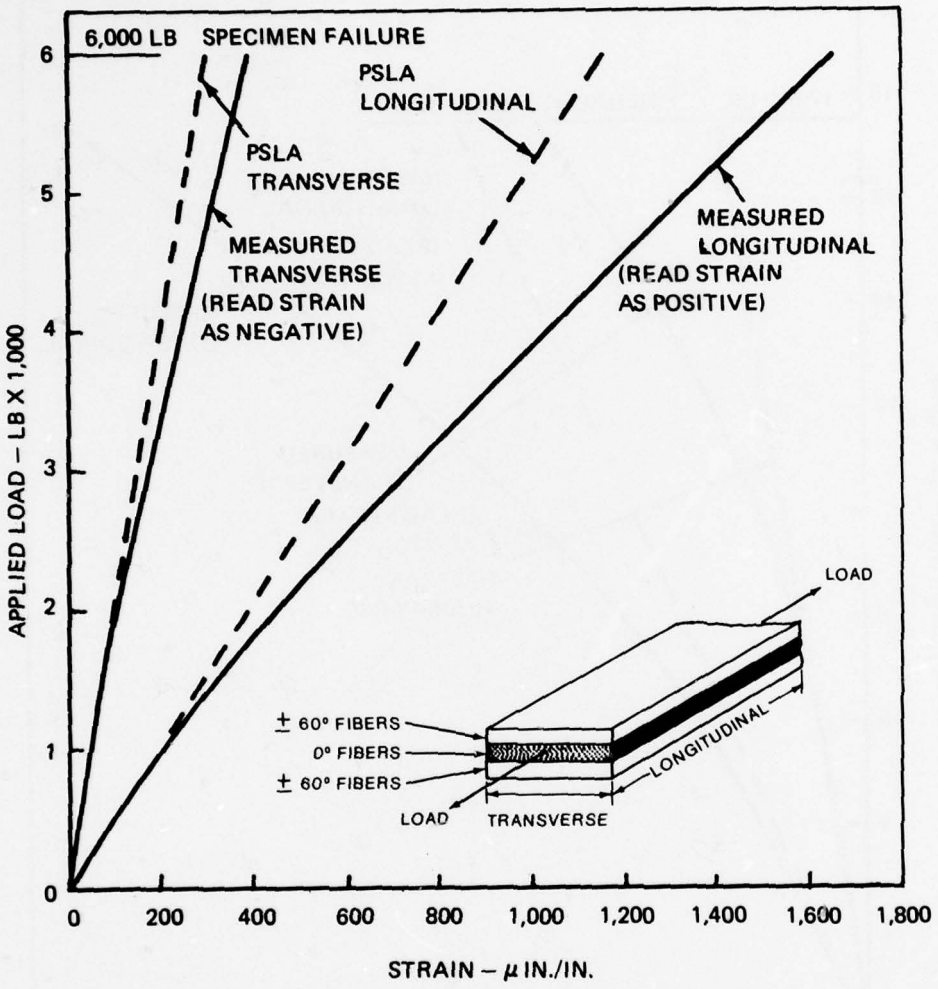

NOTE: PSLA IS POINT STRESS LAMINATE ANALYSIS.

Figure 59. Longitudinal and Transverse Load-Strain Curve of Outer-Rim Tension Coupon 7674-4-I of Fiber FP/Magnesium Composite ($\pm 60^{o}/0^{o}/\pm 60^{o}$).

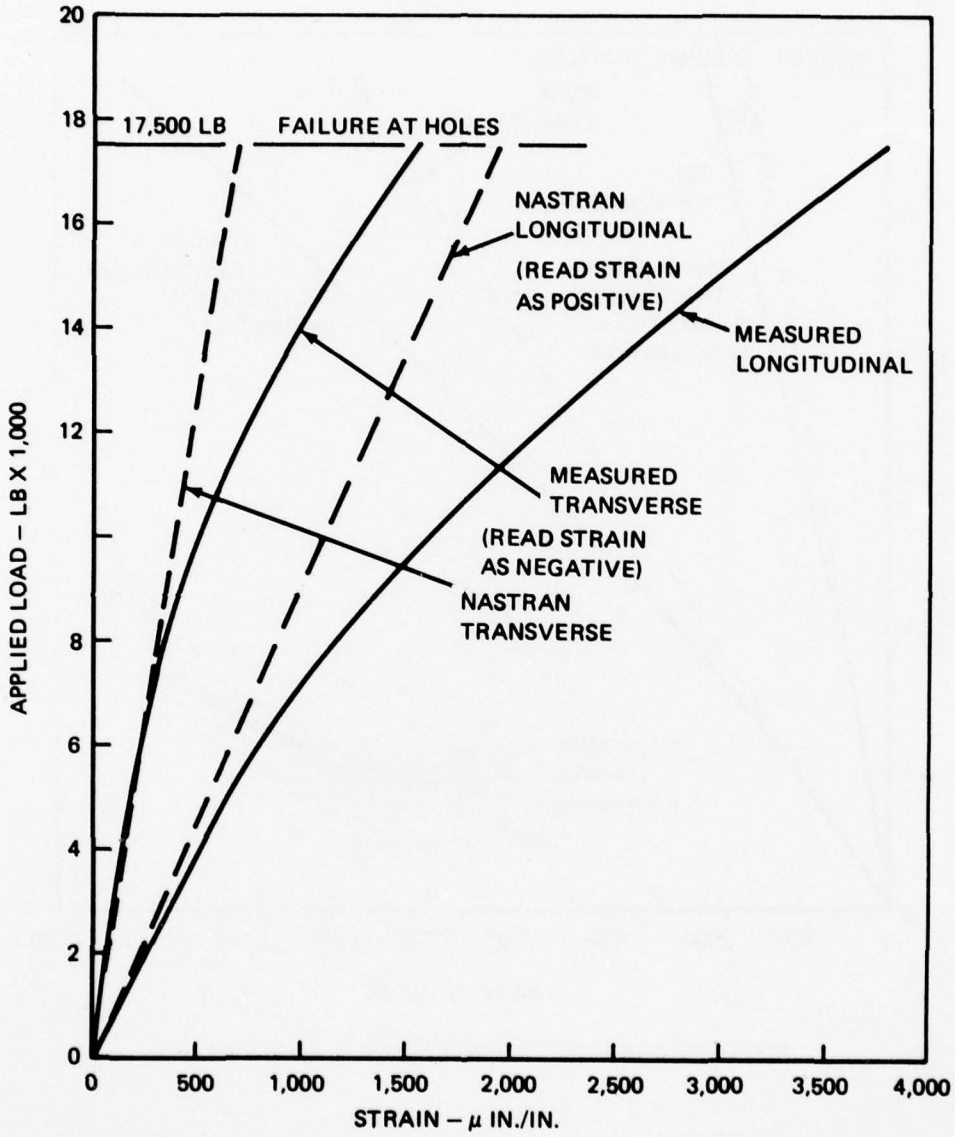

Figure 60. Longitudinal and Transverse Load-Strain Curve of Outer-Rim Cross-Section Specimen SK27376-2 of Solid AZ91C-T6 Magnesium Alloy.

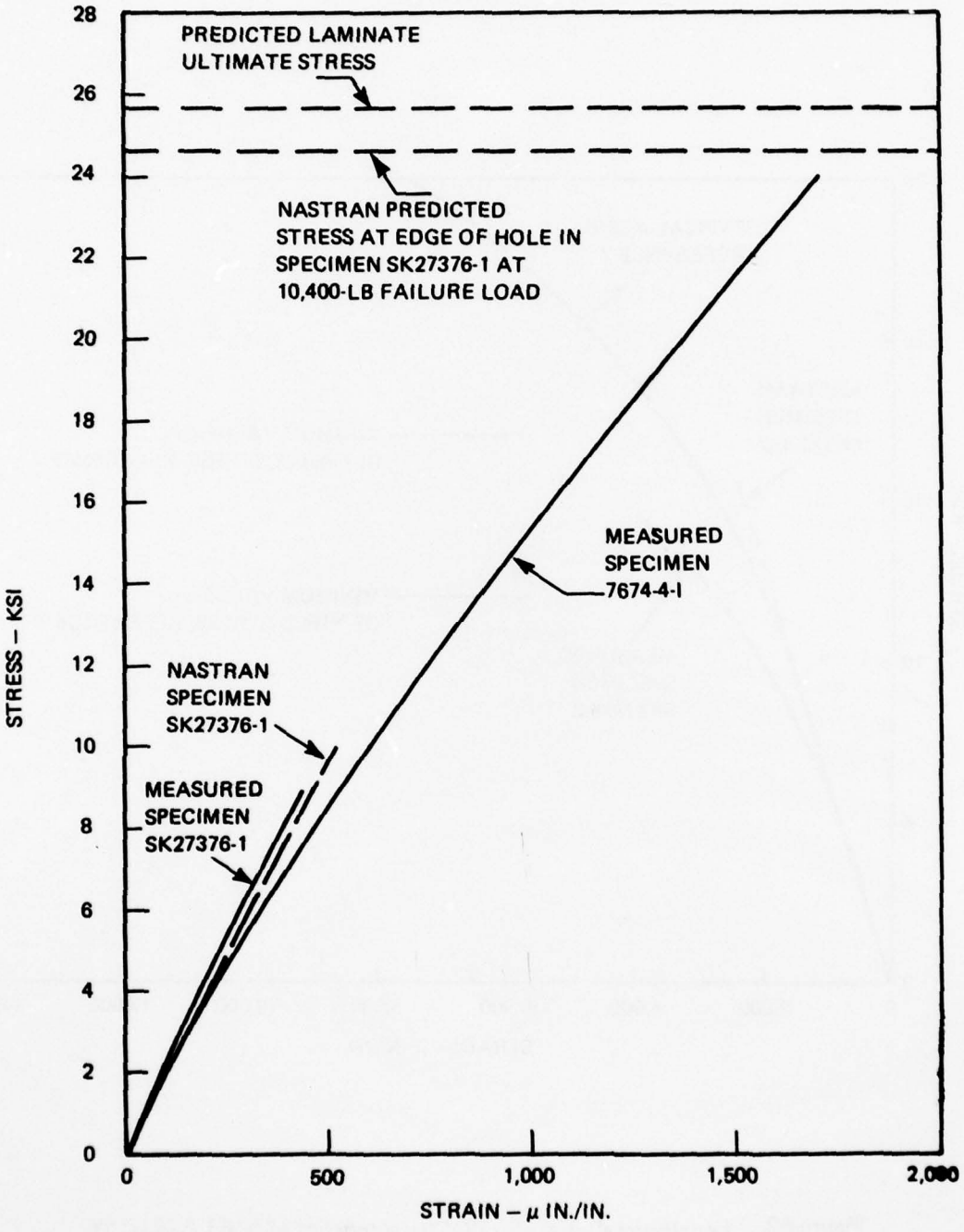

Figure 61. Longitudinal Stress-Strain Characteristics of Fiber FP/Magnesium Composite Specimens.

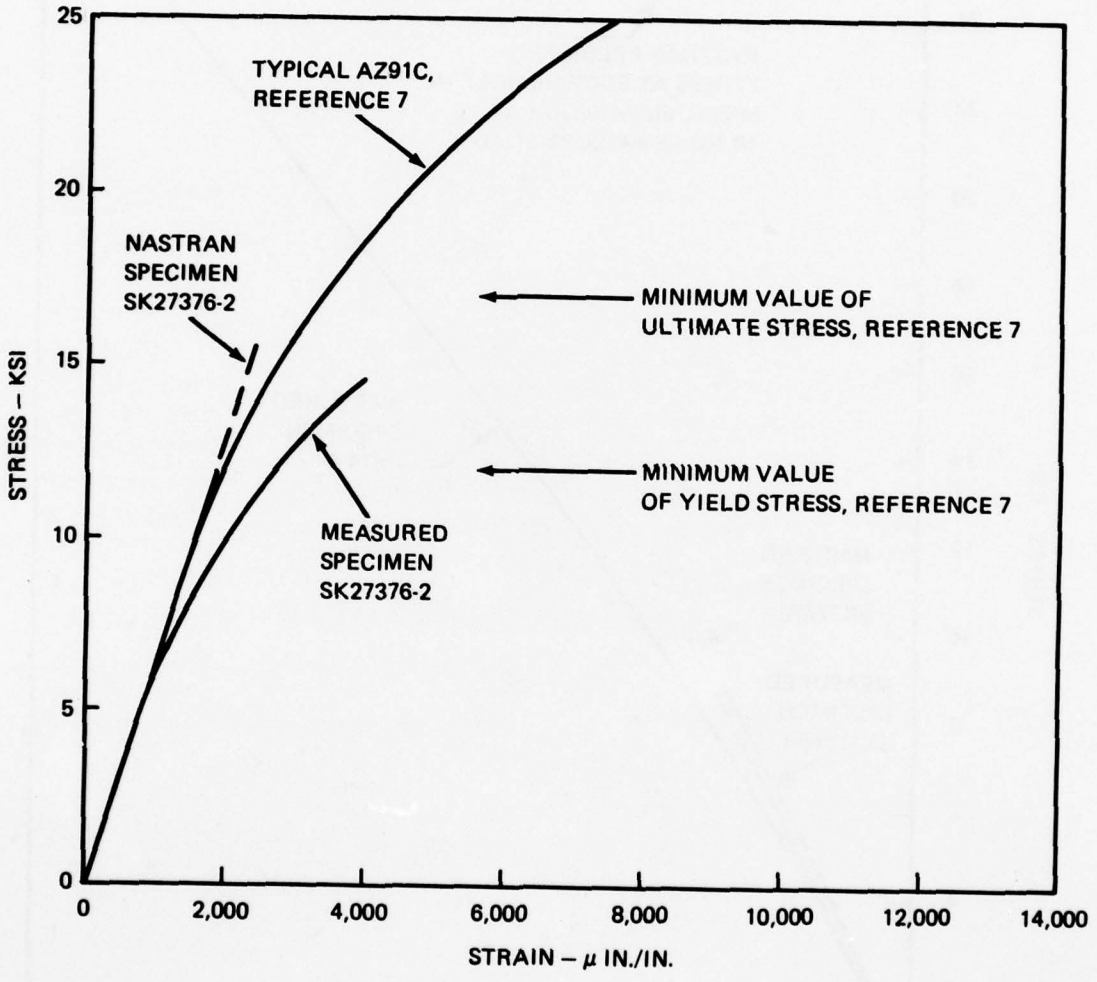

Figure 62. Longitudinal Stress-Strain Characteristics of Solid AZ91C-T6 Magnesium Alloy Specimens.

laminate was generated by the Point Stress Laminate Analysis computer progtam described in a previous section of this report. This material properties data was used by the NASTRAN finite-element analyses to calculate the specimen stress and strain data. For the AZ91C-T6 magnesium alloy specimen analysis, material properties were obtained from Reference 7. A comparison of these published values with the FP/magnesium composite material properties is given in Table 9.

TABLE 9. PREDICTED AND EXPERIMENTAL MECHANICAL PROPERTIES OF AZ91C-T6 MAGNESIUM AND FP/MAGNESIUM COMPOSITE $\pm 60^{\circ}/0^{\circ}/\pm 60^{\circ}$ LAMINATE CONFIGURATION

Property	AZ91C-T6 Reference 7	Predicted by Analysis	From Test
Elastic Modulus (Avg), Longitudinal	6.5×10^6 psi	19.6×10^6 psi	20.7×10^6 psi
Poisson's Ratio (Avg), Longitudinal	0.35	0.26	0.24
Longitudinal Ultimate Strength (Nominal)	17–35 ksi	25.7 ksi	24.0 ksi

Agreement between the SK27376-1 and 7674-4-I specimen test data seems quite good, as evidenced by the plots in this section. These results also agree with the analytical results in the strain region where material behavior is linear in nature. The Point Stress Laminate Analysis and NASTRAN analytic methodologies presuppose linear material behavior. Indeed, transmission design allowable stresses for continuous operation are generally well below the yield stress range, as shown in Figure 62. A comparison of the material properties shown in Table 9 indicates that the longitudinal elastic modulus for the FP/magnesium composite is approximately three times that of the AZ91C-T6 alloy. This represents a threefold increase in stiffness over the AZ91C-T6 and consequently a threefold decrease in deflection for a given stress for the FP/magnesium composite. Agreement between analytical and experimental properties is on the order of 5 to 8 percent. The analytical load-versus-strain data correlates well with the data from specimen testing.

OUTER RIM/WEB/INNER RIM TEST AND ANALYTICAL RESULTS

The FP/magnesium SK27377-2 outer rim/web/inner rim section specimen was tested in two configurations. In the first test, two SK27377-2 specimens were tested in a back-to-back arrangement analogous to the cylindrical inner rim/web/outer rim of the bevel gear bearing support structure. An offset load was applied to the test fixture to simulate the bearing thrust and moment resultants as shown previously in Figure 46. Load was applied incrementally to 5,000 pounds, with longitudinal strains measured at each load level. The 5,000-pound offset load produces an equivalent 5,000-pound thrust and 5,000-inch-pound overturning moment at the simulated support bearing location. These load values are approximately twice the actual support bearing loads for the CH-47C transmission operating at 100-percent rated power. Furthermore, the width of the test specimens is only 64 percent of the minimum web section width for the CH-47C bearing support webs. This would indicate that test specimen stress levels are even higher than the doubled rated load condition implies. The sketch in Figure 63 shows

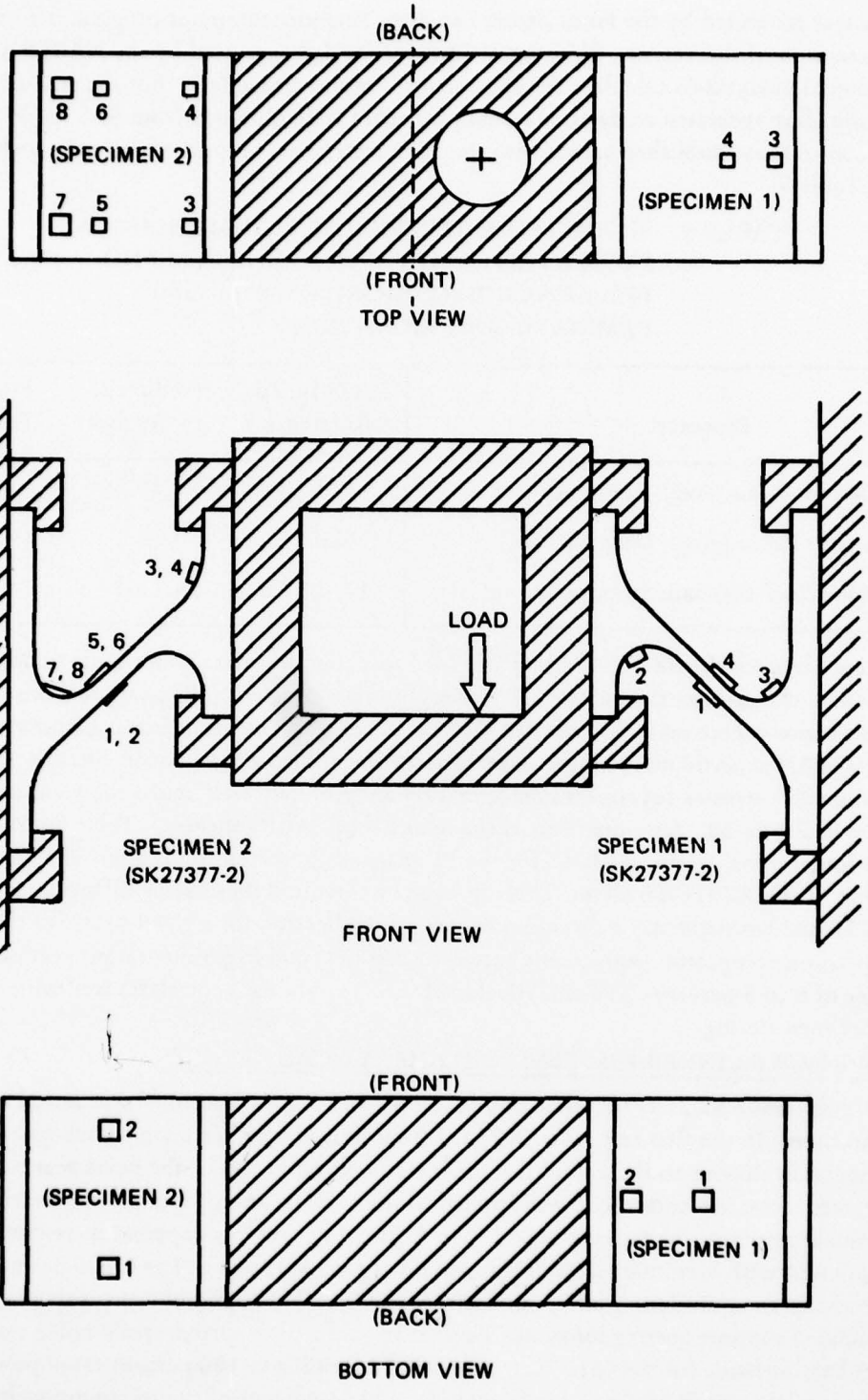

Figure 63. Back-to-Back FP/Magnesium Test Specimen Setup.

the geometric relationship between specimens and load as well as the location and numbering of the strain gages. The reduced data from this test is presented in the form of plots (Figure 64) showing average measured strain versus applied load; also contained in these figures are curves showing the results of the NASTRAN analyses performed for this test configuration. The analytical strain-versus-applied-load behavior in the web region of the FP/magnesium SK27377 specimens is indicated. The specimens were also analyzed as if they were fabricated from AZ91C-T6 magnesium alloy. Although no outer rim/web/inner rim AZ91C alloy specimens were tested, the analytical data is also included in Figure 64 for purposes of comparison.

Deflections of the loading fixture center section were also measured during the back-to-back specimen test. These deflections represent displacements and rotations of the specimen's inner rim flanges. The plots presented in Figure 65 show the measured average vertical displacements and rotations of the fixture center section as a function of load. For comparison, analytical data representing the displacements and rotations of hypothetical AZ91C-T6 specimens is included.

The second outer rim/web/inner rim cross section specimen test consisted of subjecting a single specimen (SK27377-2) to loading conditions as shown in Figure 66. In this setup the specimen was loaded incrementally until failure. Failure was initiated at a load level of approximately 350 pounds and was characterized by an audible report and a small crack in the area of strain gage 5. The specimen, however, continued to carry load. Testing was continued and the load was increased until ultimate failure occurred at 525 pounds. A plot of strain gage readings is shown in Figure 67. This figure also shows the NASTRAN strain-versus-load data for FP/magnesium and AZ91C-T6 magnesium alloy analysis. Figure 68 contains measured and analytical AZ91C-T6 displacement and rotation versus load data for the single-specimen test configuration.

The material property data used in the analyses of the composite specimens was generated by the Point Stress Laminate Analysis computer program. AZ91C-T6 properties were taken from Reference 7. The complexity of the test specimen geometry and loading conditions precludes verification of predicted outer rim/web/inner rim laminate material properties on other than a comparative basis. The correlation between analytical and experimental results seems reasonable, especially for the single-specimen test where the complexities of load paths are less likely to obscure the material characteristics. Table 10 presents the material properties used in the analysis of the outer rim/web/inner rim test specimens.

TABLE 10. COMPARISON OF FP/MAGNESIUM AND AZ91C-T6 MATERIAL PROPERTIES FOR OUTER RIM/WEB/ INNER RIM SPECIMENS

Property	AZ91C-T6 Reference 7	FP/Mag Outer and Inner Rim	FP/Mag Web
Longitudinal Elastic Modulus	6.5×10^6 psi	20.6×10^6 psi	22.7×10^6 psi
Transverse Elastic Modulus	6.5×10^6 psi	19.2×10^6 psi	18.3×10^6 psi
Poisson's Ratio	0.35	0.26	0.25
Ultimate Tensile Strength (Long.)	17–35 ksi	31.4 ksi	42.8 ksi

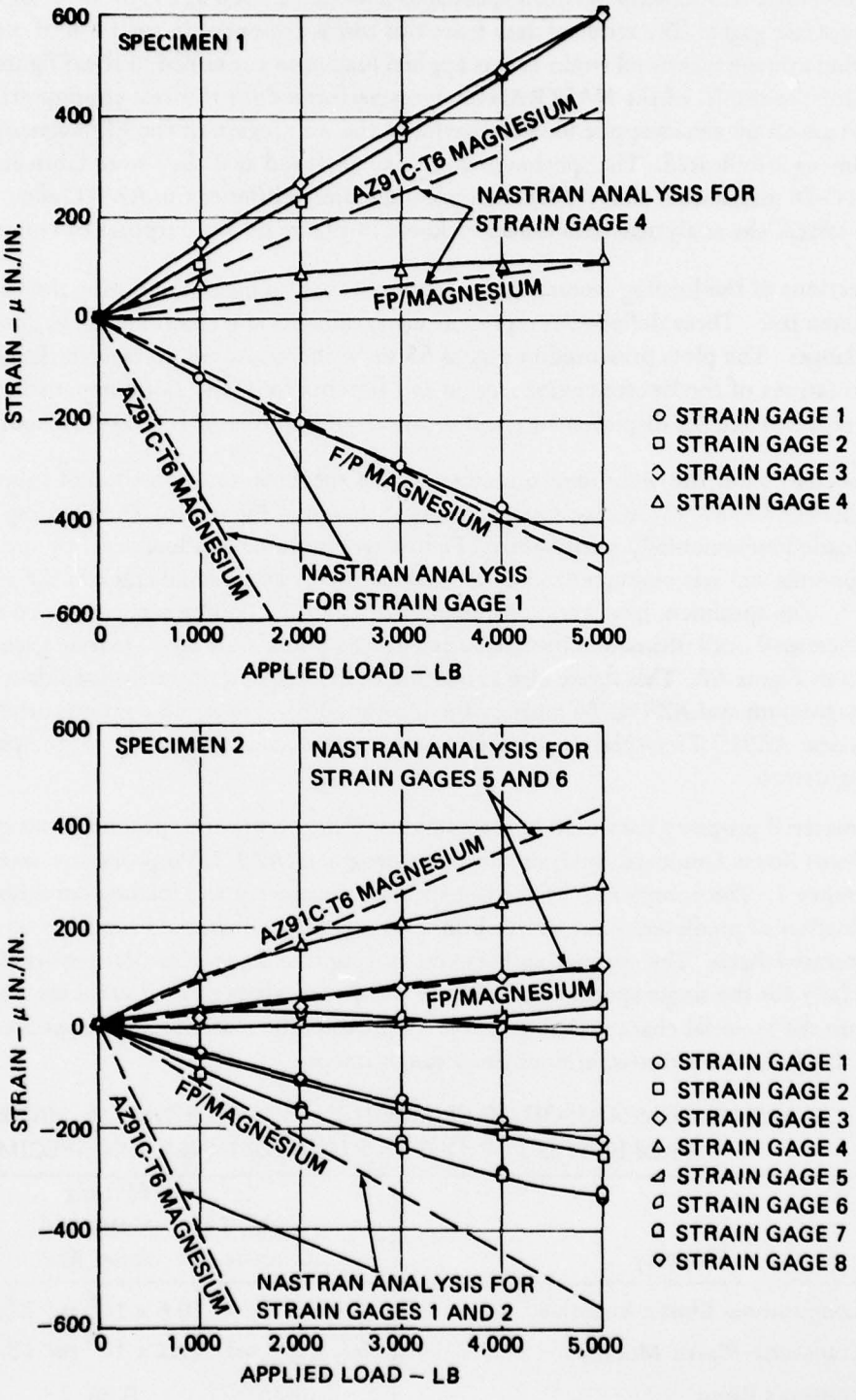

Figure 64. Strain Versus Load Data From Back-to-Back Test of Specimens SK27377.

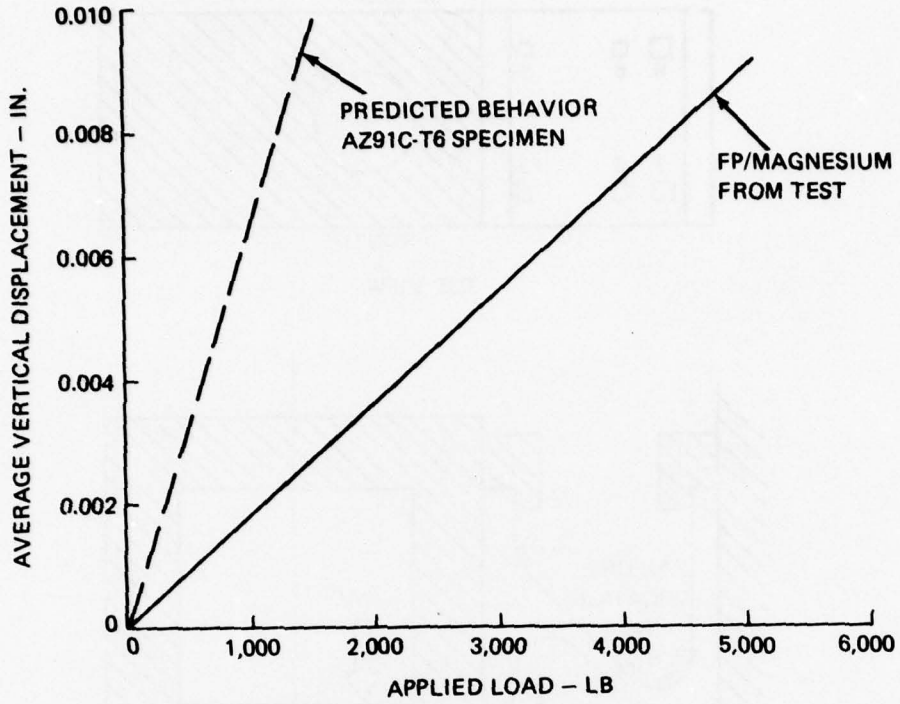

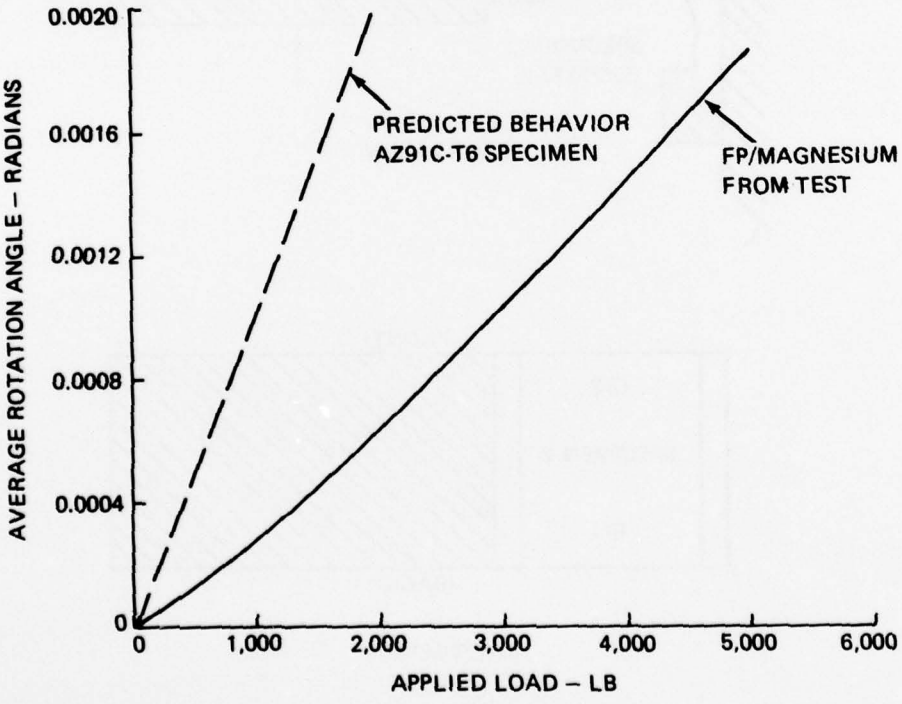

Figure 65. Vertical Displacement and Rotation of Center Section Versus Load From Back-to-Back Test of Specimens SK27377.

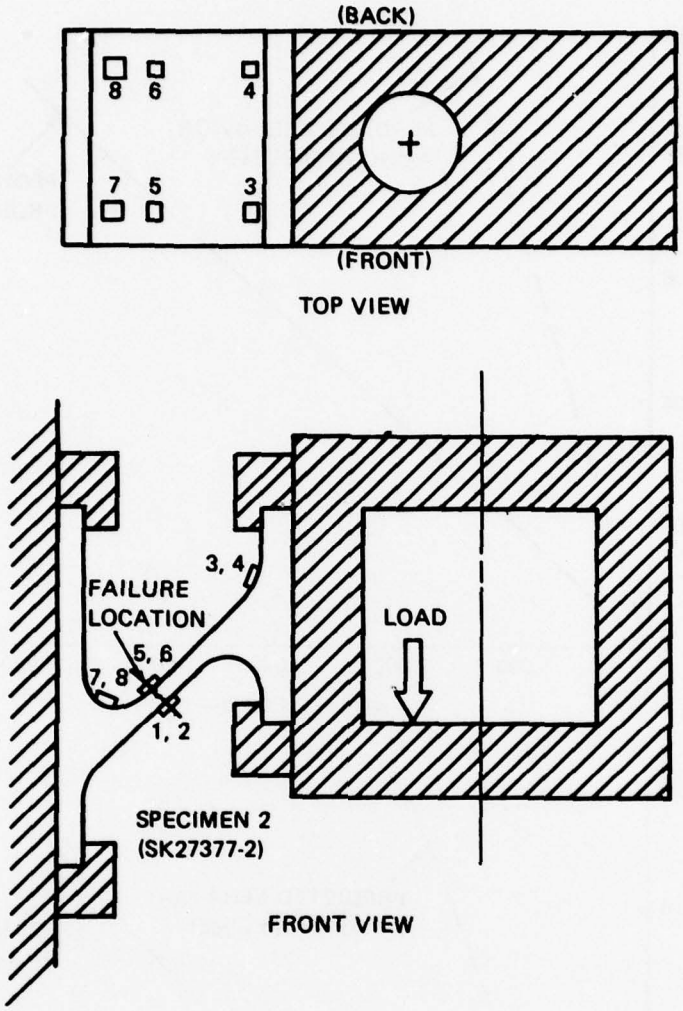

Figure 66. Single-Specimen FP/Magnesium Test Specimen Setup.

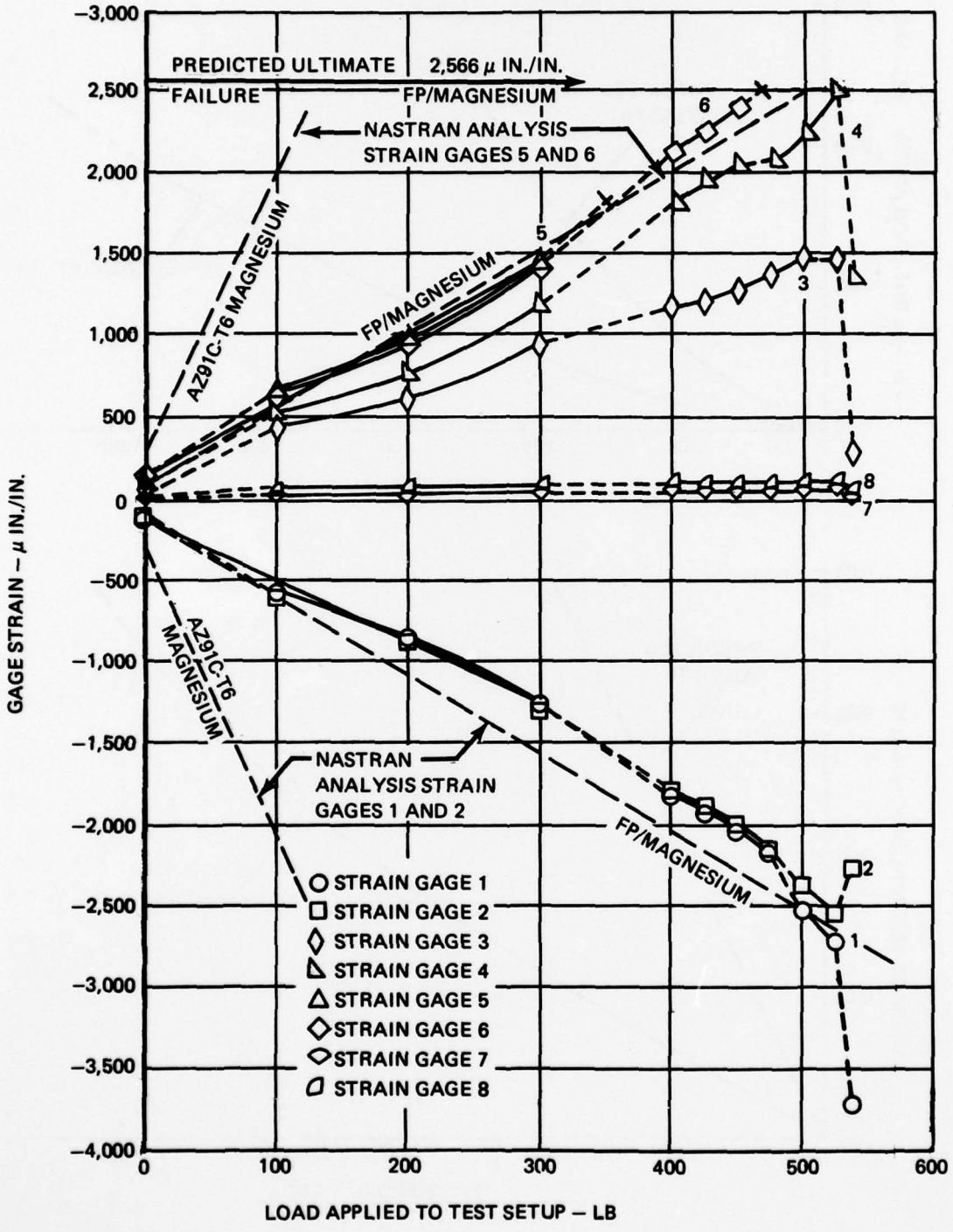

Figure 67. Strain Versus Load Data From Single-Specimen Test of SK27377.

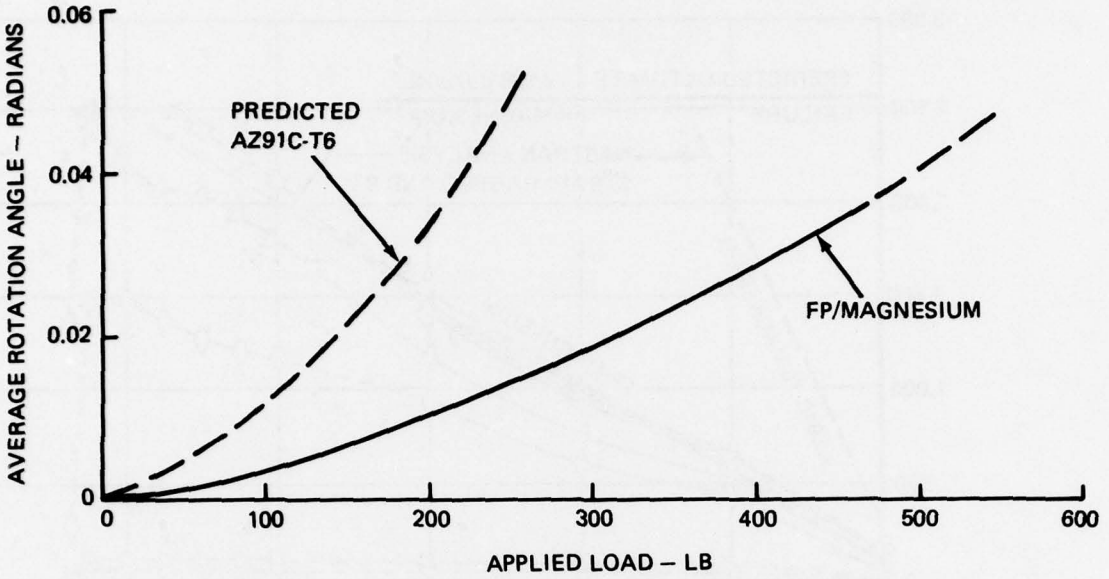

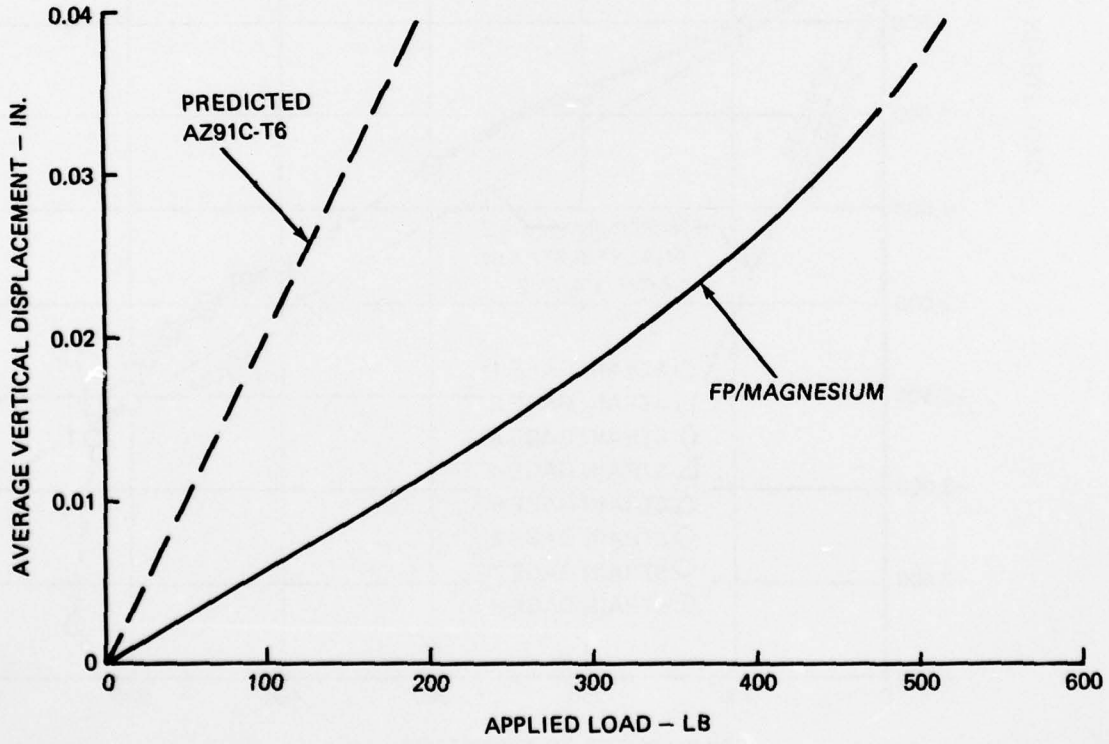

Figure 68. Vertical Displacement and Rotation of Inner Ring Flange Versus Load From Single-Specimen Test of SK27377.

The analytical strain-versus-load data is in general agreement with the experimental results. The back-to-back test and analytical results in Figure 64 display nearly linear strain-load behavior. This is expected for data in the relatively low strain region where material characteristics are linear. It should be noted that in the analyses no attempt was made to model the stress riser effect at the specimen web-rim intersection. Strains, however, were monitored during the test at these fillet locations to investigate the effects of the stress concentration and to detect any tendency for the composite to delaminate in these areas; no such tendencies were noted. A comparison of analytical results for FP/magnesium and AZ91C-T6 specimens indicates a strain-to-load ratio approximately 3.5 times greater for AZ91C-T6 than that of the FP/magnesium. This implies that the deflections for the AZ91C-T6 specimen would be greater than the FP/magnesium specimen by approximately the same ratio. Indeed, the analytical displacements reflected a 3.4 times increase for the AZ91C-T6 specimen over the FP/magnesium specimen. This ratio was applied to the measured FP/magnesium back-to-back configuration deflections and rotations and was plotted as dashed lines in Figure 65. The stiffening provided by FP/magnesium composites would have a pronounced effect on the vibrational characteristics of a structure. The strain-gage data in the lower plot of Figure 64 indicates that a slight twisting of the specimen web section occurred as load was applied. This twisting is seen as a slight difference in gage readings between gages located on opposite sides of the specimen centerline, gages 1 and 2 on specimen 2, for example.

FP/magnesium experimental and analytical data in Figure 67 for the single-specimen test correlates well. The slight deviation from linear behavior can be attributed to material nonlinearities. Again, web-rim fillet effects were not modeled. Note the apparent lack of response for gages 7 and 8. The analytical results for an AZ91C-T6 specimen indicate a substantial increase in strain-to-load ratio. The predicted ultimate strain for the web section agrees closely with the measured value at failure. The displacement and rotation versus load plots in Figure 68 exhibit the same tendencies discussed previously in relation to the back-to-back testing.

The predicted material properties for the FP/magnesium laminates comprising the SK27377 specimens have provided reasonable correlation between analytical and experimental data.

CONCLUSIONS

The analytical and fabrication technology developed for complex metal-matrix structures made from Fiber FP-reinforced cast magnesium has been demonstrated successfully in this program. This progress offers considerable encouragement for the full-scale development, fabrication, and evaluation of a metal-matrix composite helicopter main transmission housing.

The following specific conclusions have been reached as a result of this program:

- It is possible to construct a finite-element model (NASTRAN) of composite structure elements from engineering drawings and available material properties. The model predicts stresses and strains which correlate with experimentally measured values.

- The analysis indicates that composite metal-matrix materials (Fiber FP/magnesium) can be effectively employed to selectively stiffen a helicopter main transmission housing.

- The manufacturing technology necessary to fabricate a complex metal-matrix structure using Fiber FP and a magnesium alloy has been demonstrated. Procedures for developing preforms of Fiber FP and the use of vacuum-metal-infiltration techniques have also been proven.

- Good manufacturing quality of cast magnesium reinforced with Fiber FP has been demonstrated.

- Structurally sound test specimens representing various critical elements of a transmission housing have been fabricated from Fiber FP/magnesium and tested to evaluate the material properties under simulated load conditions.

AD-A066 794 BOEING VERTOL CO PHILADELPHIA PA F/G 1/3
HELICOPTER TRANSMISSION VIBRATION AND NOISE REDUCTION PROGRAM. --ETC(U)
JAN 79 J W LENSKI DAAJ02-74-C-0040
UNCLASSIFIED D210-11442-1 USARTL-TR-78-2C NL

2 OF 2
AD A066794

END
DATE FILMED
5-79
DDC

RECOMMENDATIONS

Based on the results of this program, it is recommended that the following specific items be considered for future investigation:

- Additional work is required to provide an adequate data bank on the properties of Fiber FP/magnesium composites. This information should precede the development of a production helicopter main transmission housing. Several areas to be investigated are the following:
  - Compatible alloy selection
  - Thermal processing
  - Gating and filling techniques
  - Fatigue and fracture toughness properties
  - Installation of stud inserts
  - Material properties at elevated temperatures
- The development of a monolithic investment-casting technology for large, complex structures using continuous, one-piece fiber preforms should be investigated. This technology would result in high joint efficiency, minimum machining, and a single-step casting process. Methods of providing preselected fiber orientation and location in a casting must also be developed.
- Development of ceramic shell-casting techniques is required to replace the presently used metallic expendable tooling. This new technology will be needed to cast full-scale helicopter transmission housings at relatively low cost.
- Additional work will be required to modify existing analytical methodology to incorporate the effects of the nonlinear material properties of magnesium. Present input to computer programs uses the material properties of magnesium valid only in the small strain range. This input should be varied as load and strain change in order to improve the correlation between calculated and experimental stresses and deflections.

REFERENCES

1. Sciarra, John J., Howells, Robert W., Lenski, Joseph W., Jr., Drago, Raymond J., and Schaeffer, Edward G., HELICOPTER TRANSMISSION VIBRATION AND NOISE REDUCTION PROGRAM, Volume I – Technical Report, Boeing Vertol Company, Philadelphia, Pennsylvania; USARTL-TR-78-2A, Applied Technology Laboratory, U.S. Army Research and Technology Laboratories (AVRADCOM), Fort Eustis, Virginia, March 1978, AD A055104.

2. Sciarra, John J., Howells, Robert W., Lenski, Joseph W., Jr., and Drago, Raymond J., HELICOPTER TRANSMISSION VIBRATION AND NOISE REDUCTION PROGRAM, Boeing Vertol Company, Philadelphia, Pennsylvania; USARTL-TR-78-2B, Volume II – User's Manual, Boeing Vertol Company, Philadelphia, Pennsylvania; USARTL-TR-78-2B, Applied Technology Laboratory, U.S. Army Research and Technology Laboratories (AVRADCOM), Fort Eustis, Virginia, March 1978, AD A054827.

3. Howells, R. W., and Sciarra, J. J., FINITE ELEMENT ANALYSIS FOR COMPLEX STRUCTURES (HELICOPTER TRANSMISSION HOUSING STRUCTURAL MODELING), Boeing Vertol Company, Philadelphia, Pennsylvania; USAAMRDL-TR-77-32, Applied Technology Laboratory, U.S. Army Research and Technology Laboratories (AVRADCOM), Fort Eustis, Virginia, January 1978, AD A052759.

4. Champion, A. R., Krueger, W. H., Hartmann, H. S., and Dhingra, A. K., FIBER FP REINFORCED METAL MATRIX COMPOSITES, Second International Conference on Composite Materials, Toronto, Canada, April 1978.

5. Prewo, K. M., Report R77-912245-3, United Technologies Research Center, East Hartford, Connecticut, May 1977.

6. Reed, D. L., POINT STRESS LAMINATE ANALYSIS, Document FZM-5494, Advanced Composite Division, U.S. Air Force Materials Laboratory, Wright-Patterson Air Force Base, Ohio, April 1970.

7. MIL-HDBK-5C, MILITARY STANDARDIZATION HANDBOOK, METALLIC MATERIALS AND ELEMENTS FOR AEROSPACE VEHICLE STRUCTURES, FSC1560, Department of Defense, Washington, D.C., September 1976.

8. Emley, E. F., PRINCIPLES OF MAGNESIUM TECHNOLOGY, London, England, Pergamon Press, 1966.

GLOSSARY

Al_2O_3	aluminum oxide
Fiber FP	an experimental aluminum oxide fiber under development by Du Pont
GPa	gigaPascals, $N/m^2 \times 10^9$
HM graphite	high-modulus graphite
HT graphite	high-tensile graphite
kHz	kiloHertz, thousands of cycles per second
kip	thousands of inch-pounds
ksi	thousands of pounds per square inch
LP	lower planetary
Mg	magnesium
MPa	megaPascals, $N/m^2 \times 10^6$
micron	one one-millionth of a meter
psi	pounds per square inch
PSLA	point stress laminate analysis
ϵ	strain, μ in./in.
μ	micro, one one-millionth of

DEPARTMENT OF THE ARMY

Applied Technology Laboratory
U.S. Army Research and Technology
Laboratories (AVRADCOM)
DAVDL-ATL-TSD
Fort Eustis, Virginia 23604

OFFICIAL BUSINESS

PENALTY FOR PRIVATE USE, $300

POSTAGE AND FEES PAID
DEPARTMENT OF THE ARMY
DOD-314

THIRD CLASS